THEORETICAL INVESTIGATION OF PROPANE DEHYDROGENATION AND COKE INHIBITION ON Ni(111) Ni-Au/Ni(111) AND Ni-Sn/Ni(111) CATALYSTS

TINNAKORN SAE-LEE

DOCTOR OF PHILOSOPHY

IN CHEMISTRY

GRADUATE SCHOOL

CHIANG MAI UNIVERSITY

AUGUST 2019

THEORETICAL INVESTIGATION OF PROPANE DEHYDROGENATION AND COKE INHIBITION ON Ni(111) Ni-Au/Ni(111) AND Ni-Sn/Ni(111) CATALYSTS

TINNAKORN SAE-LEE

A THESIS SUBMITTED TO CHIANG MAI UNIVERSITY IN PARTIAL FULFILLMENT OF THE REQUIREMENTS FOR THE DEGREE OF DOCTOR OF PHILOSOPHY IN CHEMISTRY

GRADUATE SCHOOL, CHIANG MAI UNIVERSITY
AUGUST 2019

THEORETICAL INVESTIGATION OF PROPANE DEHYDROGENATION AND COKE INHIBITION ON Ni(111) Ni-Au/Ni(111) AND Ni-Sn/Ni(111) CATALYSTS

TINNAKORN SAE-LEE

THIS THESIS HAS BEEN APPROVED TO BE A PARTIAL FULFILLMENT OF
THE REQUIREMENTS FOR THE DEGREE OF
DOCTOR OF PHILOSOPHY
IN CHEMISTRY

Examination Committee:

..... Chairman
(Dr. Supawadee Namuangruk)

..... Member
(Asst.Prof.Dr. Nawee Kungwan)

..... Member
(Dr. Anchalee Junkaew)

..... Member
(Dr. Chanisorn Ngaojampa)

..... Member
(Asst.Prof.Dr. Praput Thavornyutikarn)

Advisory Committee:

..... Advisor
(Asst.Prof.Dr. Nawee Kungwan)

.....Co-advisor
(Dr. Anchalee Junkaew)

.....Co-advisor
(Dr. Chanisorn Ngaojampa)

26 August 2019

ACKNOWLEDGEMENT

I would like to acknowledge my advisor Asst. Prof. Dr. Nawee Kungwan for kindly giving me the great opportunity to be a part of his research group. He has been giving all the support and continual inspiration to me along my PhD program. His willingness in giving his time has so generously been very much appreciated. I would also like to express my sincere gratitude to my co-advisors, Dr. Anchalee Junkaew and Dr. Chanisorn Ngaojampa for their advice, inspiration, and assistance in solving problems occurring during my PhD time. The publications in this thesis will not be possible without their collaborations. Moreover, I would like to offer my special thanks to Dr. Supawadee Namuangruk from National Nanotechnology Center (NANOTEC) for her indispensable suggestions which make this research more complete. In addition, I would like to sincerely thank Dr. Suwit Suthirakun from Faculty of Chemical Engineering, Suranaree University of Technology, who has taught me know how to use the useful microkinetic model to get the rate constants for the reaction studied in my PhD research. Furthermore, I would like to thank Asst. Prof. Dr. Praput Thavornyutikarn for serving on my thesis examination as a committee.

In addition, I am very thankful to my friends and colleagues: all members in CCL-CMU especially Ms. Khanittha Kerdpol and all members in Nanoscale Simulation Laboratory (SIM-NANOTEC) as well as my friends in the Department of Chemistry, Faculty of Science, Chiang Mai University. Furthermore, I am particularly grateful for the financial support given by the Thailand Graduate Institute of Science and Technology (TGIST) and the Graduate School of Chiang Mai University. Moreover, I wish to thank all teachers for giving me valuable suggestions and courage. I also would like to thank other people who have helped me but their names are not mentioned here.

Finally, my special thanks go to members in my family who encourages me and pull me up from all the sadness and negative emotions during my PhD.

Tinnakorn Sae-lee

หัวข้อดุษฎีนิพนธ์	การศึกษาเชิงทฤษฎีของการเกิดปฏิกิริยาโพรเพนดีไฮโดรจีเนชันและการยับยั้งการเกิดโค้กบนตัวเร่งปฏิกิริยานิกเกิล(111) นิกเกิล-ทอง/นิกเกิล(111) และนิกเกิล-ดีบุก/นิกเกิล(111)	
ผู้เขียน	นายทินกร แซ่หลี	
ปริญญา	ปรัชญาดุษฎีบัณฑิต (เคมี)	
คณะกรรมการที่ปรึกษา	ผู้ช่วยศาสตราจารย์ ดร. นาวี กังวาลย์	อาจารย์ที่ปรึกษาหลัก
	ดร. อัญชลี จันทร์แก้ว	อาจารย์ที่ปรึกษาร่วม
	ดร. ชนิสร เหง้าจำปา	อาจารย์ที่ปรึกษาร่วม

บทคัดย่อ

การศึกษาปฏิกิริยาโพรเพนดีไฮโดรจีเนชัน (PDH) ในการผลิตโพรพิลีน และปฏิกิริยาข้างเคียง เช่น ปฏิกิริยาการแตกพันธะ C-C และปฏิกิริยาดีไฮโดรจีเนชันภายหลังกระบวนการ PDH (deep dehydrogenation) บนตัวเร่งปฏิกิริยานิกเกิล (Ni) รวมไปถึงนิกเกิลที่เจือด้วยทองคำ (Au) และดีบุก (Sn) ถูกนำมาศึกษาโดยใช้ทฤษฎีฟังก์ชันความหนาแน่น (DFT) เพื่อทำความเข้าใจถึงกลไกการเกิดปฏิกิริยา PDH และปฏิกิริยาข้างเคียงดังกล่าวบนพื้นผิวนิกเกิลเปล่าและนิกเกิลที่เติมโลหะเจือ นอกจากนี้อิทธิพลของโลหะเจือที่มีต่อการปรับปรุงความจำเพาะของการผลิตโพรพิลีน การยับยั้งการเกิดโค้ก และความว่องไวของตัวเร่งปฏิกิริยานิกเกิลที่เจือด้วยโลหะทองคำและดีบุกถูกศึกษาอย่างเป็นระบบ

ในส่วนแรกของงานวิจัยนี้เป็นการศึกษาความเป็นไปได้ทั้งหมดของปฏิกิริยา PDH และปฏิกิริยาข้างเคียงบนตัวเร่งปฏิกิริยานิกเกิล เพื่อหาสาเหตุของความจำเพาะในการผลิตโพรพิลีน (propylene selectivity) ที่ต่ำ ในงานวิจัยนี้แบบจำลอง Ni(111) ถูกนำมาใช้เป็นตัวแทนของตัวเร่งปฏิกิริยานิกเกิล ซึ่งจากผลการคำนวณพลังการดูดซับพบว่าโพรเพนจะเกิดการดูดซับเชิงกายภาพกับพื้นผิว Ni(111) ขณะที่โพรพิลีนเกิดการดูดซับเชิงเคมี ซึ่งยืนยันด้วยผลการวิเคราะห์ประจุภายหลังการดูดซับ เมื่อพิจารณากลไกการเกิดปฏิกิริยา PDH และปฏิกิริยาข้างเคียงบนพื้นผิว Ni(111) พบว่าปฏิกิริยา PDH สามารถเกิดผ่านสารมัธยันตร์ได้สองรูปแบบ คือ 1-โพรพิล และ 2-โพรพิล ซึ่งการเกิดปฏิกิริยา PDH ผ่าน 1-โพรพิลนั้นเกิดได้ง่ายกว่าการเกิดปฏิกิริยาผ่าน 2-โพรพิลในเชิงจลนพลศาสตร์ สำหรับศึกษาปฏิกิริยาข้างเคียงบนพื้นผิว Ni(111) พบว่าปฏิกิริยาการแตกพันธะ C-C

ซึ่งเป็นปฏิกิริยาแข่งขันกับปฏิกิริยา PDH สามารถเกิดขึ้นได้ยากกว่า ในขณะที่ปฏิกิริยาดีไฮโดรจีเนชันภายหลังกระบวนการ PDH ซึ่งเป็นปฏิกิริยาแข่งขันกับการคายซับ (desorption) ของโพรพิลีนนั้นสามารถเกิดได้ง่ายกว่า ซึ่งส่งผลให้ตัวเร่งปฏิกิริยานิกเกิลเป็นตัวเลือกที่น่าสนใจสำหรับปฏิกิริยา PDH แต่มีความจำเพาะของการผลิตโพรพิลีนที่ต่ำ

งานวิจัยในส่วนที่สองเป็นการออกแบบตัวเร่งปฏิกิริยานิกเกิล เพื่อปรับปรุงความจำเพาะของการผลิตโพรพิลีนโดยการเจือโลหะทองคำสองความเข้มข้นบนพื้นผิวของ Ni(111) ทั้งความเข้มข้นต่ำ ($Ni_3Au/Ni(111)$) และความเข้มข้นสูง ($Ni_2Au/Ni(111)$) ซึ่งจากผลการคำนวณพลังการดูดซับของโพรเพนและโพรพิลีนบนตัวเร่งปฏิกิริยาพบว่า การเจือโลหะทองคำบนตัวเร่งปฏิกิริยานิกเกิลไม่มีผลต่อการดูดซับโพรเพน แต่ส่งผลให้พลังงานการดูดซับโพรพิลีนลดลงอย่างมีนัยสำคัญเมื่อปริมาณของโลหะเจือทองคำเพิ่มขึ้น สำหรับกลไกการเกิดปฏิกิริยาพบว่า การเพิ่มความเข้มข้นของโลหะเจือทองคำส่งผลให้ความว่องไวของตัวเร่งปฏิกิริยาในการเกิดปฏิกิริยา PDH และการแตกพันธะ C-C ลดลง ยิ่งไปกว่านั้นการเจือโลหะทองคำบนพื้นผิว Ni(111) จะไปลดอันตรกิริยาระหว่างโพรพิลีนและตัวเร่งปฏิกิริยา Ni-Au/Ni(111) นำไปสู่การลดลงของกำแพงพลังงานในการคายซับของโพรพิลีน ส่งผลให้ความจำเพาะของการผลิตโพรพิลีนเพิ่มขึ้น

ส่วนสุดท้ายเป็นการศึกษาอิทธิพลของโลหะเจือทองคำและดีบุกที่มีต่อการเกิดโค้ก (coke formation) ซึ่งนำไปสู่การสูญเสียสภาวะเร่ง (deactivation) ของตัวเร่งปฏิกิริยา โดยศึกษาการดูดซับอะตอมคาร์บอน (C) บนตัวเร่งปฏิกิริยา $Ni_3Au/Ni(111)$ $Ni_2Au/Ni(111)$ $Ni_3Sn/Ni(111)$ และ $Ni_2Sn/Ni(111)$ เทียบกับตัวเร่งปฏิกิริยา Ni(111) ซึ่งพบว่าอะตอมคาร์บอนถูกดูดซับได้ดีที่สุดบนตำแหน่ง hcp ระหว่างสามอะตอมของนิกเกิลบนตัวเร่ง Ni(111) ทั้งนี้การเติมโลหะเจือทองคำและดีบุกจะลดอันตรกิริยาระหว่างอะตอมคาร์บอนบนตำแหน่ง hcp ของตัวเร่ง $Ni_3Au/Ni(111)$ และ $Ni_3Sn/Ni(111)$ ซึ่งสอดคล้องกับผลการวิเคราะห์ประจุภายหลังการดูดซับ แสดงให้เห็นถึงการยับยั้งการเกิดโค้กบนพื้นผิว Ni(111) ที่เติมโลหะเจือ นอกจากนี้การเพิ่มความเข้มข้นของโลหะเจือทองคำและดีบุกทำให้ตำแหน่งดูดซับเปลี่ยนไปเป็นตำแหน่ง bridge ระหว่างสองอะตอมของนิกเกิล ส่งผลให้จำนวนพันธะระหว่างอะตอมคาร์บอนและนิกเกิลบนพื้นผิวของตัวเร่งปฏิกิริยาลดลง เมื่อพิจารณาผลของโลหะเจือต่างชนิดกันพบว่าโลหะเจือดีบุกแสดงผลการยับยั้งการเกิดโค้กได้ดีกว่าโลหะเจือทองคำ

แม้ว่าการเจือโลหะทองคำและดีบุกจะสามารถปรับปรุงความจำเพาะของการผลิตโพรพิลีนและยับยั้งการเกิดโค้กบนพื้นผิวของตัวเร่งปฏิกิริยาได้ แต่ก็ทำให้ตัวเร่งปฏิกิริยาสูญเสียความว่องไวได้เช่นกัน ดังนั้นการเลือกโลหะเจือใดๆบนตัวเร่งปฏิกิริยานิกเกิล นักวิจัยควรคำนึงถึงการเพิ่มความจำเพาะของการเกิดโพรพิลีนและสูญเสียความว่องไวของตัวเร่งในการเร่งปฏิกิริยา PDH ให้น้อย

Dissertation Title	Theoretical Investigation of Propane Dehydrogenation and Coke Inhibition on Ni(111), Ni-Au/Ni(111) and Ni-Sn/Ni(111) Catalysts	
Author	Mr. Tinnakorn Sae-Lee	
Degree	Doctor of Philosophy (Chemistry)	
Advisory Committee	Asst. Prof. Dr. Nawee Kungwan	Advisor
	Dr. Anchalee Junkeaw	Co-advisor
	Dr. Chanisorn Ngaojampa	Co-advisor

ABSTRACT

Studies of propane dehydrogenation (PDH) yielding propylene and side reactions such as C-C bond cracking and deep dehydrogenation on bare and doped Ni surfaces have been theoretically investigated using density functional theory (DFT) to understand the insight mechanisms of PDH and side reactions on bare Ni and Ni doped with Au and Sn surfaces. Moreover, the effects of Au and Sn on doped Ni surfaces on selectivity improvement of propylene production, coke inhibition, and reactivity change are also systematically investigated.

The first part of this study is mechanistic exploration of all possible PDH and side reactions on pure Ni catalyst to investigate the cause of low selectivity of propylene production. The Ni(111) surface was modeled to represent the Ni catalyst. Based-on the adsorption energies, propane is physisorbed whereas propylene is chemisorbed on Ni(111) surface, supported by electronic charge analyses after adsorption. For PDH reaction, propane can be transformed to propylene via two possible intermediates; 1-propyl and 2-proply. The PDH reaction through 1-propyl intermediate is more kinetically favorable than 2-propyl intermediate. For side reactions, the C-C bond cracking during PDH process is more difficult to occur than PDH reaction. The deep dehydrogenation after PDH process is easier to take place than propylene desorption. Hence, the Ni(111) surface is a good candidate for PDH reaction but low selectivity for propylene production.

The second part of this research is a design better Ni(111) to improve the selectivity of propylene production. Two concentrations of Au are doped on the Ni(111) surface to construct models of low Au concentration of Ni_3Au/Ni(111) and high Au concentration of Ni_2Au/Ni(111). The calculated results of propane and propylene adsorptions on Ni-Au/Ni(111) surfaces reveal that doping of Au has no effect on propane adsorption but significantly reduces adsorption energy of propylene when the concentration of Au is increased. For the reaction mechanisms, increment of Au concentration decreases reactivity of catalyst for both PDH and C-C cracking reaction. Additionally, doping of Au on Ni(111) surface reduces the interaction between propylene and Ni-Au/Ni(111) surfaces leading to decreasing of propylene desorption barrier, which enhances the selectivity of propylene production.

The final part of this research is about the effect of Au and Sn doping on coke formation which leads to deactivation of catalyst. In this section, C atom adsorption on Ni_3Au/Ni(111), Ni_2Au/Ni(111) Ni_3Sn/Ni(111) and Ni_2Sn/Ni(111) surfaces are comprehensively compared to Ni(111) surface. The investigation of C atom adsorption shows that the C atom prefers to adsorb on hcp hollow site between three Ni atoms. Introduction of Au and Sn dopants weakens the interaction between C and hcp sites of three Ni atoms on Ni_3Au/Ni(111) and Ni_3Sn/Ni(111) surfaces, supported by electronic charge analyses. Weakening of C atom adsorption inhibits of coke formation on modified Ni(111) surface. Moreover, increment of Au and Sn concentrations changes the favorite adsorption site of C atom from hcp to bridge site between two nearest Ni atoms causing reduction of number of bond formation between C atom and catalyst surface. Comparison of different Au and Sn dopants on coke formation reveals that the Sn dopant shows more positive effect than Au on coke inhibition.

Although doping Au and Sn can improve the selectivity of propylene production and inhibit coke formation on Ni catalyst surface, the catalytic reactivity is reduced. Therefore, choosing any elements to dope on Ni catalyst, researcher should take the compromising between the enhancement of propylene selectivity and lowering catalytic reactivity for PDH reaction into the developed Ni.

CONTENTS

LIST OF TABLES

LIST OF FIGURES

LIST OF ABBREVIATIONS

ABS	Acrylonitrile-butadiene-styrene
BOA	Born-Oppenheimer approximation
CI-NEB	Climbing image nudge elastic band
d-DOS	Electron density at d-state
DFT	Density functional theory
DOS	Density of state
FCC	Fluid catalytic cracking
FS	Final state
GGA	Generalized-gradient approximation
HF	Hartree-Fock
IS	Initial state
Int	Intermediate state
LDA	Local density approximation
MLE	Monolayer equivalent
MMA	Methyl methacrylate
MTP	Methanol to propylene
NBR	Nitrile rubber
PAW	Projector-augmented wave
PBE	Perdew, Burke, and Ernzerhof
PDH	Propane dehydrogenation
PDOSs	Projected density of states
p-DOS	Electron density at p-state
PES	Potential energy surface
PP	Pseudopotential
PVC	Polyvinyl chloride
PW91	Perdew-Wang 91
QM	Quantum mechanics

QM/MM	Quantum mechanics/molecular mechanics
SAN	Acrylonitrile-styrene
SAPs	Superabsorbent polymers
SC	Steam cracking
s-DOS	Electron density at s-state
TS	Transition state
TST	Transition state theory
UPRs	Unsaturated poly ester resins
VASP	Vienna a*b initio* simulation package

LIST OF SYMBOLS

$\Psi(r)$	Wave function at ground state
U_{ext}	Unique external potential
$\rho(r)$	Electron density
ε_d	The d-band center
∇^2	Laplacian
$\Phi_{PW}(x)$	Plane wave basis set equation
$F[\rho(r)]$	Universal function
A	Area of catalyst surface
Å	Angstrom unit
d	Atomic distance
E_a	Activation energy
ΔE_{des}	Desorption energy
E_{el}	Electronic energy
E_{gs}	Ground state energy
T_{kin}^{non}	Kinetic energy of non-interacting *n* electrons
E_H	Classical Coulomb energy
$E_{2H/Ni(111)}$	Total energy of Ni(111) surface with two H atoms
E_{xc}	Exchange correlation energy
ε_{xc}^{GGA}	Exchange correlation energy per electron
E_{ads}	Adsorption energy
$E_{\text{molecule, C/surface}}$	Total energy of the complex
$E_{surface}$	Total energy of clean surface
$E_{molecule,\ C}$	Total energy of isolated molecule
eV	Electron volt unit
$\hat{H}$	Hamiltonian operator
$\hat{H}_{el}$	Hamiltonian operator of only electron motion
$\Delta\delta$	Partial charge difference

δ_i^{ads}	Partial charge of atom *i* of after adsorption
$\delta_i^{isolate/clean}$	Partial charge of atom *i* of before adsorption
ΔG_i	Gibbs free energy of isolated gas *i*
p_i	Partial pressure of gas species *i*
R	Gas constant 1.43×10^{-28} eV·K^{-1}·mol^{-1}
T	Temperature in Kelvin
T	Kinetic energy
$T_e(r)$	Kinetic energy operator of electron
$T_N(R)$	Kinetic energy operator of nucleus
V	Potential energy
$V_{eN}(r,R)$	Potential energy operator of electron-nucleus
$V_{ee}(r)$	Potential energy electron-electron
$V_{NN}(R)$	Potential energy between nucleus-nucleus
$V_{\text{ext}}[\rho(r)]$	External field
E_{ZPE}	Zero-point energy
Q_{vib}	Total vibrational partition function of adsorbed system
k_{ads}	Adsorption rate constant
k_B	Boltzmann constant (8.62×10^{-5} eV·K^{-1})
K	Kelvin
k^{TSA1}	Rate constant of TS at pathway A
k^{TSB1}	Rate constant of TS at pathway B
h	Planck's constant (4.14×10^{-15} eV/s)
ΔG_f	Activation free energy of forward reaction
K_{eq}	Equilibrium rate constant
ΔG^0	Change in standard Gibbs free energy
ΔS^0	Standard state difference of entropy
ΔH^0	Standard state enthalpy change
ε_d	The *d*-band center
Au	Gold
C	Carbon
C_3H_8	Propane

C_3H_7	Propyl
C_3H_6	Propylene
E_a	Activation energy
$CH_3CH_2CH_3$	Propane
$CH_3CH_2CH_2^*$	1-propyl
$CH_3CHCH_2^*$	Adsorbed propylene
$CH_3CH_2^*CH_3$	2-propyl
$CH_3CH\ CH^*$	1-proppenyl
$CH_3CCH_2^*$	2-proppenyl
CH_3^*	Methyl
CH_4	Methane
$CH_3CH_2^*$	Ethylene
CH_2^*	Methylidene
CH_3CH^*	Ethylidene
$CH_3CCH_2^*$	2-propenyl
H	Hydrogen
Ni	Nickel
Ni-Au/Ni(111)	Nickel-gold surface alloy on Ni(111)
Ni-Sn/Ni(111)	Nickel-tin surface alloy on Ni(111)
Pt	Platinum
Pt-Sn	Platinum-Tin
Sn	Tin

ข้อความแห่งการริเริ่ม

1) ปฏิกิริยา PDH เป็นปฏิกิริยาสำคัญในการเปลี่ยนโพรเพนไปเป็นโพรพิลีน ซึ่งเป็นสารผลิตภัณฑ์มูลค่าเพิ่มสำหรับเป็นสารตั้งต้นในอุตสาหกรรมเคมีอื่นๆที่หลากหลายนั้น สามารถเกิดขึ้นได้บนตัวเร่งปฏิกิริยากลุ่มแพลทินัม อย่างไรก็ตามต้นทุนของแพลทินัมเป็นข้อจำกัดในการใช้งานในปริมาณมาก ดังนั้นการพัฒนาตัวเร่งปฏิกิริยากลุ่มนิกเกิล ซึ่งมีความว่องไวในการเกิดปฏิกิริยา PDH และมีมูลค่าที่ถูกกว่าแพลทินัมจึงได้รับความสนใจในปัจจุบัน

2) การทำความเข้าใจกลไกการเกิดปฏิกิริยา PDH และปฏิกิริยาข้างเคียงอื่นๆ บนตัวเร่งปฏิกิริยานิกเกิลโดยใช้ระเบียบวิธีเชิงคำนวณมีความสำคัญอย่างมาก เนื่องจากรายละเอียดของกลไกการเกิดปฏิกิริยาดังกล่าวไม่สามารถศึกษาโดยทำการทดลองในห้องปฏิบัติการเพียงอย่างเดียว ซึ่งผลที่ได้จากการศึกษาเชิงทฤษฎีจะให้ข้อมูลที่เป็นประโยชน์ต่อการพัฒนาประสิทธิภาพของตัวเร่งปฏิกิริยากลุ่มนิกเกิลสำหรับปฏิกิริยา PDH

3) จากข้อมูลผลการทดลองการเจือโลหะทองคำลงบนพื้นผิวของตัวเร่งปฏิกิริยานิกเกิล แสดงให้เห็นถึงการปรับปรุงความจำเพาะของการผลิตโพรพิลีน อย่างไรก็ตามบทบาทของโลหะทองคำนั้น ยังไม่เป็นที่เข้าใจอย่างถ่องแท้ ดังนั้นการใช้ระเบียบวิธีเชิงคำนวนในการศึกษารายละเอียดของกลไกการเกิดปฏิกิริยา คาดว่าจะได้เข้าใจบทบาทของโลหะทองคำในการเพิ่มความจำเพาะของการผลิตโพรพิลีน

4) ปฏิกิริยาการเกิดโค้กส่งผลให้ตัวเร่งปฏิกิริยานิกเกิลสูญเสียสภาวะเร่งเกิดจากพันธะที่แข็งแรงระหว่างอะตอมคาร์บอนบนพื้นผิวของตัวเร่งปฏิกิริยา และการเติมเจือโลหะทองคำและดีบุกอาจจะลดการเกิดโค้กบนพื้นผิวของตัวเร่งปฏิกิริยาได้ ดังนั้นการศึกษาบทบาทของโลหะเจือทองคำและดีบุกจะให้ข้อมูลสำคัญในการยับยั้งการเกิดโค้กบนพื้นผิวของตัวเร่งปฏิกิริยา ด้วยการศึกษาโดยใช้ระเบียบวิธีเชิงความหนาแน่นในการศึกษาการดูดซับและการคายซับของอะตอมคาร์บอนบนตัวเร่งปฏิกิริยานิกเกิลที่เติมโลหะเจือนั้นจะได้ข้อมูลที่สำคัญเกี่ยวการลดลงของการโค้กบนพื้นผิวของตัวเร่งปฏิกิริยานิกเกิลเจือด้วยโลหะ

STATEMENTS OF ORIGINALITY

1. PDH reaction, a promising process to transform propane to propylene as a value-added product for precursor in various chemical processes, can conventionally take place on the Pt based catalyst. However, the cost of Pt has limited it for large scale use. Thus, development of Ni based catalyst, which is highly reactive for PDH reaction and cheaper than Pt, has recently been gained more attention.

2. Understanding the complete PDH mechanism and side reactions on Ni surface using DFT method is very important since the detailed reaction mechanisms occurring on the surface catalysis are not easily obtained by experiment alone. The theoretical study could provide the useful information for development of the efficient Ni-based catalyst for PDH process.

3. The results of experimental study of doping Au into Ni surface show the improvement of propylene selectivity; however, the role of Au is not completely understood yet. Therefore, by using DFT method to investigate the detailed mechanism, the role of Au on the increasing propylene selectivity is expected to be obtained.

4. Coke formation causing catalytic deactivation can occur on the pristine Ni surface by creating a strong bond formation of C on catalyst surface and doping of inactive Au and Sn might reduce the coke formation. So, the role of dopants (Au and Sn) is very important information to understand the anti-coking process on the Ni surface doped with Au and Sn. By carrying on a fast screening using DFT method based-on adsorption and desorption of C atom on doped Ni surfaces, the important information on how coke formation being reduced will be given.

CHAPTER 1

Introduction

1.1 Propylene

Propylene or propene, an unsaturated organic compound, is the colorless fuel gas with a pungent smell like petroleum. It is a liquefied gas under storage pressure and can be soluble in water. Generally, a propylene gas is created by the burning of fossil fuels, wood and foliage and is also present in cigarette smoke and automobile exhaust. Moreover, it is given off naturally from garlic oil, some pine trees and certain seeds such as bean and corn. The chemical structure of propylene is consisted of three carbon (C) and six hydrogen (H) atoms with one double bond (unsaturated) between the first and second C atoms. These C atoms connect with six H atoms as shown in 2D and 3D structures in Figure 1.1. The existence of double bond between C^1 and C^2 elucidates that propylene molecule can be transformed to many chemical products upon further chemical reactions. Hence, propylene is commonly used as an essential commercial precursor to further produce other chemicals used in various applications.

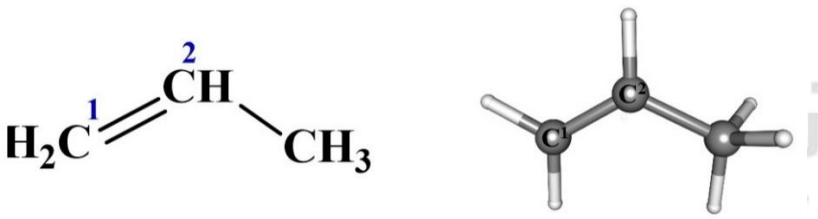

Figure 1.1 Chemical structure of propylene in (a) 2D and (b) 3D views

1.2 Applications of Propylene

Since beginning of the modern petroleum and foundation of the natural gas industry, propylene has been gained more attention in many industries because its unsaturated double bond can be easily initiated to form other compounds including polypropylene, propylene oxide, acrolein, acrylic acid, acrylonitrile, oxo alcohols and cumene [1, 2]. The compounds derived from propylene are shown in Figure 1

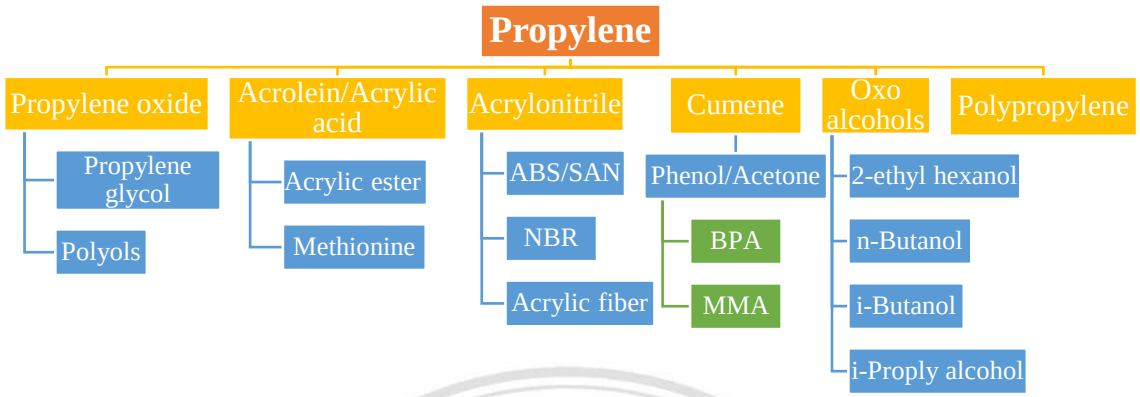

Figure 1.2 Chart of propylene consumption in many applications [3-12]

For propylene oxide, it is the important reactant in the manufacture of polyether and polyols for urethane production. Moreover, it can be employed to synthesize propylene glycols which is used as precursor for unsaturated poly ester resins, heat transfer fluid, anti-freeze and aircraft deicing fluids [9].

For acrolein and acrylic acid [4, 10], acrolein is produced by vapor phase oxidation of propylene. The main usage of acrolein is the essential precursor of acrylic acid production, while acrylic acid is used as superabsorbent polymers, water treatment chemicals and the raw material for acrylic esters production (60% of global demand).

For acrylonitrile, it is manufactured by ammoxidation of propylene [5]. It has numerous demands from many applications such as acrylic fiber (to produce sweaters, blankets, scarves, hats, rugs hand knitting yarn, toys, wigs and furnishings), acrylonitrile-butadiene-styrene (ABS) [12] and acrylonitrile-styrene (SAN) [7] (to produce TVs, phones, computers, vehicles toys, etc.), nitrile rubber (NBR) [3, 6] (to produce automobile parts, cables, rubber gloves, hoses and conveyor belts), polyacrylamide [13, 14] (using in water treatment and enhanced oil recovery applications) and carbon fiber [11, 15, 16] (to produce auto motive parts of aircraft military, racing car, passenger car, wind turbine etc.).

For cumene [8], it is synthesized from alkylation reaction of propylene with benzene. The crucial application of cumene is the essential precursor to synthesize phenol and acetone which are the useful chemical reagent to produce phenolic resins, nylon

intermediates, epoxy resins, polycarbonates, methyl methacrylate (MMA) and the solvents in many chemical processes.

For oxo alcohols [17], they are conventionally synthesized via hydroformylation of propylene by addition of carbon monoxide and H to form an aldehyde. Then, the aldehyde is reduced to form many kinds of alcohols. The oxo alcohols which are produced from propylene are applied in many industries for example, using of 2-ethy hexanol to be the intermediates for acrylic surface coating, the additives for diesel fuel and oil lubricant and plasticizer for flexible poly (vinyl chloride) (PVC), using of n-butanol and i-butanol to be the reagents for water-based coating formulation, textile production, the modifier for rigid PVC, the plasticizer for amino resins and butylamines and the solvents for purification of olefins, and using of iso-propyl alcohol to be the common ingredients in chemical solvent as well as anti-bacterial solution [18].

Moreover, propylene is the necessary monomer to produce polypropylene which is the useful polymer for automotive part, textile, furniture, clothing, tube, and packaging applications [19, 20]. Around 40% of propylene productions is PP because of the advantages of high chemical and bacterial resistance, good weldability, outstanding in mechanical properties, light weight, non-toxic, excellent optical clarity as well as low moisture transmission [21]. Polypropylene is commonly used in many industries such as packaging [22] including food packaging, automotive [23], fiber and fabric [20], medical [24], film and sheet [25] applications.

1.3 Technologies of Propylene Production

Due to variety applications of propylene as well as versatile properties of the derived products, demanding of propylene has been quickly enlarged [26, 27]. Indeed, propylene consuming has been continuously increased since the 20th century [28]. Up to date, all technologies of propylene production are summarized in to Figure 1.3. Currently, the approaches for propylene production can be classified into two technologies, which are the steam cracking (SC) of liquid feedstocks [29-32] and catalytic cracking refineries in units (FCC) [29, 33].

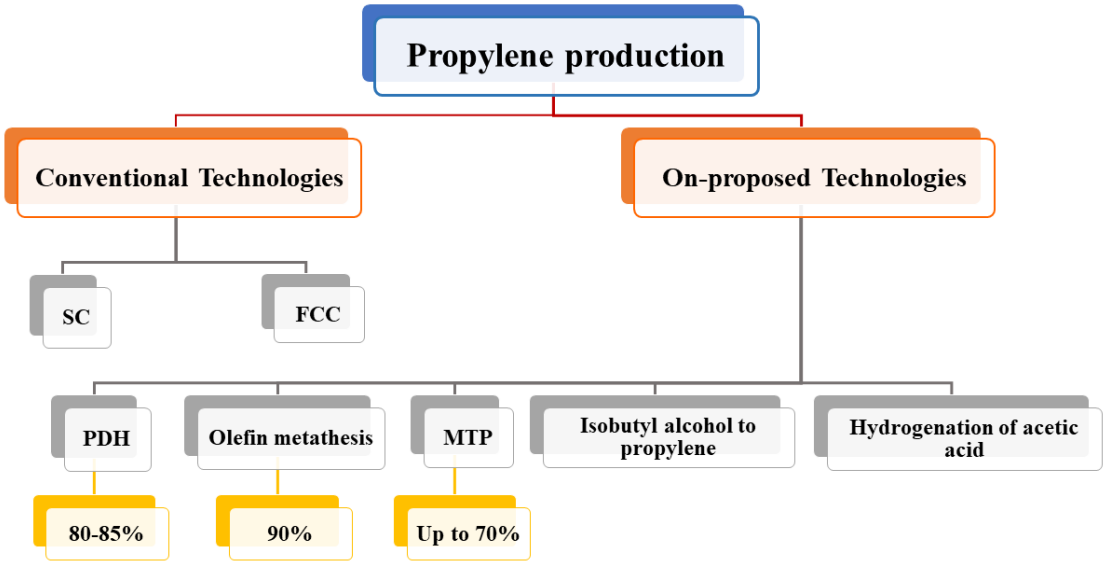

Figure 1.3 Technologies of propylene production

The most important technology for propylene production is SC. In this technology, various feedstocks of hydrocarbon from light alkanes such as ethane and propane to complex mixtures including naphtha and gas oil are introduced in the tubular reactor [31]. Then, the temperature in the reactor is used to crack the hydrocarbon feedstock to be smaller olefin gas in the hot reactor. After that, the hot gas is transferred to the cold reactor where the gases will be cooled down and separated into different products. One of these products is the propylene.

Another important technology for propylene production is FCC in which the preheated oil is transferred into the reactor containing the catalyst powder. The oil vapor, air and steam are used as the conveying media to transfer the inlet gas into the reactor. Then, the temperature of reactor is raised up to heat the catalyst. When the preheated gas enters to the hot fluidized reactor, the contacting of feeding gas and hot catalyst generates cracking reaction of inlet oil gas into smaller gas products. Then, the gas products and catalyst are separated in the separator vessel. The lighter gases are injected to the separator while the heavier gases and catalyst as well as deactivated catalyst with the coke deposition are separated to the next treatment unit before being regenerated to the reactor [34].

According to the diverse applications of propylene, the faster growing propylene consumption rate than the propylene production rate from the two important SC and FCC processes leads to the gap between a high demand and a low supply of the global

propylene resulting in pushing up of propylene price in the global market [35]. To satisfy the propylene gap [34], other on-propose technologies including olefin metathesis [36], methanol to propylene (MTP), isobutyl alcohol to propylene, hydrogenation of acetic acid and propane dehydrogenation (PDH) have been developed.

For olefin metathesis process [36, 37], the ethylene and n-butene are mixed before disproportioning to provide the propylene. However, the prices of ethylene and n-butene reactants are currently comparable to propylene, making this technique not widely interesting. However, if propylene value is higher than ethylene, this technique may become increasingly attractive.

For MTP process [36, 38, 39], the new technology to produce propylene from methanol becomes the interesting method to manufacture propylene. Generally, the methanol which is the typical produced from coal and natural gas resources is fed via the porous of zeolite. Then, the methanol is reacted itself to form propylene. The abundant yield of propylene production makes methanol overcome the historical barrier against using natural gas or coal to make olefins. The products from this MTP process are ethylene and propylene. However, the ratios of propylene and ethylene is still low [40, 41]. Thereby, establishing of MTP plant is still under developing and planning such as a gas-based MTP plant in the United States [42].

Other newer on-proposed technologies for propylene production via isobutyl alcohol to propylene [43] and hydrogenation of acetic acid [44] have been developed. These technologies attempt to produce propylene from other sustainable resources such as alcohols from fermented source and acetic acid from economically inexpensive natural gas source. However, these technologies are still under development in terms of finding effective catalyst and operating condition. Hence, filling the propylene gap via these processes is still an ideal and needs more time and development to find the appropriate operation conditions.

Another on-proposed approach which influences the satisfaction of the lacking gap of propylene supply from the conventional technologies of SC and FCC is PDH in which propylene is directly produced from propane [45]. Recently, the discovery of natural and shale gas resources reveals that propane is the second rich gas production form these alternative resources. Because of the very large amount of the propane generated from

the shale and natural gas resources, the inexpensive propane is great interest for the energy and chemical markets [28]. Thus, transformation of cheap propane into be propylene via has recently gained more attention and it is possible to have a large scale of manufacture propylene [46]. From the chemical perspective, PDH reaction is endothermic and taken place through hydrogen elimination of propane, resulting in propylene as the main product while the detached H atoms can be transformed into H_2 gas as a byproduct illustrated below:

$$C_3H_8 \longleftrightarrow C_3H_6 + H_2 \quad \Delta H^0_{298} = 129 \text{ eV}$$

1.4 Propane Dehydrogenation Process

In 2011, a PDH process was first started in the United States and has been continuously developed because of the increasing amount of propylene demand in the market. And the production of propylene from the PDH process has increased and it tends to continuously enlarge as one of the promising processes for propylene production in the future [47]. Figure 1.4 shows proposed reaction mechanisms of PDH and side reactions including C-C bond cracking and deep dehydrogenation of propylene [48]. The PDH mechanisms can be classified into two possible pathways based on the order of eliminated H position. One is through 1-propyl ($^*CH_2CH_2CH_3$) intermediate in pathway A, in which one H of the primary C is eliminated first. Another is via 2-propyl ($CH_3{}^*CHCH_3$) intermediate in pathway B, in which one H of the secondary C is eliminated first. The side reactions of the C-C bond cracking of propane, propyl intermediates and propylene, described in steps 1C, 2C, 2C′ during PDH and 3C after PDH, can be taken place [49-51]. Moreover, another side reaction namely the deep dehydrogenation of propylene to 1-propenyl (CH_3CHCH^*) and 2-propenyl ($CH_2^*CCH_3$) via steps 3D and 3E leading to coke formation is also possible resulting in deactivation on the active site of the catalyst surface. Thus, high effective catalysts with high selectivity of propylene are very essential for PDH reaction with high selectivity of propylene species on catalyst surface by inhibiting the side reactions of C-C bond cracking and deep dehydrogenation. To transform propane to propylene by PDH process, the high effective catalyst which can speed up the reaction as well as providing high propylene production yield is needed.

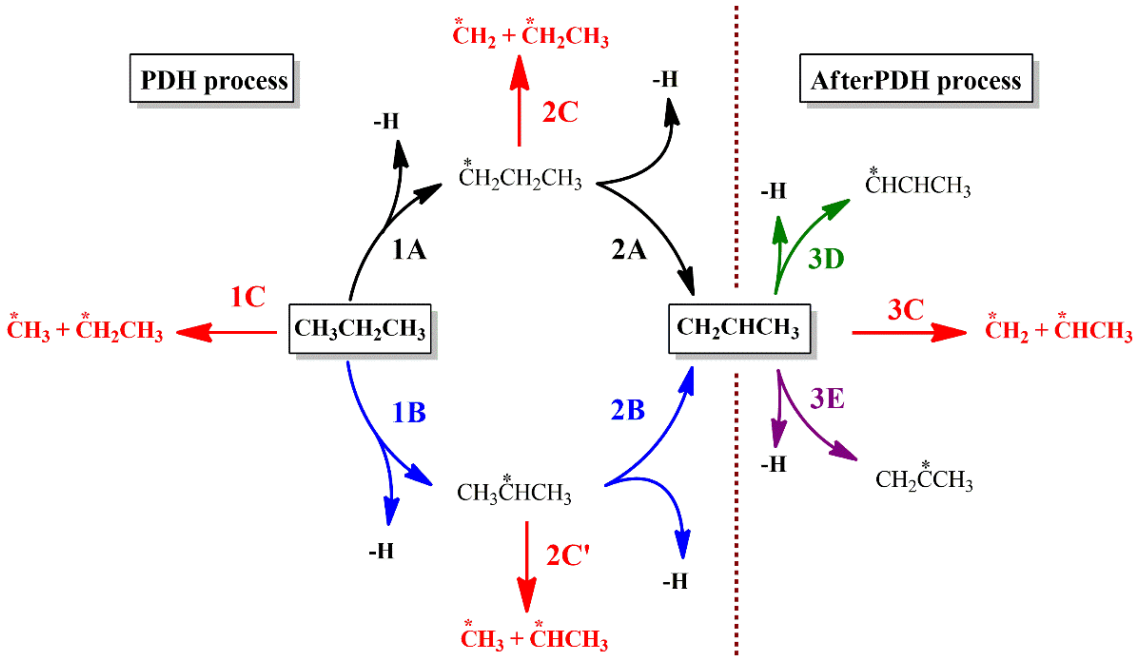

Figure 1.4 Proposed mechanisms of PDH and side reactions on catalytic surface

1.5 Conventional Catalyst for PDH Process

Generally, catalysts in chemical reactions can be classified into two types; homogenous and heterogeneous catalysts. For the homogenous catalyst, the similar phase of catalyst and chemical reactants well homogenize the catalyst and the reactant in the reactor. However, the main disadvantage of the homogenous catalyst system is a difficult separation of the products from the reactor after the reaction is complete leading to losing of catalytic material during reaction process. For heterogeneous catalyst, the separation of catalyst from a product is easy, leading to recovery of the heterogeneous catalyst. Therefore, the heterogeneous catalyst has received more attention in the PDH industry owing to its selective dehydrogenation to produce propylene and can accelerate the reaction [52].

Many heterogeneous catalysts are available in the market including (1) metal catalysts as non-oxidative dehydrogenation such as platinum (Pt) [53-57] and nickel (Ni) [58, 59], (2) metal oxides as oxidative catalysts such as chromium oxide [60-63], vanadium oxide [64-67], molybdenum oxide [67, 68] and gallium oxide [61, 69-71] and (3) carbon-based materials such as carbon nanofibers [72], mesoporous carbons [73]. Among them, the metal-based catalysts especially Pt has been widely employed in industries due to its high reactivity for C-H bond activation and low activity of C-C bond

cleavage which is appropriate for direct PDH suppressing side reaction of C-C bond cracking.

In literature, the PDH reaction mechanisms in Pt-based catalyst have been intensively investigated [48, 49, 74, 75]. Yang and co-workers [48, 74] studied activity and selectivity of PDH reaction on different facets of Pt including Pt(111) and Pt(100), and Pt(211) which represent flat and step surfaces of Pt catalyst, respectively. Among different shapes of Pt surfaces, the flat surface of Pt(111) is less active for PDH reaction than that of Pt(100), and Pt(211) surfaces. However, the selectivity of propane conversion to form propylene by suppressing C-C bond cracking on Pt(111) surface is the highest. Furthermore, the PDH mechanism and side reactions of C-C bond cracking and deep dehydrogenation reactions have been studied on Pt(111) [48, 76]. During PDH process, the selectivity of C-H activation was found to be higher than C-C cracking reaction on Pt(111) supported by lower energy barrier. However, after PDH, the propylene was more difficult to desorb than undergoing deep dehydrogenation causing coke formation indicating low selectivity of propylene production on Pt(111) surface. Although Pt are currently employed to be the conventional catalyst for direct PDH reaction, the main drawback of coke formation on Pt surfaces leads to low selectivity of propylene production. Moreover, existence of coke formation on Pt surface poisons the active site of Pt surface leading to deactivation of the catalyst [53, 77]. Furthermore, the cost is also very important for designing the new catalysts for large-scale industries. Consequently, improvement better catalysts which provide higher performance as well as lower price have been sought to replace Pt-based catalyst.

1.6 Improvement of Ni-Based Catalyst for PDH Process

Among various choices of reactive metal-based catalysts, Ni could be a good candidate because it has been widely used in many applications such as stream reforming process [78, 79], water gas shift reaction [80, 81], biomass gasification [82], hydrogenation [83], dehydrogenation reaction of small alkane [84-86], and PDH [87-90]. Moreover, Ni has more advantages in term of lower cost than Pt [87]. However, the undesired side reactions include the coke formation and fast deactivation on bare Ni surface result in low selectivity of propylene production on bare Ni catalyst [58, 91-93]. Yan and co-workers [58] experimentally studied PDH reaction on Ni supported by SiO_2

(Ni/SiO_2). They found that the reaction rate of propane conversion is very high (about $1x10^{14}$ molecule·s^{-1} at 523 K). The high propane conversion refers to high reactivity of Ni/SiO_2. The comparison of reactivity of Ni-based catalyst for methane (CH_4) conversion is higher than that of Pt-based catalyst [76, 94, 95]. Although the reactivity of propane conversion on Ni/SiO_2 is very high, CH_4 as the main product from the C-C bond cracking. This predominant side reaction leads to low selectivity of PDH in this catalyst [58]. Moreover, the deactivation of Ni/SiO_2 from coke formation induced by deep dehydrogenation causing low propylene production was also reported [58]. The selectivity of propylene production might be the interrupted from C-C bond cracking of propane during PDH process because Ni is also the high reactive catalyst for cracking reaction of alkane [91]. Moreover, Ni-based catalyst has been reported as the high reactive catalyst for deep dehydrogenation leading to creation of coking on Ni surface [92, 93]. To prevent occurrence of cracking and low selectivity of propylene production during PDH process on bare Ni catalyst, modification of the Ni for improving its selectivity and activity for PDH reaction is needed for producing propylene from propane. Recently, promoting gold (Au) into Ni has been reported [96-99] to improve selectivity of PDH reaction by inhibiting the cracking reaction and deep dehydrogenation. Yan and co-workers [96] experimentally studied production of propylene from propane via PDH process on bare Ni and Ni-Au catalysts. They found that the bare Ni catalyst is more reactive than the Ni-Au catalyst measuring from the reaction rate of propane transformation at 523 K. However, this reaction rate of propane transformation tends to decrease when amount of Au increases. Moreover, the selectivity of propylene which is the wanted product from PDH process tends to increase as a function of Au loading. In addition, Yan and Goodman [58] also experimentally investigated the effect of Au doping for the side reaction of C-C bond cracking on the Ni surface. They found that doping of Au into Ni catalyst can retard amount of CH_4 production, which refers to decrease C-C bond cracking but facilitate PDH pathway on the Ni surface.

1.7 Roles of Computational Chemistry on Catalytic Design

Nowadays, computational calculations have become a powerful tool to locate the elementary configurations and investigate reaction mechanisms of heterogeneous catalyst systems in the atomic scale which are not easily accessible by experiments [100].

This tool provides the information of electronic structure properties of surface and adsorbate, interaction between surface and adsorbate molecule in terms of physisorption and chemisorption as well as reaction mechanism which are important to predict the reactivity and selectivity of catalytic system for investigated reactions from simple model such as metal, or single crystal surface to more complex catalyst model of bimetallic catalyst, alloys as well as supported catalysts [101, 102]. Moreover, the computational calculations also describe the nature of an active site, which is the key concept of designing the new effective catalyst. In addition, the advance microkinetic modeling is very useful technique to extend theoretical calculations to predict the results of complex chemical reactions under various conditions. The reaction rate constants of elementary steps which is determined through computational calculations can be further converted to the turnover rate under calculated condition. Moreover, applying linear correlation of activation energy and other descriptors can describe the activity and selectivity of catalyst in chemical process.

Furthermore, the information from microkinetic calculation can be used to explain the reaction rate in many calculated conditions which are useful for designing the new catalyst as well as predicting the reaction conditions such as pressure and temperature based on the certain reaction. Barghi and co-workers [103] combined both of experimental and theoretical studies of PDH on platinum-tin (Pt-Sn) catalyst to develop the appropriate kinetic model. In the experimental section, the small amounts of water or methanol were detected when the PDH reaction was carried out under atmospheric pressure in the temperature of 575 - 620 °C. In the theoretical part, the kinetics model of the main dehydrogenation reaction as well as the effects of presented water and methanol on coke deposition and catalyst sintering were described to explain the observed optimum level in the amount of added oxygenated compounds. The results from the prediction model were in good agreement with experimental data. Hook and Celik [104] predicted the suitable promoter for enhancing high the ethane dehydrogenation pathway and retarding the coke formation pathway. Metals from groups 7 to 15 are considered to understand the reduction of carbon formation on catalyst surface and enhanced selectivity during ethane dehydrogenation. From this study, platinum-lead (Pt-Pb) and platinum-antimony (Pt-Sb) alloys show the most promise at low and high alloy coverages resulting to selection of lead and antimony promoters to investigate more in the experimental part.

1.8 Research Objectives

In this work, the dehydrogenation reaction in Ni-based catalysts has been studied. The detailed mechanisms of PDH and side reactions including deep dehydrogenation, C-C bond cracking during and after PDH process, and coke formation on Ni-based catalysts are investigated. From previous experimental studies, the improvement of Ni catalyst was observed by adding dopants. Therefore, this work determines role of doping Au and tin (Sn) elements on the performance of the Ni catalyst. The mechanistic investigations of PDH and side reactions on those Ni-based catalysts are divided into three parts.

The first part is involved the explorations of PDH and side reactions including deep dehydrogenation and C-C bond cracking on bare Ni(111) comparing with Pt(111) surface to find that what factors suppress the selectivity PDH reaction on Ni(111). The results from this section is useful for improving the better Ni(111) catalyst for increasing the selectivity of propylene production as described in Chapter 3.

The second part is about the effect of Au doping on catalytic reactivity on PDH reaction as well as enhancing the reactivity of propylene production. Moreover, the effects of Au concentrations for reactivity changes of Ni(111) and selectivity change of propylene production are investigated. In addition, the roles of Au dopant for increasing the selectivity of propylene production and suppressing the unwanted side reactions are also explored as given in Chapter 4.

The last part focuses on investigation coke formations on Ni(111), Ni-Au/Ni(111) of Ni_3Au/Ni(111) and Ni_2Au/Ni(111) as well as Ni-Sn/Ni(111) of Ni_3Sn/Ni(111) and Ni_2Sn/Ni(111) surfaces. The roles and compositions of Au and Sn dopants and the composition for the coke inhibition on Ni-based catalysts are reported in Chapter 5.

The information from all investigations in this thesis provide the models for exploring the intrinsic nature of Ni atom on Ni(111), Ni-Au/Ni(111) and Ni-Sn/Ni(111) surface for PDH reaction. Moreover, the information of Au and Sn dopants for improving the Ni(111) surface is essential for designing and developing the efficiency of Ni catalyst by increasing the reactivity of propylene desorption and inhibiting the side reactions of C-C bond cracking, deep dehydrogenation and coking reaction.

CHAPTER 2

Theory and Computational Detail

2.1 Computational Chemistry

Computational chemistry, a subfield of chemistry focuses on solving the chemical problems such as molecular structures, electronic properties, chemical properties, and reaction pathways [105-107] by using theoretical methods and mathematic calculations. Recently, development of theoretical and mathematical methods, the improvement of computational algorithms, and the development of computer lead to advances of solving important chemical questions. The computational chemistry has become well accepted as a powerful tool to study systems in various field such as chemistry, physics, material science and biochemistry since Nobel Prize in Chemistry in 1998 which was given to Walter Kohn and John Pople who developed the methods in computational physics and computational chemistry, respectively. After that, the computational chemistry has obviously proved again as the currently powerful tool for even bigger systems in biological science when Nobel Prize in Chemistry in 2013 was awarded to Martin Karplus, Michael Levitt, and Arieh Warshel who were successful in development hybrid quantum mechanics/molecular mechanics (QM/MM) for the multiscale models of complicated chemical systems. Nowadays, computational chemistry is a useful and popular tool to assist both theoretical and experimental chemists for understanding the chemical phenomena which could be complementary to the experiment results. Moreover, the calculated results of computational chemistry can help chemists to make predictions before doing actual experiments or prediction the properties of unknown chemical compounds and to reduce the laboratory cost particularly in chemical synthesis. Furthermore, the calculated results can be used to explain and reasonable well-known observations or reactions in chemistry as well as to explore new or controversial reactions and properties of on new catalytic materials [105].

2.2 Quantum Mechanics

Generally, the motion of macroscopic objects such as spacecraft, planets, stars, and galaxies can be correctly described by classical mechanics [106] However, the classical mechanics theory cannot correctly explain the behaviors of microscopic particles leading to development of quantum mechanics (QM). QM is fundamental knowledge for studying the nature particle, atom and molecule to understand the microscopic phenomena involving the electron motion in the atoms and the molecules. The theory of QM is more complicated than that of classical mechanics, but it can provide the accurate results microscopic systems especially about the phenomena involving electron motion of where classical mechanics fails to explain. Currently, QM defined as Schrödinger equation in computational chemistry has been employed in all branches of chemistry to investigate many interested systems for example physical chemistry (kinetics and thermodynamic calculation using statistical mechanics), organics chemistry (understanding the reaction pathway via reaction mechanism simulation) and material science (electronic properties and catalytic activity).

2.3 Schrödinger Equation

QM is the mathematical function which can explain how the electrons behave in both particle-like and wave-like characteristics. The QM was developed by Werner Heisenberg [107] which is used the matrix approach to give the exact solution and Erwin Schrödinger which is proposed about partial differential equation was developed. The partial differential equation shows clearer physical meaning of the classical wave equation applied to describe duality behavior of particle. The Schrödinger equation, an eigen function, contains all information of any molecular system. By solving eigen value problem normally in the time-independent Schrödinger equation, one can get the total energy of any system as shown in equation 2.1.

$$\hat{H}\Psi = E\Psi \tag{2.1}$$

where $\hat{H}$ is the Hamiltonian operator, and Ψ is the wave function, which is a function of the positions dependent of all electrons, and E is the total energy of electrons in the system. Normally, $\hat{H}$ is the kinetic (T) energy of all particle in a considered system combining with the potential (V) energy defined as:

$$\hat{H} = T + V \tag{2.2}$$

The first term, *T*, is calculated by summation of Laplacian (∇^2) with respect to x, y and z components over all particles in molecule given by:

$$\mathrm{T} = -\frac{h^2}{8\pi^2}\sum_{\mathrm{i}}\frac{1}{m}\nabla_{\mathrm{i}}^2 \quad \text{where} \quad \nabla_{\mathrm{i}}^2 = \frac{\partial^2}{\partial \mathrm{x}^2}+\frac{\partial^2}{\partial \mathrm{y}^2}+\frac{\partial^2}{\partial \mathrm{z}^2} \tag{2.3}$$

where *h* is the Planck' s constant and *m* is the mass of particle (electron or nucleus). Another term, *V*, is calculated by the Coulomb repulsion between each pair of charge entity (electron-electron, nuclear-nucleus and electron-nucleus interactions) which is defined as:

$$V = \frac{1}{4\pi\varepsilon_0}\sum_{\mathrm{j}}\sum_{k<j}\frac{e_j e_k}{\Delta r_{jk}} \tag{2.4}$$

where ε_0 is the permittivity of free space, r_{jk} and e_j *and* e_k are the charge of electron *i* and *j*, respectively. Therefore, the full $\hat{H}$ corresponding *T* and *V* can be written as:

$$\hat{H} = -\frac{h^2}{8\pi^2}\sum_i\frac{1}{m}\nabla_{\mathrm{i}}^2 - \frac{h^2}{8\pi^2}\sum_k\frac{1}{M}\nabla_{\mathrm{k}}^2 - \frac{1}{4\pi\varepsilon_0}\sum_{ik}\frac{e^2 Z_k}{r_{ik}}+\frac{1}{4\pi\varepsilon_0}\sum_{i<j}\frac{e^2}{r_{ij}}+\sum_{k<l}\frac{e^2 Z_k Z_l}{r_{kl}} \tag{2.5}$$

where *i* and *j* refer to electrons, *k* and *l* refer to nucleus, *m* and *M* are the mass of electron and nucleus, respectively. *e* is a charge of electron, *Z* is an atomic number and r_{kl} is the distance between particles *k* and *l*, respectively. The simple form of $\hat{H}$ can be rewritten as:

$$\hat{H} = T_e(r) + T_N(R) + V_{eN}(r,R) + V_{ee}(r) + V_{NN}(R) \tag{2.6}$$

where the $T_e(r)$ and $T_N(R)$ are kinetic energy operators of electron and nucleus, respectively, the $V_{eN}(r,R)$ represents the potential energy operators of electron-nucleus, $V_{ee}(r)$ is potential energy electron-electron and $V_{NN}(R)$ is the potential energy between nucleus-nucleus.

The Schrödinger equation proposed in equation (2.6) can be solved for only one-electron systems such as H atom, He^+ and Li^{2+}. For the complex systems having many-electrons, it is too complicated to solve the Schrödinger equation. Therefore, a new approximation regarding the motions of nuclear and electron is proposed to this complicated mathematical equation.

2.4 Born-Oppenheimer Approximation

The Born-Oppenheimer approximation (BOA) is a fundamental approximation that separately considers the motions of nuclear and electron because the mass of nucleus is too much greater than that of electron (about 1,000 times). Moreover, the velocity of nucleus is much slower than that of electron. By this assumption, the $T_N(R)$ and $V_{NN}(R)$ are omitted from the $\hat{H}$ leading to the new $\hat{H}_{el}$ form consisting of only the motion of electron written as:

$$\hat{H}_{el} = T_e(r) + V_{eN}(r,R) + V_{ee}(r) \tag{2.7}$$

The electronic Schrödinger equation under BOA can be defined as:

$$(\hat{H}_{el} + V_{NN})\Psi_{el}(q_i,q_k) = E_{el}\Psi_{el}(q_i,q_k) \tag{2.8}$$

where q_i and q_k represent the electronic and nuclear coordinates, respectively. The solution of the electronic Schrödinger equation is electronic energy (E_{el}). Because the V_{NN} is a constant, the Schrödinger equation can be solved without the V_{NN} so the eigenvalue is called the pure electronic energy. Furthermore, by adding V_{NN} to this eigenvalue, it can be recognized as the total energy of a given system. In addition, the numerical methods for solving the electronic Schrödinger equation have intensively been developed to use in computational chemistry consisting of *ab initio*, density functional theory and higher level of calculations.

2.5 *Ab Initio* and Hartree-Fock

The word of "*ab initio*" is the Latin word which means "from the first principles" or "from the beginning". The *ab initio* methods consider nucleus and electrons as the basis particles and describe event in a subatomic world. The basis for *ab initio* method is solving the differential equation of Schrödinger equation based on the BOA to obtain the approximate solution without reference to experimental information. The results of the electronic Schrödinger equation solution through *ab initio* methods yield the useful information such as the electron densities, the energies and the other properties of the interesting systems. The simplest type of *ab initio* method is the Hartree-Fock (HF) which is the good example to be starting calculation for many types of *ab initio* calculations.

HF method is the simplest wavefunction-based calculation beginning with assumption of independent-particle model that the motions of each electron are independent from others in the systems. Hence, the $V_{ee}(r)$ value can be accounted as an average value called mean-field approximation in the HF method. The total wavefunctions of each electron which are accounted by HF model called the Hartree product (Ψ_{HP}), which can be written as:

$$\Psi_{HP}(r_1,r_2,\ldots,r_n) = \phi_1(r_1)\phi_2(r_2)\cdots\phi_N(r_N) \tag{2.8}$$

The Ψ_{HP} does not satisfy the antisymmetry principle of Pauli [108]. It states that the wave function describing electrons must be antisymmetric with respect to the interchange of the space-spin coordinates set. Hence, the antisymmetric wavefunction can be modified in terms of a Slater determinant [109] for *N* electron systems neglecting the spin variable is defined as:

$$\Psi_0(x_1,x_2,\ldots,x_N) = \frac{1}{\sqrt{N!}}\begin{vmatrix} \chi_1(x_1) & \chi_2(x_1) & \cdots & \chi_N(x_1) \\ \chi_1(x_2) & \chi_2(x_2) & \cdots & \chi_N(x_2) \\ \vdots & \vdots & \ddots & \vdots \\ \chi_1(x_N) & \chi_2(x_N) & \cdots & \chi_N(x_N) \end{vmatrix} \tag{2.9}$$

The HF approximation demonstrates that the Ψ_0 is the wave function approximated by an antisymmetrized product of *n* orthonormal spin orbitals $\chi_i(x)$ and $1/\sqrt{N!}$ is the normalization factor for *N* electron systems.

2.6 Density Functional Theory

Unlike HF method with treating electron as wave function, the density functional theory (DFT) method proposed by Kohn and Sham [106] defines the electron in the system as the electron density. The electron can be divided to be core electrons densities close to the nucleus and valence electrons densities diffusing around the nucleus. If the electron density can be adopted to be the single variable for the electronic calculation, it will be more realistic and convenient than the wave function-based treatments. In addition, the computational effort for DFT calculation is drastically decreased for the calculation.

The combination of the theorems by Kohn and Sham generates the final expression of E including four energy terms in the DFT framework:

$$E = T_{kin}^{non} + V_{ext} + E_H + E_{xc} \quad (2.10)$$

where T_{kin}^{non} is the kinetic energy of non-interacting *n* electrons (ideal system), V_{ext} is the external field, E_H is the classical Coulomb energy and E_{xc} is the exchange correlation energy. Nevertheless, the last term of E_{xc} is still controversial for accepting in the DFT formalism leading to approximation of E_{xc}.

2.7 Exchange Correlation Approximation

As shown in equation 2.10, the first three terms are relatively easy to calculate. For the *n*-electron system, the last term of E_{xc} which consists of all quantum effects is exactly unknown. Hence, the approximation of this E_{xc} term takes the electron correlation effect into account which is missing in HF method. The exchange correlation approximation terms include the local density approximation (LDA) and generalized-gradient approximation (GGA). Brief detail for each approximation is given in the following sections. In this work, the GGA approximation proposed by Perdew, Burke, and Ernzerhof (PBE) given in section 2.7.2 is employed for all DFT calculations using the Vienna *ab initio* simulation package (VASP) program.

2.7.1 Local Density Approximation

One simple way of accounting for the varying electron density in the system by assuming that the density can be treated locally as a uniform electron gas in which the exchange correlation energy in each point of system is the same as the electron density called LDA. This approximation was originally introduced by Kohn and Sham [110]. As aforementioned, the LDA becomes exact only in homogenous gas or very slowly varying density. In practical calculations, the values of local exchange correlation energy per electron with electron density ($\varepsilon_{xc}^{hom}[\rho(r)]$) per volume of constant electron density (ρ) of homogenous gas are parameterized before multiplying with local electron density and integrating over the space as:

$$E_{xc}^{LDA}[\rho(r)] = \int \rho(r)\varepsilon_{xc}^{hom}[\rho(r)]dr \quad (2.11)$$

The limitation of using LDA is that the real systems are far from the homogenous electron gas. So, the LDA works well when the charge density slowly varied such as in the covalent system and simple metals. Furthermore, the typical drawbacks of LDA include overestimating of cohesive energy and bulk modulus of solid, the calculated

adsorption energy (E_{ads}) is too high and diffusion energy is too low, incorrect describing the transition metal or strong correlation systems and unsuitable for working in materials that involve weak hydrogen bond or Van der Waals attraction. Therefore, the development of better approximations is indispensable for material field.

2.7.2 Generalized-Gradient Approximation

An incompletely homogeneous electron with varying density landscape in the real systems makes the deviation of calculated results far from the actual systems. Hence, the more accurate of exchange correlation of GGA which captures both local and semilocal information is introduced. In principle, GGA should provide better results with the general formula with density gradient as an additional variable:

$$E_{xc}^{GGA}[\rho(r)] = \int \rho(r)\varepsilon_{xc}^{GGA}[\rho(r), \rho(r)]dr \quad (2.12)$$

where the ε_{xc}^{GGA} is the exchange correlation energy per electron and $\rho(r)$ is the generalized-gradient electron density. In fact, there is no simple functional form of $E_{xc}^{GGA}[\rho(r)]$. Therefore, the general form of GGA is expressed based on modification of LDA energy with an additional enhancement factor $F(s)$:

$$E_{xc}^{GGA}[\rho(r),s] = \int \varepsilon_{xc}^{LDA}[\rho(r)]\, \rho(r)F(s)dr \quad (2.13)$$

where, the $F(s)$can be calculated by:

$$F(s) = (1+1.29s^2+14s^4+0.2s^6)^{1/15} \quad (2.14)$$

when, the s factor depends on both electron gradient and its density:

$$s = C\frac{|\rho(r)|}{\rho^{4/3}(r)} \quad (2.15)$$

In the solid system, the typical range of electron density s is in the range of 0 to 3 corresponding with the $F(s)$ from 1.0 to 1.6. the GGA approximation works very well giving structure properties. The various GGA forms have been continuously proposed such as Perdew-Wang 91 (PW91) which was developed in 1992 [111]. This functional is popular in material science because it provides the reasonable accuracy with cost effectiveness. It is based on the constrains of exchange correlation hole using the data from the uniform electron gas and keep a nonempirical system. However, the main limitation of this functional is tendency to provide wiggles in exchange correlation

potential at high and low electron densities which leads development of new functional, PBE developed by Perdew, Burke and Ernzerhof. Based on PW91, PBE shows the simplified GGA version with no empirical elements. The PBE functional includes features of local electron density and its gradient and second order to enhance the factors of $F(x)$ and $F(c)$. The PBE function has proven to be higher accuracy and better than the previous PW91. Now, the PBE is the most frequently used because it does not show wiggles in exchange correlation potential at high and low electron densities. Therefore, using of PBE is better off with pseudopotential.

2.8 Periodic Boundary Condition

The periodic boundary condition is a set of boundary condition which is selected to represent a large (infinite) system of solid by constructing a small unit cell. All unit cells are just duplicated in all directions surrounding the primary unit cell as illustrated in Figure 2.1. Based on periodic boundary condition, the actual calculation can be taken place only in single unit cell to represent image in super cell. The super cell under periodic boundary condition can be extended to many systems such as bulk, atom, slab and cluster. Therefore, the actual solid behaviors can be effectively simulated via the periodic boundary condition.

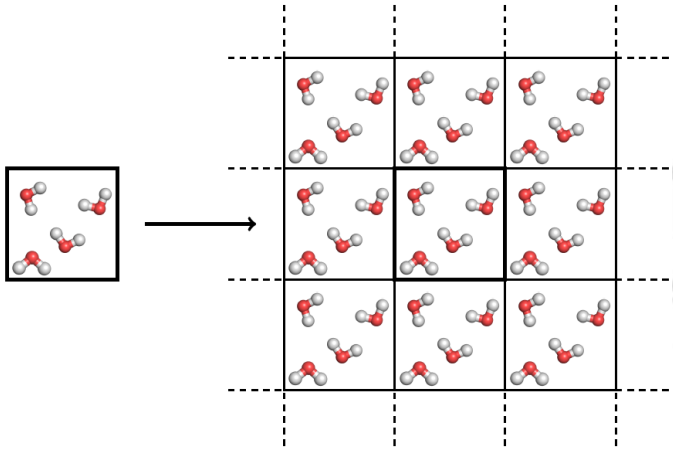

Figure 2.1 Schematic representation of the ideal of periodic boundary condition [112]

2.9 Pseudopotential Approach

Pseudopotential (PP) is an important method of treating core electrons in the solid catalytic model system because the core electrons are not particularly essential for defining chemical bonding and other physical characteristics of materials while these

properties are dominated by the valence electrons in reaction of solid catalytic system. Therefore, the electron density of core electrons is replaced with smoothed density called frozen core model. Exclusion of the core electrons from the calculation affects smaller number of total energy differences leading to more accuracy of total energy calculations and reduce computational time.

2.10 Plane Wave Based DFT Method

Plane wave is one of basis wave functions which is the simplest and frequently used for solid model. The plane wave basis set ($\Phi_{PW}(x)$) equation can be written by the combination of cosine and sine mathematic forms as:

$$\Phi_{PW}(x) = \cos(kx)+i\sin(kx)=\exp(ikx) \tag{2.16}$$

Plane wave basis set for free electron satisfies the Bloch condition representing the smoothly varying function. The systematic improvement of convergence and accuracy is possible with increasing the size of basis set. Moreover, the plane wave basis set is ionic position independent due to the nonlocal nature. Hence, the calculation can be accomplished without avoiding the atomic-centered basis set. These advantages effect that plane wave basis set is commonly adopted in the DFT codes.

2.11 Treating Solid Model using Periodic Boundary Condition

For any solid model, a number of electrons are introduced into the solid system of varying the potentials and identified the result. Then the formulation of Kohn-Sham equations in terms of Fourier coefficient which is an important property of solid is created. However, two issues are firstly resolved: one is the number of electrons become infinite and another is the number of atoms in solid. In practical, the large number of electrons can be treated by the PP methods. Normally, the three common types of PP are normconserving PP, ultrasoft PP and PAW. However, the PAW potential provides the results that are in good agreement with all-electron calculations and gives more reliable results than other PP methods for materials which have strong magnetic moments or large difference in electronegativity.

The PAW potential can be used to provide the accurate results as the all electron full-potential approach with much less computational effort. Moreover, this method can provide all electron charge density if valence orbitals cannot be obtained by other

standard PP methods. Then, the data from a small number of atoms are involved to periodic boundary condition and supercell schemes to physically represents real material in the concept of periodic nature of solid.

2.12 Procedure of Calculation in this Work

In this dissertation, the plane wave based DFT method as the suitable method for surface calculation is selected for investigating of the PDH mechanisms and side reactions on Ni-based catalysts with different dopants. Detailed procedure is given in the following sections.

2.12.1 Geometry Optimization

All periodic boundary calculations in this thesis were performed by a plane wave-based DFT [110] using VASP [113, 114] program. The PAW method [115, 116] with the GGA refined by PBE [117] was employed. The geometry optimization was obtained by minimizing the Hellman-Feynman forces with the conjugate-gradient algorithm until the forces between atoms were below 0.01 eV/Å and the criterion for electronic self-consistent field iteration was 1.0×10^{-6} eV/atom. The k-point grid of 3×5×1 was generated by Monkhorst-Pack scheme [118] and the cut-off value for plane wave basis set was 400 eV. The electron occupancies were determined by using Methfessel-Paxton scheme [119] with smearing energy of 0.2 eV. The Van der Waals dispersion correction was applied using DFT-D3 method proposed by Grimme [120].

2.12.2 Adsorption Energy Calculation

The E_{ads} values of each adsorbed molecule (*i.e.* propane and propylene) on both Ni(111) and Ni-Au/Ni(111) surfaces presented in Chapter 3 and Chapter 4, and C atom on Ni(111), Ni-Au/Ni(111) and Ni-Sn/Ni(111) surfaces given in Chapter 5 are calculated as follows:

$$E_{ads} = E_{molecule,\ C/surface} - E_{surface} - E_{molecule,\ C} \qquad (2.17)$$

where $E_{\text{molecule, C/surface}}$ is the total energy of adsorbate molecule and C atom on the substrate complex, E_{surface} is the total energy of a clean Ni(111), Ni-Au/Ni(111) and Ni-Sn/Ni(111) surfaces, and $E_{\text{molecule, C}}$ is the total energy of isolated molecule and C atom in vacuum. A negative E_{ads} indicates energetically favorable adsorption.

2.12.3 Reaction Mechanism Calculation

To explore the PDH mechanism as well as side reactions of C-C bond cracking and deep dehydrogenation of propylene on Ni(111) and Ni-Au/Ni(111) surfaces, the TS calculation was systematically carried out by using a climbing image nudged elastic band (CI-NEB) method [121] and refined using DIMER method [122-124]. The force tolerance of 0.05 eV/Å and the energy convergence of 1.0×10^{-7} eV/atom were used as the criteria for searching TS in each elementary step. The attained TS structures were confirmed by a single imaginary frequency in vibrational analysis.

2.12.4 Partial Atomic Charge Calculation

The partial charge difference ($\Delta\delta$) of atom *i* before and after adsorption process was calculated from:

$$\Delta\delta = \delta_i^{ads} - \delta_i^{isolate/clean} \tag{2.18}$$

where δ_i^{ads} is the partial charge of atom *i* of stable configuration and $\delta_i^{isolate/clean}$ is the partial charge of atom *i* of isolate gas species or clean surface.

2.12.5 Free Energy and Reaction Rate Constant

The DFT calculations were performed to provide the energies and frequencies which are the important input parameter for thermodynamic and microkinetic investigations. For the adsorption and desorption of gas species (propane and propylene), the Gibbs free energy (ΔG_i) of isolated gas *i* is calculated according to:

$$\Delta G_i = E_0 + \mu + RTlnp_i \tag{2.19}$$

where E_0 is the total energy of gas species *i*, p_i is the partial pressure of gas species *i*, *R* is the gas constant 1.43×10^{-28} eV·K^{-1}·mol^{-1} and *T* is the temperature in Kelvin (K). For the adsorbed system the Gibbs free energy is given by:

$$\Delta G_i = E_0 + E_{ZPE} - RTlnQ_{vib} \tag{2.20}$$

where E_{ZPE} is the zero-point energy of adsorbed system, Q_{vib} is the total vibrational partition function of adsorbed system.

The collision theory was employed to determine rate constants for adsorption and desorption processes which are calculated as followed:

$$k_{ads} = \frac{A \times 10^5}{\sqrt{2\pi m_A k_B T}} \tag{2.21}$$

where A is the area of catalyst surface in angstrom (Å), k_B is the Boltzmann constant (8.62×10^{-5} eV·K^{-1}) and m_A is the molecular weight of the species. Moreover, the rate constants for dehydrogenation and deep dehydrogenation reactions are typically calculated using transition state theory. The forward rate constant (k_f) is given as:

$$k_f = \frac{k_B T}{h} exp\left(\frac{-\Delta G_f}{k_B T}\right) \tag{2.22}$$

where h is the Planck's constant (4.14×10^{-15} eV·s^{-1}). The ΔG_f is the activation free energy of forward reaction in the temperature range of 500 to 1200K. The forward and reverse rate constants (k_f and k_r) and the equilibrium rate constant (K_{eq}) are linked through the following relation:

$$K_{eq} = \frac{k_f}{k_r} \tag{2.23}$$

where the K_{eq} is given as:

$$K_{eq} = exp\left(-\frac{\Delta G^0}{k_B T}\right) = exp\left(\frac{\Delta S^0}{k_B}\right) exp\left(-\frac{\Delta H^0}{k_B T}\right) \tag{2.24}$$

where ΔG^0 is the change in standard Gibbs free energy, ΔS^0 denotes the standard state difference of entropy and ΔH^0 is the enthalpy change which is deviated from standard state.

CHAPTER 3

Theoretical Insight into Catalytic Propane Dehydrogenation on Ni(111)

In the literature [58, 96], the bare Ni which is the high reactive catalyst for alkane reaction is not the appropriate catalyst PDH reaction due to low selectivity of propylene production. To explore the cause of low propylene selectivity, the insight into mechanisms of PDH as well as side reactions of deep dehydrogenation, C-C bond cracking during and after PDH process as well as coke formation on Ni-based catalysts are investigated. The information from this calculation can be used determine that what is the limitation of Ni catalyst in the low selectivity of propylene production. Moreover, the suitable method to improve the batter Ni catalyst for increasing yield production of propylene during PDH process is also investigated.

3.1 Slab Information

For a slab model, a 6×4 Ni(111) slab with a dimension of 14.73 Å x 8.51 Å x 21.02 Å was constructed. As illustrated in Figure 3.1a and 3.1b, four Ni layers consisting of 107 Ni atoms is separated by ~15 Å of vacuum region along the z-axis to avoid interactions between periodic images. The two bottom layers of Ni(111) slab were fixed to their bulk lattice positions, while two top layers and adsorbed species were allowed to fully relax during the calculation. The possible active sites of Ni(111) slab are exhibited in Figure 1c; there are atop site of Ni atom (atop site), bridge site between Ni-Ni atoms (bridge site) and three-fold hollow sites (hcp- and fcc-sites).

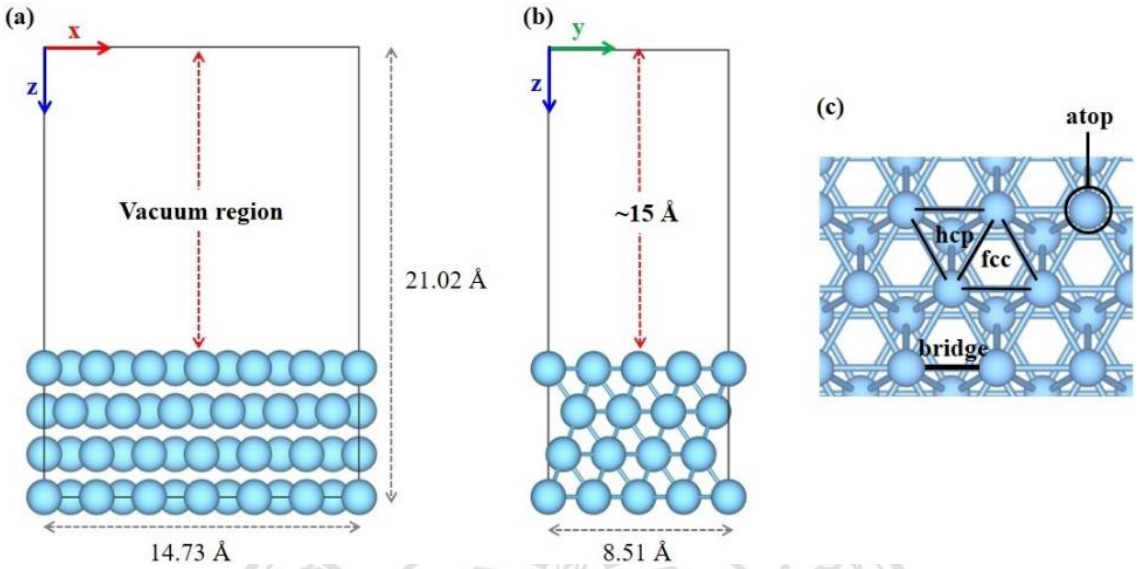

Figure 3.1 Structure of Ni(111) slab projected along (a) the (010)-direction, (b) (100)-direction, and (c) the possible active sites on the Ni(111) surface

3.2 Results and Discussion

3.2.1 Adsorption of Propane and Propylene on Ni(111)

The interaction of a reactant and a product of PDH reaction on Ni(111) surface is discussed in this part. The possible adsorption configurations of propane and propylene were optimized by varying location of the adsorbates (*i.e.* propane and propylene), which are atop, bridge and fcc and hcp sites of Ni(111) (see Figure 3.1c). The optimized structures of all possible configurations of propane and propylene adsorption on Ni(111) and E_{ads} in eV are given in Figure 3.2 and Figure 3.3, respectively.

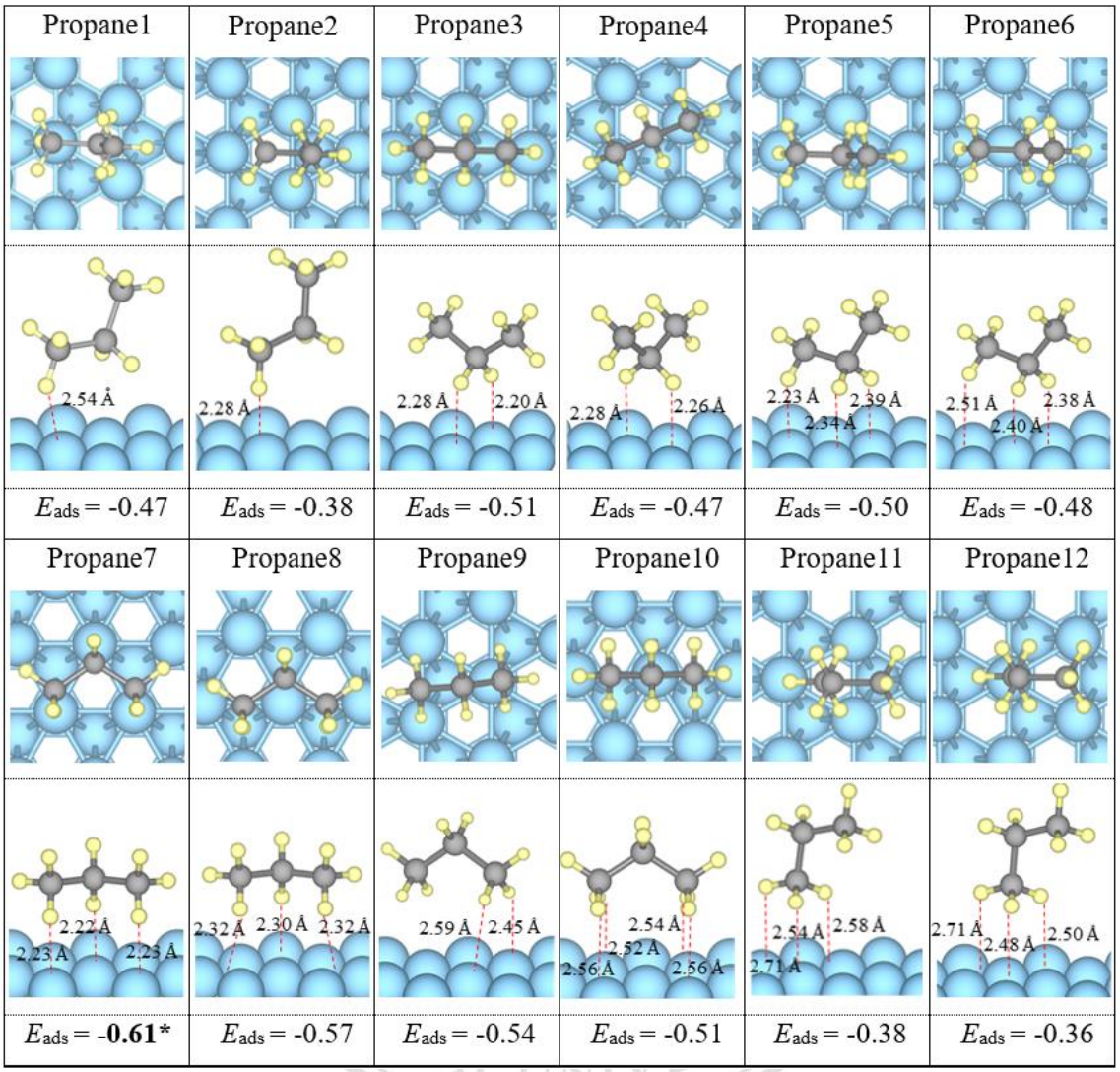

Figure 3.2 All possible configurations of propane adsorption on Ni(111) and E_{ads} in eV

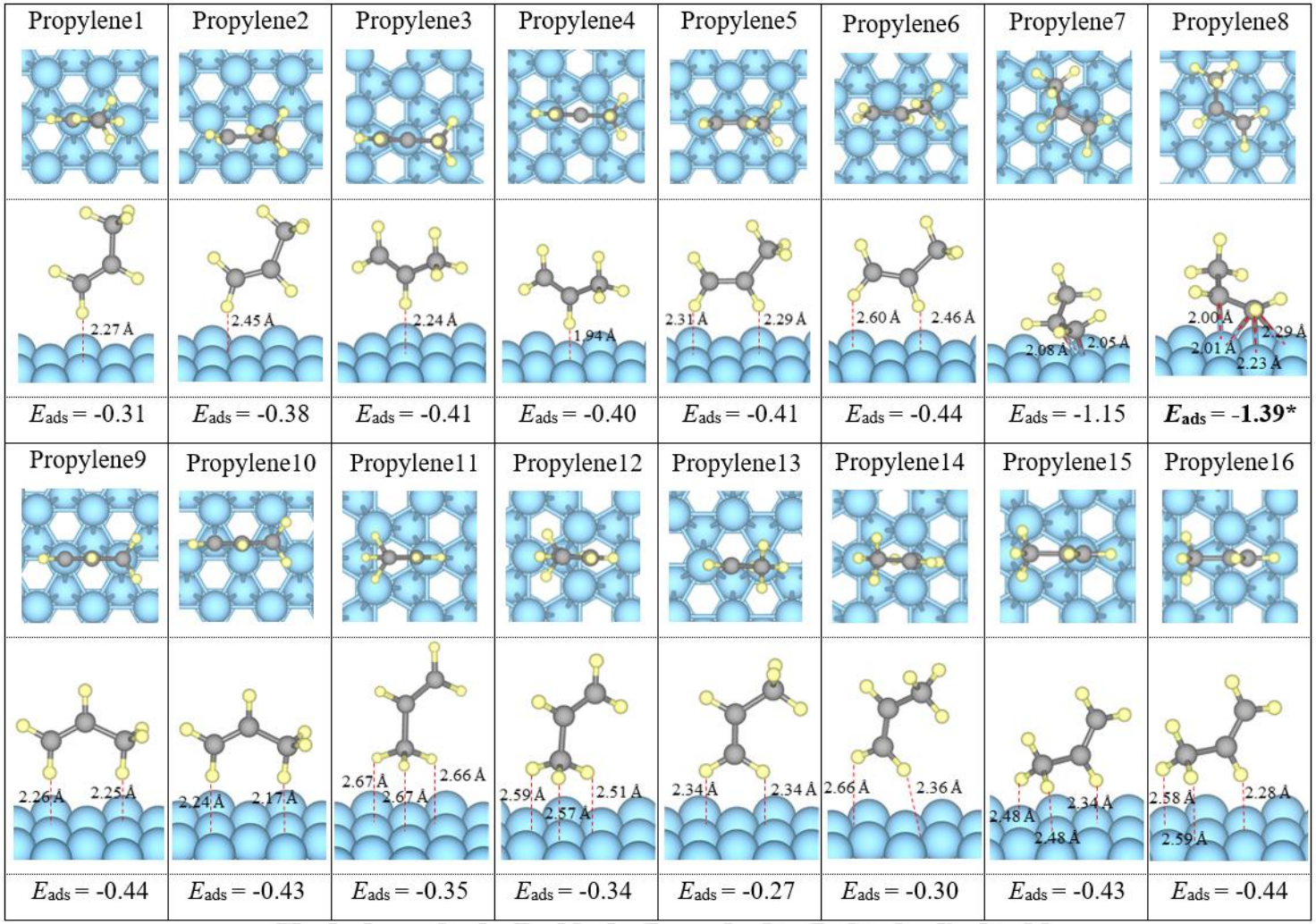

Figure 3.3 All possible configurations of propylene adsorption on Ni(111) and E_{ads} in eV

The most stable configurations of propane and propylene on Ni(111) surface are shown in Figure 3.4a and Figure 3.4b, respectively. The calculated E_{ads} values and selected interatomic distances of propane and propylene on Ni(111) are summarized in Table 3.1.

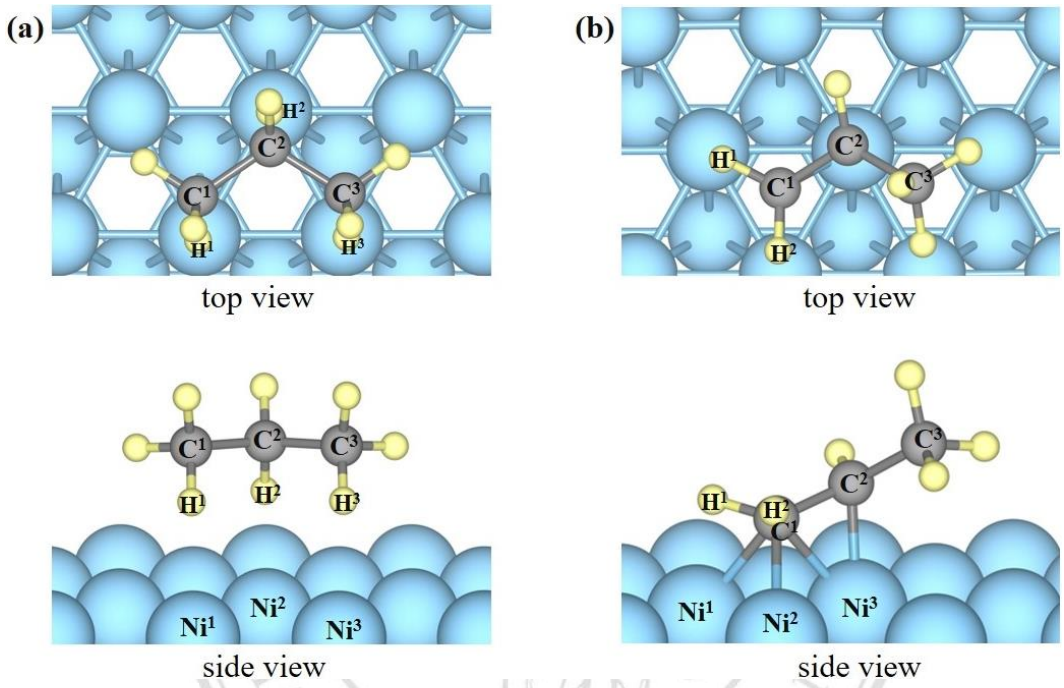

Figure 3.4 Top and side views of the most stable configurations of (a) propane and (b) propylene on Ni(111) surface

Table 3.1 Adsorption energies (E_{ads}) in eV and interatomic distances (d) in Å of propane and propylene on Ni(111) surface

Adsorbate	E_{ads} (eV)	Favored site	$d_{C\text{-}Ni}$ (Å)	$d_{H\text{-}Ni}$ (Å)	$d_{C\text{-}C}$ (Å)	$d_{C\text{-}H}$ (Å)
propane	-0.61	atop	$C^1\cdots Ni^1 = 3.23$ $C^2\cdots Ni^2 = 3.15$ $C^3\cdots Ni^3 = 3.25$	$H^1\cdots Ni^1 = 2.34$ $H^2\cdots Ni^2 = 2.14$ $H^3\cdots Ni^3 = 2.36$	$C^1\text{-}C^2 = 1.52$ $C^2\text{-}C^3 = 1.52$	$C^1\text{-}H^1 = 1.11$ $C^2\text{-}H^2 = 1.12$ $C^3\text{-}H^3 = 1.11$
propylene	-1.39	fcc and atop	$C^1\text{-}Ni^1 = 2.23$ $C^1\text{-}Ni^2 = 2.17$ $C^1\text{-}Ni^3 = 2.11$ $C^2\text{-}Ni^3 = 1.99$	$H^1\cdots Ni^1 = 2.00$ $H^2\cdots Ni^2 = 1.89$	$C^1\text{-}C^2 = 1.44$ $C^2\text{-}C^3 = 1.50$	$C^1\text{-}H^1 = 1.12$ $C^1\text{-}H^2 = 1.13$

For propane adsorption, propane prefers to adsorb on atop sites of Ni(111) surface as shown in Figure 2a. The adsorbed propane interacts with Ni(111) surface by H^1-Ni^1, H^2-Ni^2 and H^3-Ni^3 interactions. The equilibrium adsorption height of propane from the Ni(111) surface is 2.14 Å measured from the nearest distance between H^2 atom of propane and atop of Ni^2. The E_{ads} of propane on Ni(111) surface is -0.61 eV. The undistorted of the adsorbed propane structure and the low E_{ads} value indicate the physisorption of propane and Ni(111). It is worth mentioning that this value is more negative than that on Pt(111) (-0.42 eV) [49] suggesting the stronger adsorption of propane on Ni surface than Pt surface.

For propylene adsorption, the propylene prefers to adsorb on Ni(111) surface on two adsorption sites; fcc and atop sites as illustrated in Figure 3.4b. The C^1 atom of propylene binds to Ni^1, Ni^2 and Ni^3 atoms at the hollow site of Ni(111) while C^2 of propylene binds to atop of Ni^3. The adsorption height of propylene from Ni(111) calculated from the bond length between C^2 and Ni^3 atoms is 1.89 Å. The strong bond formations between propylene and Ni(111) surface causes the elongation of the C^1=C^2 bond of propylene from 1.34 Å to be 1.44 Å. The E_{ads} value of -1.39 eV and the distorted structure of the adsorbed propylene molecule signify that interaction between propylene and Ni(111) surface is chemisorption.

3.2.2 Electronic Charge Property

3.2.2.1 Charge Density Difference and Bader Charge Analysis

To understand the interaction between propane/propylene and Ni(111) during adsorption process, electronic charge properties are elucidated herein. The charge density differences of the most stable adsorption configurations of propane and propylene on Ni(111) are displayed in Figure 3.5a and 3.5b. Charge accumulation and charge depletion are represented by green and red regions, respectively. In addition, charge transfer between adsorbed molecules and Ni(111) surface were quantitatively analyzed by performing Bader charge analysis [125]. The number of valence electrons of neutral atom/molecule is used as a reference for calculating the Bader charge change. More Bader charge information of individual atoms on the top layer of Ni(111) surface and adsorbate such as Ni^1, Ni^2 and Ni^3 atoms of Ni(111) and C and H atoms of propane and propylene are reported in Table 3.2.

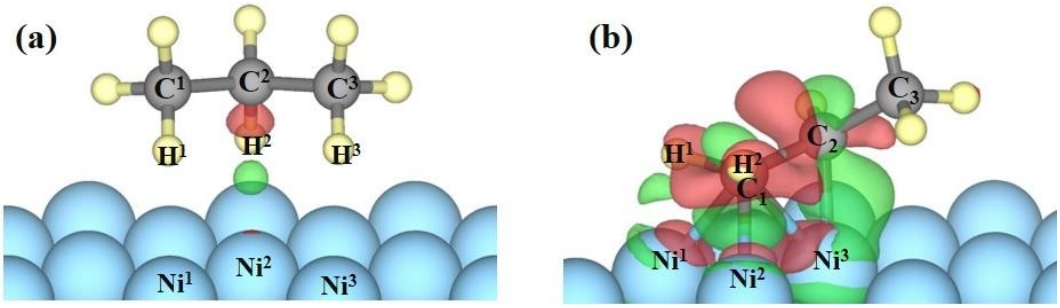

Figure 3.5 Charge density differences (green for charge accumulation and red for charge depletion) of (a) propane and (b) propylene adsorption on the Ni(111) surface with isovalue of ±0.003 e $Å^{-3}$

Table 3.2 Bader charge analysis of selected atoms of Ni(111), propane and propylene before and during adsorption represented in Figure 3.4

Bader charge change (|*e*|)						
System	**Ni(111)**		**Adsorbed molecules**			
			Propane		**Propylene**	
Isolated phase	Total	(0.000)	Total	(0.000)	Total	(0.000)
	Subsurface layer	(-0.084)	C^1	(+0.178)		
	Top layer	(-0.060)	C^2	(-0.221)		
			C^3	(+0.162)		
	Ni^1	(-0.026)	H^1	(-0.048)		
	Ni^2	(+0.046)	H^2	(-0.047)		
	Ni^3	(-0.150)	H^3	(-0.039)		
	Ni^1	(-0.057)			C^1	(-0.109)
	Ni^2	(-0.041)			C^2	(-0.102)
	Ni^3	(+0.046)			C^3	(-0.192)
					H^1	(+0.134)
					H^2	(-0.042)
Propane adsorption	Total	(-0.264)	Total	(+0.264)		
	Subsurface layer	(-0.027)	C^1	(-0.097)		
	Top layer	(-0.236)	C^2	(-0.206)		

Table 3.2 Bader charge analysis of selected atoms of Ni(111), propane and propylene before and during adsorption represented in Figure 3.4 (continued)

Bader charge change (|*e*|)						
Propane adsorption			C^3	(-0.161)		
	Ni^1	(+0.129)	H^1	(+0.272)		
	Ni^2	(+0.316)	H^2	(+0.202)		
	Ni^3	(+0.072)	H^3	(+0.135)		
Propylene adsorption	Total	(-0.545)			Total	(+0.545)
	Subsurface layer	(-0.643)				
	Top layer	(+0.303)				
	Ni^1	(+0.020)			C^1	(+0.013)
	Ni^2	(+0.139)			C^2	(+0.085)
	Ni^3	(-0.138)			C^3	(-0.186)
					H^1	(+0.154)
					H^2	(+0.160)

For propane adsorption (see Figure 3.5a), the interaction can be observed from charge accumulation and depletion between H^2 of propane and Ni^2 of the substrate. In addition, the Bader charge analysis signifies electron transfer from Ni substrate to propane approximately 0.26 |*e*| during the adsorption process. Figure 3.5b shows charge density difference of propylene adsorbed Ni(111). There are four chemical bonds between propylene and Ni(111) surface, which are three bonds of C^1 atom to Ni^1, Ni^2, Ni^3 and one C^2---Ni^3 bond. Similar to the propane adsorption, the Bader charge result indicates the charge transfer from Ni(111) to adsorbed propylene approximately 0.55 |*e*|.

At the same isosurface value of charge density difference, the electron density of the propylene adsorbed Ni(111) system is more obviously changed than that of the propane adsorbed Ni(111) system. Moreover, a greater number of electrons are transferred from the substrate to propylene than propane. These evidences support that the propylene adsorption is stronger than the propane adsorption. This aspect corresponds well with the E_{ads} results discussed in adsorption part.

3.2.2.2 Density of State Analysis

The detailed information on interactions of propane/propylene and Ni(111) was investigated by projected-density of states (PDOSs). The PDOSs of propane, propylene and Ni(111) before and during adsorption processes are plotted in Figure 3.6a and 3.6b. The Fermi level (E_F) is set at 0 eV. The bonding and anti-bonding states are represented in lower and higher regions from E_F, respectively. The density of state (DOS) of C, H and Ni atoms is projected into the p-state (p-DOS), the s-state (s-DOS) and the d-state (d-DOS), respectively. In Figure 3.6, the PDOSs of isolated propane and propylene are presented in panel I. The PDOSs of adsorbates when they are adsorbed on the Ni surface are shown in panel II. Panel III presents PDOSs of Ni(111) of pre-adsorption and during adsorption.

For the pre-adsorption condition, the overlapping of p-DOS peaks of C atoms and s-DOS peaks of H atoms expresses the C-H bonds in propane and propylene molecules (see panel I of Figure 3.6a and 3.6b). For bare Ni(111) surface, the d-DOS of Ni atoms is demonstrated in panel III (blue peaks). The *d*-band center (ε_d) of bare Ni(111) surface is -1.43 eV which is similar to the result reported by Hammer and Nørskov (-1.48 eV) [126].

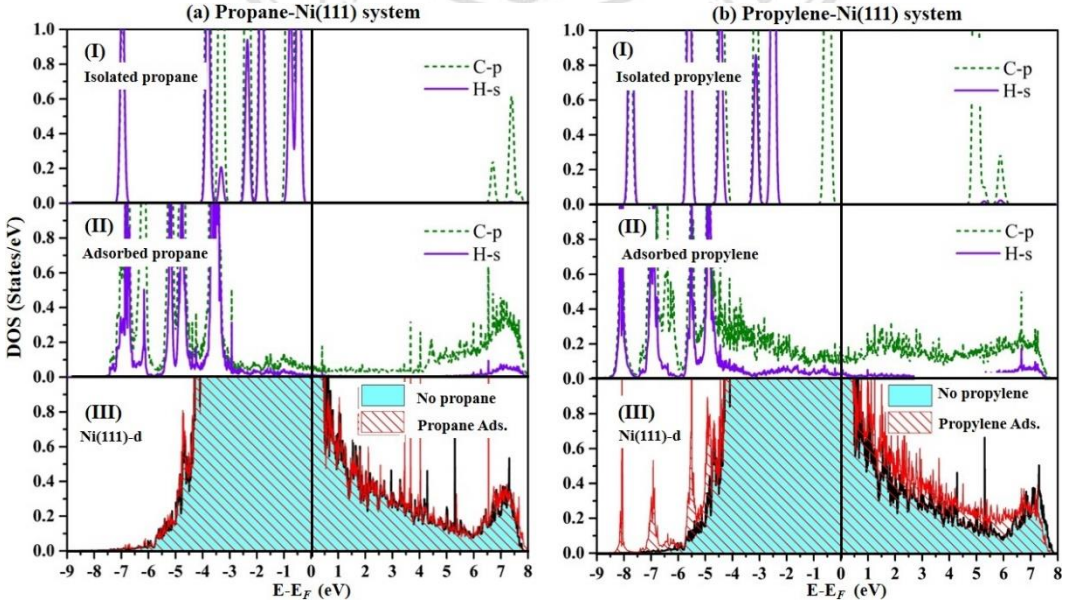

Figure 3.6 Comparison projected density of states (PDOS) of (a) propane-Ni(111) and (b) propylene-Ni(111) system where I, II and III representing isolated molecule, adsorbed molecule, and Ni(111) surface (before and during adsorption), respectively

For the propane adsorption, PDOS peaks of adsorbed propane are shown in panel II of Figure 3.6a. The interactions between H atoms of propane and Ni atoms of Ni(111) surface can be explained by the s-DOS of H atoms of adsorbed propane and d-DOS of Ni atoms of Ni(111) surface. The PDOS peaks from H and C atoms of adsorbed propane are shifted and broadening compared with those of isolated propane in panel I of Figure 3.6a. However, no significant change of d-DOS of Ni(111) surface can be observed when comparing red- and blue-peaks in panel III of Figure 3.6a. This aspect signifies the weak physisorption of propane on Ni(111) surface.

For the propylene adsorption, the PDOS peaks of adsorbed propylene are depicted in panel II of Figure 3.6b. As discussed in the adsorption part, propylene binds on the Ni(111) surface via four chemical bonds (see Figure 3.4b). These interactions of propylene on Ni(111) surface can be described by the overlapping of the p-DOS of propylene (C^1 and C^2 atoms) and d-DOS of Ni(111) surface (Ni^1, Ni^2, Ni^3 atoms). The redistribution of p-DOS signal of adsorbed propylene indicates bond formations of C^1 and C^2 atoms of propylene to Ni atoms on Ni(111) surface. The d-DOS curve of Ni(111) surface obviously changes after propylene adsorption (red peaks in panel III of Figure 3.6b). The strong overlapping of d-DOS of Ni(111) surface with p-DOS of C^1 and C^2 of adsorbed propylene at the range of -8.37 to -4.47 eV indicates d-p hybridization of C atoms of propylene and Ni atoms of Ni(111) surface. In summary, PDOS results describe the strong chemical bonding between propylene and Ni(111) and the weak interaction between propane and Ni(111), which correspond very well with the E_{ads}, charge density difference and Bader charge results.

3.2.3 PDH Reaction on Ni(111) Surface

Detailed mechanisms of PDH on Ni(111) are discussed in this part. The mechanism of PDH reaction of propane to propylene involves two dehydrogenation steps: the first step is propane (C_3H_8) to propyl species (C_3H_7) and the second step is C_3H_7 to form propylene (C_3H_6) as described in Figure 1.4. The propyl species from the first step can be produced from two possible pathways; pathway A and pathway B. These two possible pathways start from the same IS of adsorbed propane to yield the same final structure of adsorbed FS of adsorbed propylene. As a result, the geometries of IS, transition states

(TSA1, TSA2, TSA-diff, TSB1, TSB2 and TSB-diff), intermediates (Int A-1, Int A and Int B) and FS of pathways A and B are displayed in Figure 3.7a and 3.7b, respectively.

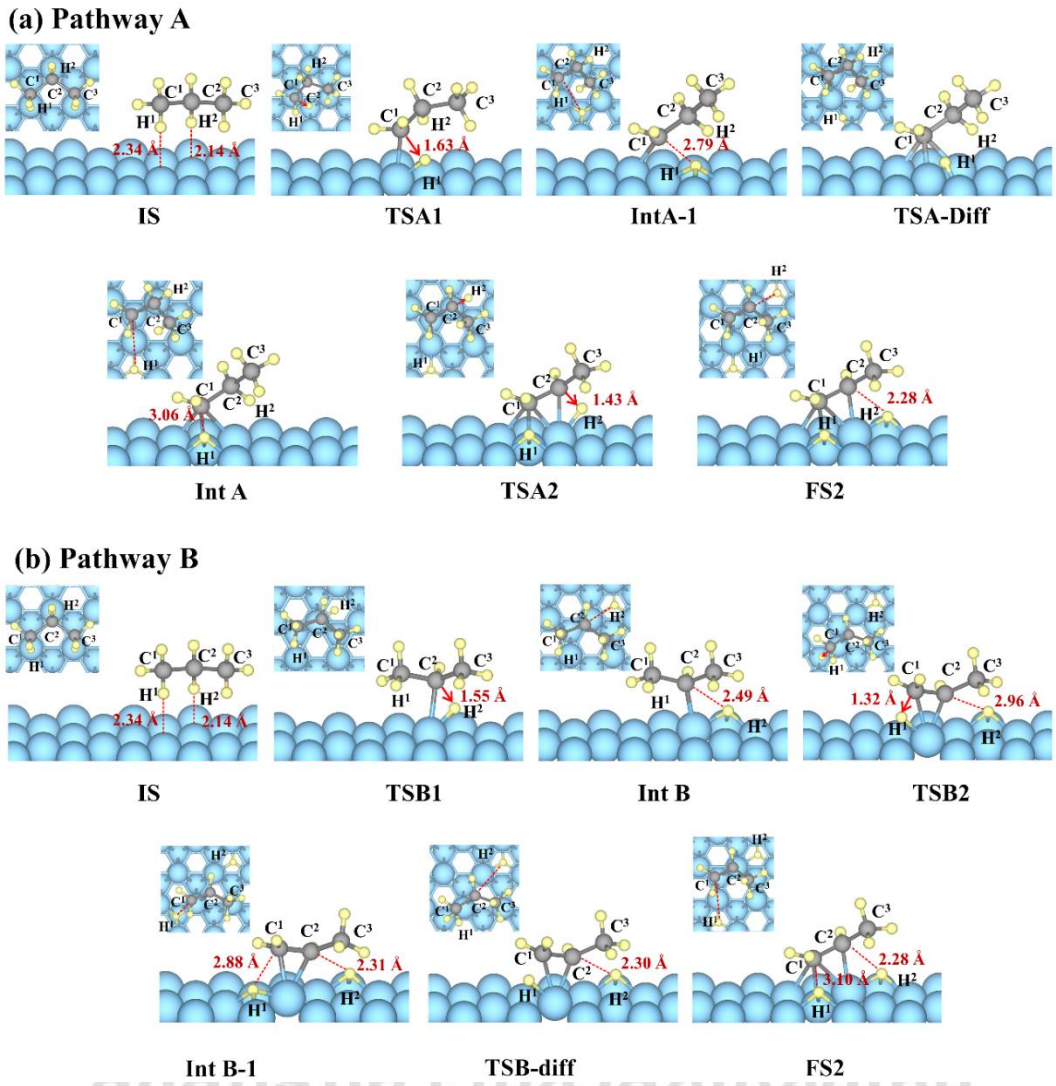

Figure 3.7 Geometries of initial state (IS), transition state (TS) intermediate (Int) and final state (FS) structure for PDH reaction in (a) pathway A and (b) pathway B

The potential energy surfaces (PES) of both pathway A (black line) and pathway B (blue line) are presented in Figure 3.8. Their corresponding activation energies (E_a) and relative energies of each state of reaction on Ni(111) surface are summarized and compared with PDH on Pt(111) surface [48, 74] in Table 3.3. The summation of total energies of isolated propane and bare Ni(111) surface was set as the reference value for relative energy calculation. For the pathway A (Figure 3.7a), the first dehydrogenation (step 1A) of adsorbed propane ($CH_3CH_2CH_3$) denoted as IS to form 1-propyl

($CH_3CH_2CH_2^*$) intermediate denoted as Int A starts from C^1-H^1 bond stretching of propane from 1.11 Å to 1.63 Å.

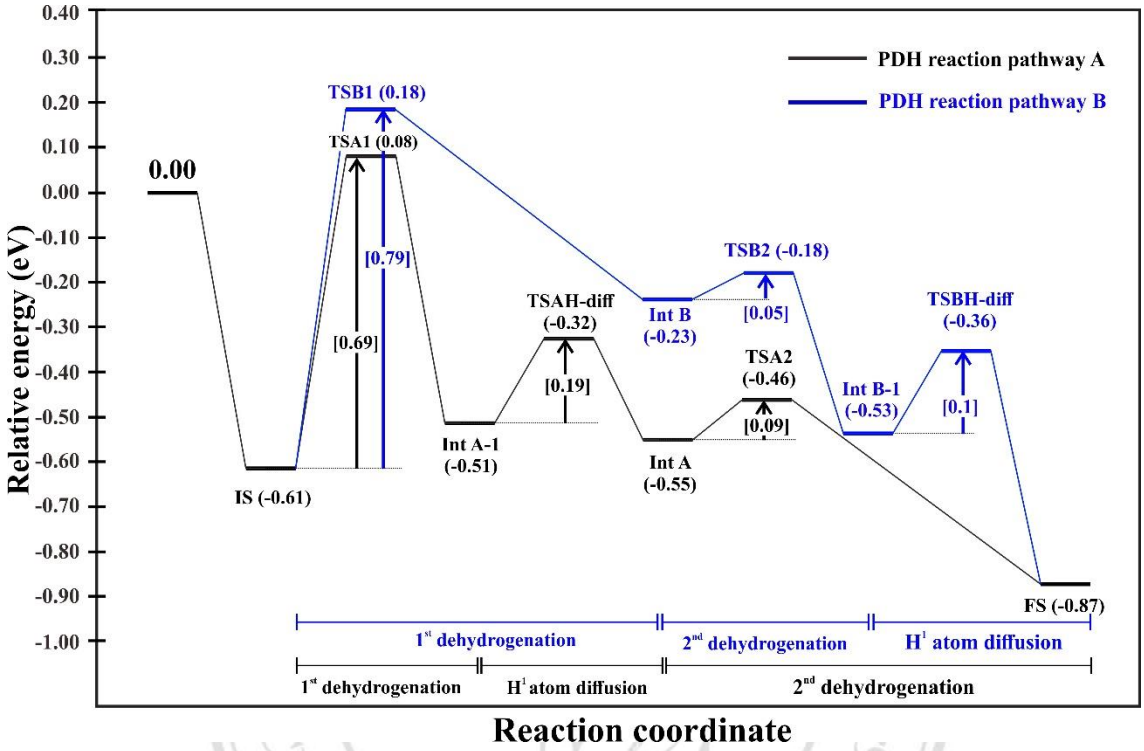

Figure 3.8 Energy profiles of PDH for pathway A (—) and pathway B (—) (Relative energies are displayed in the parenthesis and the E_a barriers are denoted in the bracket)

Table 3.3 Activation energies (E_a) in eV unit for PDH, C-C cracking and deep dehydrogenation reactions on Ni(111) and Pt(111) surfaces

Reaction	Elementary step		E_a (eV)	
			Ni(111) (This work)	Pt (111) [48][a]
PDH	Step 1A	$CH_3CH_2CH_3 \longrightarrow CH_3CH_2CH_2^* + H^*$	0.69	0.69
	Step 1B	$CH_3CH_2CH_3 \longrightarrow CH_3CH\,CH_3^* + H^*$	0.79	0.70
	Step 2A	$CH_3CH_2CH_2^* \longrightarrow CH_3CH\,CH_2^* + H^*$	0.09	0.73
	Step 2B	$CH_3CH\,CH_3^* \longrightarrow CH_3CH\,CH_2^* + H^*$	0.05	0.70
Propylene desorption		$CH_3CH\,CH_2^* \longrightarrow CH_3CH\,CH_{2\,(g)}$	1.16	0.97

Table 3.3 Activation energies (E_a) in eV unit for PDH, C-C cracking and deep dehydrogenation reactions on Ni(111) and Pt(111) surfaces (continued)

Reaction	Elementary step		E_a (eV) Ni(111) (This work)	E_a (eV) Pt (111) [48][a]
C-C cracking	Step 1C	$CH_3CH_2CH_3 \longrightarrow CH_3CH_2^* + CH_3^*$	2.39	2.44
	Step 2C	$CH_3CH_2CH_2^* \longrightarrow CH_3CH_2^* + CH_2^*$	1.45	1.69
	Step 2C'	$CH_3CH\,CH_3^* \longrightarrow CH_3CH^* + CH_3^*$	0.90	1.81
	Step 3C	$CH_3CH\,CH_2^* \longrightarrow CH_3CH^* + CH_2^*$	1.14	2.00
Deep dehydrogenation	Step 3D	$CH_3CH\,CH_2^* \longrightarrow CH_3CH\,CH^* + H^*$	0.84	0.76
	Step 3E	$CH_3CH\,CH_2^* \longrightarrow CH_3CCH_2^* + H^*$	0.85	0.77

[a]PDH on 3x3 Pt (111) surface calculated by PAW/PBE method implemented in VASP

At the TSA1 state, H^1 is dissociated to the hcp site of Ni(111) to form Int A-1. The E_a of the first dehydrogenation is 0.69 eV. Then, the unstable detached H^1 atom diffuses from hcp to more stable fcc site of Ni(111) surface (Int A). The E_a of H^1 atom diffusion via TSA-diff is only 0.19 eV. The E_a of H atom diffusion from hcp to fcc sites on Ni(111) surface in this study is in good agreement with the energy barrier of 0.15 eV reported by Kristinsdóttir and co-workers [127] For the second dehydrogenation step (step 2A), the Int A can be activated to form propylene ($CH_3CHCH_2^*$) denoted as FS by elongation of C^2-H^2 bond from 1.16 Å to 1.43 Å, leading to the strong adsorption of H^2 atom on the hcp site of Ni(111) surface. The E_a of the second dehydrogenation via TSA2 is 0.09 eV. This second step is a facile process. Therefore, the first dehydrogenation is the rate determining step for PDH reaction in pathway A.

For the pathway B (Figure 3.7b), the first dehydrogenation (step 1B) of propane (IS) starts from C^2-H^2 bond activation of adsorbed propane at the secondary C atom to produce H^2 adsorbed on the fcc site of Ni(111) surface and to form 2-propyl ($CH_3CH_2^*CH_3$) intermediate (see Int B in Figure 3.7b). Next, the activated C^2-H^2 bond is elongated from 1.12 Å to 1.57 Å at the TSB1 state, requiring energy of 0.79 eV to form Int B. The H^2 atom of adsorbed Int B is strongly adsorbed on the preferred fcc site of Ni(111) surface, so there is no diffusion to other sites. For the second dehydrogenation (step 2B), the Int B is continuously dehydrogenated by elongation of C^1-H^1 bond of Int B from 1.12 Å to 1.31 Å on Ni(111) through TSB2. The E_a of the second dehydrogenation

for C_1-H_1 bond activation is 0.05 eV. Similar with step 2A, the second dehydrogenation of pathway B occurs easily. Next, the detached H^1 atom is adsorbed on the hcp site of Ni(111) surface before moving to the more stable fcc site on Ni(111) surface with diffusion energy of 0.17 eV (Int B-1 to FS). The higher energy barrier of TSB1 than that of TSB2 in pathway B indicates that the first dehydrogenation is also the rate determining step for PDH reaction which is the same as in pathway A.

In addition, PDH on Ni(111) from this work is compared to that on Pt(111) reported in literatures. The energy barriers of the first and second dehydrogenations on Ni(111) and Pt(111) are given in Table 3.3. For the first dehydrogenation, the E_a of propane to produce 1-propyl on Ni(111) in pathway 1A is the same to that of Pt(111) with the E_a of 0.69 eV. While the E_a of the first dehydrogenation of propane on Ni(111) in pathway 1B is 0.79 eV, which is slightly higher than the E_a of 0.70 eV in Pt(111). For the second dehydrogenation, the energy barrier of 1-propyl dehydrogenation to form propylene in pathway 2A is 0.09 eV which is lower than that of Pt(111) (0.70 eV). Meanwhile the E_a of 2-propyl dehydrogenation in pathway 2B is only 0.05 eV, which is also lower than that of Pt(111) (0.68 eV). These results indicate that Ni(111) is more active catalyst for propyl species (1-propyl and 2-proply) dehydrogenation than Pt(111) surface.

From PES in Figure 3.8, pathway A is more thermodynamically favorable than pathway A by comparing the stability of intermediates. The relative energy of Int A is -0.55 eV which is more thermodynamically stable than that of Int B (-0.23 eV). By considering the energy barriers of the rate determining step in both pathway A and pathway B (see Figure 3.8), the first dehydrogenation of propane in pathway A is slightly lower than that of pathway B. To indicate the kinetically favorable pathway for the main PDH in the present study, we have compared the reaction rates of IS→TSA1 (k^{TSA1}) and IS→TSB1 (k^{TSB1}), which are the rate determining steps of pathways A and B. The details of calculations are provided in Table 3.4. As a result, the calculated k^{TSA1}/k^{TSB1} values in range of 298K to 900K signify that pathway A is more kinetically preferable than pathway B. Therefore, the PDH reaction in pathway A is a major contribution to the formation of FS on Ni(111) surface.

Table 3.4 Comparison of k^{TSA1}/k^{TSB1} at different temperature

T (K)	k^{TSA1}/k^{TSB1}
298	2.05×10^{4}
400	4.87×10^{3}
500	2.12×10^{3}
600	1.23×10^{3}
700	8.34×10^{2}
800	6.24×10^{2}
900	4.99×10^{2}

Finally, desorption of propylene after PDH process has a positive effect on the selectivity toward propylene production. The energy barrier of propylene desorption (ΔE_{des}) from Ni(111) surface after PDH reaction regarding from FS is calculated by:

$$\Delta E_{des} = E_{FS} - E_{2H/Ni(111)} - E_{propylene}$$

where E_{FS} is the total energy of adsorbed propylene and two H atoms which are detached from propane structure during PDH process on the Ni(111) surface despite, $E_{2H/Ni(111)}$ is the total energy of Ni(111) surface with two detached H atom without propylene, and $E_{propylene}$ is the total energy of isolated propylene molecule. The energy barrier of propylene desorption from Ni(111) surface is 1.16 eV.

3.2.4 Side Reactions on Ni(111) Surface

As mentioned in Chapter 1, the C-C bond cracking and deep dehydrogenation (*i.e.* dehydrogenation of adsorbed propylene on surface catalyst) as side reactions can affect the selectivity of propane conversion to form propylene on Ni(111) surface. Hence, these two side reactions have been investigated and discussed in this part. The proposed mechanisms of C-C bond cracking and deep dehydrogenation are described in Figure 1.4. The possible C-C bond cracking reactions of propane, 1-propyl, 2-propyl and propylene are denoted as steps 1C, 2C, 2C′ and 3C, respectively. Herein, the structures of C-C bond cracking reactions are displayed in Figure 3.9. The deep dehydrogenation can be triggered through 3D and 3E to produce 1-proppenyl ($CH_3CH\,CH^*$) and 2-propynyl ($CH_3CCH_2^*$) as displayed in Figure 3.10. The obtained energy profiles are

compared in Figure 3.11. The activation energies of C-C bond cracking and deep dehydrogenation are summarized in Table 3.3.

3.2.4.1 C-C Bond Cracking Mechanism on Ni(111) Surface

As presented in Figure 1.4, the first side reaction of step 1A and 1B is the C-C cracking of propane represented by step 1C. In this C-C cracking step, the C^1-C^2 bond of propane can be cleaved to form methyl (CH_3^*) and ethyl ($CH_3CH_2^*$) adsorbed on fcc and atop sites of Ni(111), respectively (see Figure 3.9). The C^1-C^2 is prolonged from 1.52 Å to 2.21 Å in the TSC1. From Table 3.3 and Figure 3.11, the E_a of C^1-C^2 breaking is 2.39 eV which is much higher than that of the first dehydrogenation of propane (about 0.70 eV). The high E_a value corresponds to the steric effect of H that obstructs the contact points between C of propane and Ni atoms on the surface. This extremely high E_a indicates that this cracking requires extremely high temperature. Therefore, the first dehydrogenation of propane, step 1A, can proceed as the preferable process.

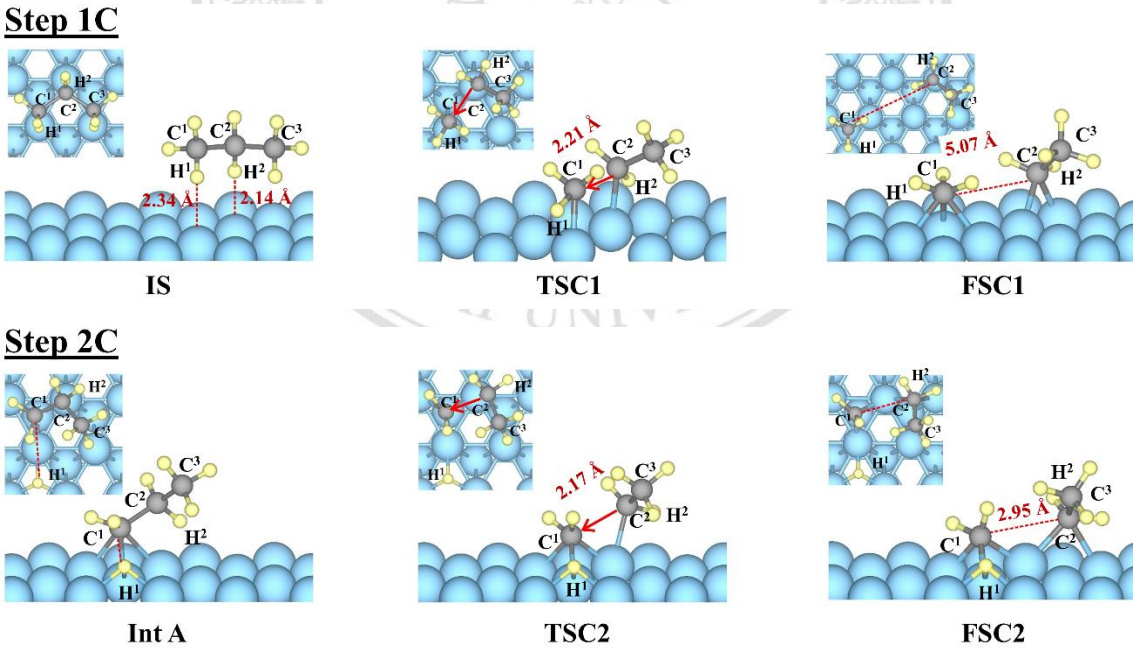

Figure 3.9 Geometries of the C-C bond cracking reactions of propane (step 1C), 1-propyl (step 2C), 2-proply (step 2C′) and propylene (step 3C)

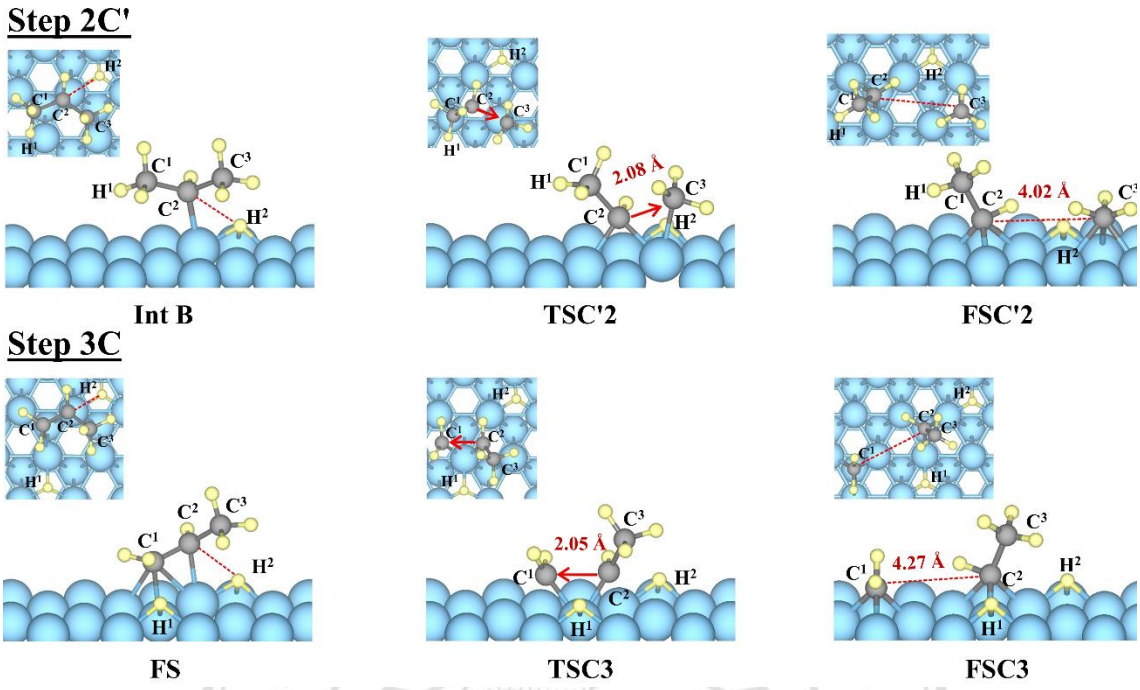

Figure 3.9 Geometries of the C-C bond cracking reactions of propane (step 1C), 1-propyl (step 2C), 2-proply (step 2C′) and propylene (step 3C) (continued)

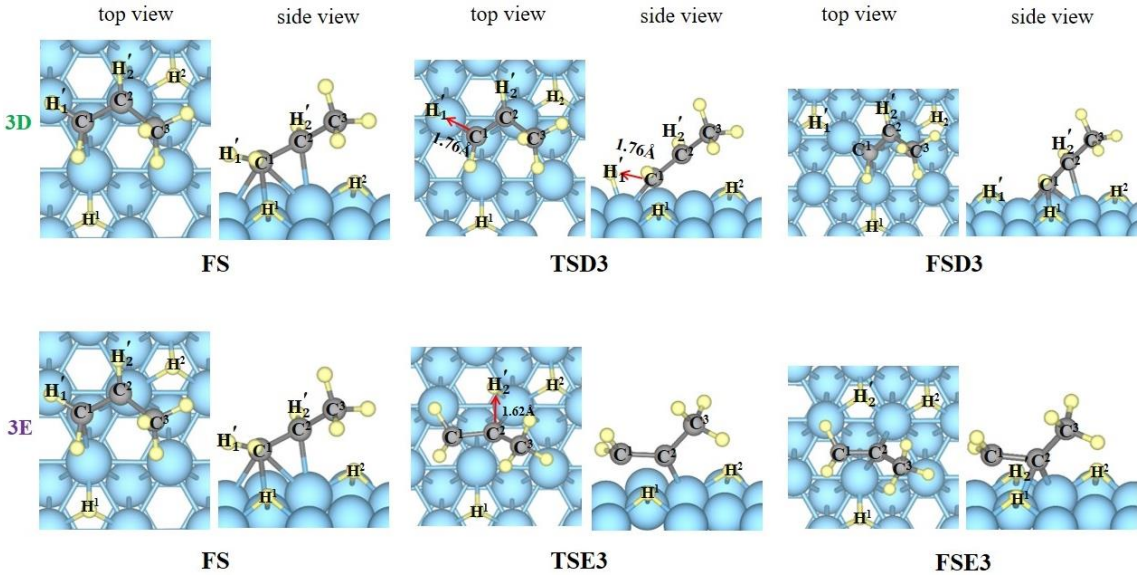

Figure 3.10 Geometries of the deep dehydrogenation producing 1-propenyl (step 3D) and 2-propenyl (step 3E) on Ni(111) surface

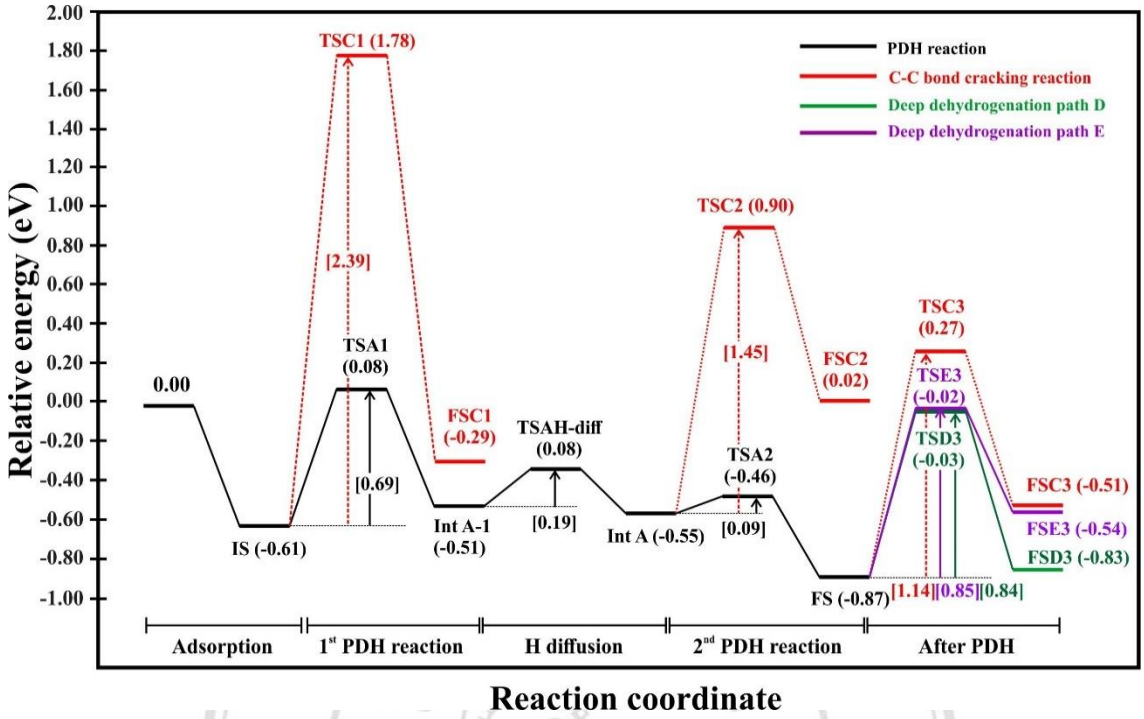

Figure 3.11 Energy profiles of dehydrogenation (—) and side reactions including cracking reaction (—) and the deep dehydrogenation of propylene (— and —)

The next possible cracking is the C-C bond cracking of 1-proply (step 2C), the cracking starts with the elongation of C^1-C^2 bond of Int A from 1.53 Å to 2.17 Å in TSC2 to form stable methylidene (CH_2^*) and ethylene ($CH_3CH_2^*$) species on hcp and atop sites of Ni(111) surface (FSC2), respectively. The E_a of C^1-C^2 bond activation of 1-propyl on Ni(111) is 1.45 eV which is higher than the energy barrier of the second dehydrogenation (step 2A) on Ni(111) surface (0.09 eV). The C-C cracking along 2C is less preferable than the 1-propyl dehydrogenation (step 2A). Another possible side reaction is the C-C bond cracking of 2-propyl (step 2C′ in Scheme 1). This C-C cracking through 2C′ is the side reaction of 2-propyl dehydrogenation (step 2B). As shown in Figure 3.9, the C-C bond cleavage begins with stretching of C2-C3 bond of Int B from 1.52 Å to 2.08 Å in TSC′2 to generate methyl (CH_3^*) and ethylidene (CH_3CH^*) which are adsorbed on fcc and hcp sites of Ni(111) surface (FSC′2), respectively. In Table 3.3, the E_a of 2-propyl cracking is 0.90 eV which is much higher than the energy barrier of the second dehydrogenation (step 2B) on Ni(111) surface (0.05 eV). For the C-C bond cracking of propylene (3C), the C^1-C^2 bond of propylene can be activated to form methylidene (CH_2^*)

and ethylidene (CH_3CH^*) adsorbed on the hcp sites on Ni(111) surface (FSC3). The activated C^1-C^2 bond of FS is prolonged from 1.43 Å to 2.05 Å with the E_a of 1.16 eV.

From overall C-C bond cracking reactions along pathway A, the activation energies of C-C bond cracking decrease in this following order: $CH_3CH_2CH_3$ > $CH_3CH_2CH_2^*$ > $CH_3CH\,CH_2^*$ which are in accordance with removal of H can enhance the interaction between C and Ni atoms due to less steric effect. This feature leads to weakening of C-C bond of adsorbed 1-propyl and propylene on Ni(111) surface resulting in lower cracking barrier along PDH process [128, 129]. Although the energy barriers of C-C bond cracking trend to decrease along PDH reaction to produce propylene, the lowest energy barrier C-C bond cracking which is located as the competitive reaction with desorption and deep dehydrogenation of propylene is still high (around 1.14 eV). Hence, this work can confirm that the C-C bond cracking cannot be taken place during PDH process. This result is in good agreement with C-C bond cracking on Pt(111) surface [48]. The C-C bond cracking in Pt(111) is more favorable over the deep hydrogenation after propyne formation.

3.2.4.2 Deep Dehydrogenation Mechanism on Ni(111) Surface

For the deep dehydrogenation, the strong adsorption of propylene on Ni(111) surface causes the further reactions of deep dehydrogenation to form 1-propenyl ($CH_3CH\,CH^*$) and 2-propenyl ($CH_3CCH_2^*$) via step 3D and step 3E, respectively. The first deep dehydrogenation of FS initiates from C^1-$H_1^{'}$ bond activation to form 1-propyenyl (step 3D in Figure 1.4). As illustrated in Figure 3.10, the activated C^1-$H_1^{'}$ bond of TSD3 is lengthened from 1.43 Å to 1.76 Å, requiring E_a of 0.84 eV. The detached $H_1^{'}$ atom is adsorbed on fcc site on Ni(111) surface (FSD3). Another deep dehydrogenation starts with C^1-$H_2^{'}$ bond activation of propylene to form 2-propenly on Ni(111) surface (step 3E). The activated C^1-$H_2^{'}$ bond of TSE3 is elongated from 1.43 Å to 1.62 Å with the E_a of 0.85 eV. The detached $H_2^{'}$ atom is also adsorbed on fcc site of Ni(111) surface (FSE3). Both deep dehydrogenations via step 3D and step 3E are possible because their E_a values are less than 1 eV [130].

According to our PES results, step 1A and step 2A are kinetically and thermodynamically favorable for PDH reaction on Ni(111) as summarized Table 3.3.

This PDH pathway also preferable than the cracking side reaction via TSC1 and TSC2. However, the E_a of propylene desorption (1.16 eV) are almost the same of the E_a of propylene cracking (1.14 eV) after PDH process. The E_a of C-C cracking comparable with that of the product desorption. Moreover, the energy barrier of deep dehydrogenation via step 3D and step 3E are 0.84 eV and 0.85 eV, respectively, which are lower than that of propylene desorption and C-C cracking. Therefore, the adsorbed propylene is preferable undergoing the deep dehydrogenation than desorption to wanted propylene. These results describe the low selectivity of propylene production using Ni(111) surface reported in previous experimental studies [58]. In Pt(111) surface, the E_a of propylene desorption is 0.97 eV, which is higher than that of deep dehydrogenation (about 0.76 eV) but lower than that of propylene cracking (2.00 eV) [48].

3.3 Summary

In summary, the insight mechanisms of PDH as well as side reactions of deep dehydrogenation of propylene and C-C bond cracking on Ni(111) and Pt(111) can be compared as follows:

i) Similar adsorption behavior of propane and propylene adsorption on Ni(111) and Pt(111) can be observed. For instance, propane shows the physisorption interaction, while propylene forms strong chemical interaction (chemisorption) with those catalyst surfaces.

ii) For the main PDH reaction, the C-H activation of propane to be 1- and 2-propyl on Pt(111) are 0.65 and 0.75 eV, respectively proposed by Yang and co-workers [48]. In contrast, the PDH reaction on Ni(111) via 1-propyl, pathway A, is obviously the most kinetically and thermodynamically preferable. After the first H is dissociated, the second dehydrogenation occurs easily with low E_a (< 0.1 eV).

iii) The C-C bond cracking is less preferable than the main dehydrogenation in both Ni(111) and Pt(111). It is to be noted that the C-C cleaving processes (*i.e.* steps 1C, 2C, 2C' and 3C) on Ni(111) in this work require less activation energies than those in Pt(111) [48].

iv) After propylene formation, the deep hydrogenation is the most preferable process compared to propylene desorption and C-C cracking in both Ni(111) and Pt(111). This feature results in low selectivity of propylene production in both catalysts.

v) Zha and co-workers [102] proposed that the first C-H activation is the rate-controlling step on Pt-based catalysts. They also suggested that propylene desorption plays an important role the key roles on activity and selectivity of PDH on Pt-based catalysts. The findings of this work also suggested similar conclusion that the first C-H activation and enhancement of propylene adsorption are the key roles affecting on activity and selectivity of PDH in Ni.

Therefore, suppressing propylene-Ni(111) interaction can enhance the selectivity of propylene production. In literature, increment the H coverage on the catalyst surface has been suggested for enhancing propylene desorption and also decrease the further deep hydrogenation on Pt(111) [131]. Moreover, improvement of PDH in Pt can be achieved by alloying Pt with other elements such as In and Sn [102]. In Ni catalyst, improvement of propylene production was observed in Ni-Au [96]. The understanding of PDH on the in Pt(111) surface serves as a good guidance for developing the efficiency of Ni-based catalyst for PDH reaction.

CHAPTER 4

Effect of Au Doping on Selectivity Improvement of Propylene Production via PDH Reaction

To improve the efficiency of Ni-based catalyst, doping another metal is one of simple method to increase the selectivity of propylene production is doping another effective metal into bare Ni surface. Recently, Au doping shows interesting experimental result of significant enlargement of propylene production on Ni surface proposed by Yan and the coworkers [58, 96]. However, the role plays of Au doping for selectivity improvement are still controversial. In this section, the effects of Au doping for selectivity enhancement of propylene production are systematically studied by computational investigation of PDH and other side reactions on Ni-Au/Ni(111) surfaces.

4.1 Slab Information

In Chapter 3, the Ni(111) surface is selected to explore the limitation of Ni catalyst on low propylene selectivity. To improve the performance of Ni(111) catalyst, doping of Au into Ni(111) surface to form Ni-Au/Ni(111) is constructed. Furthermore, the effects of Au loading for properties change in terms reactivity of catalyst and selectivity of propylene product are also investigated. So, the Ni-Au/Ni(111) surfaces were constructed by substitutions of Au into the first layer of Ni(111) with the atomic ratios of 1/3 and 1/2 are selected to create Ni_3Au/Ni(111) and Ni_2Au/Ni(111) surfaces. The stable alignments of Au atom of Ni_3Au/Ni(111) as well as Ni_2Au/Ni(111) surfaces are referred to the most stable configuration of 0.25 and 0.33 monolayer equivalent of Ni-Au/Ni(111) surfaces which were reported by Celik [132] as illustrated in Figure 4.1. So, the Ni-Au/Ni(111) surfaces compose of three atomic layers of Ni atom and one atomic layer of mix Au and Ni atoms as ratios of 1/3 and 1/2 for Ni_3Au/Ni(111) and Ni_2Au/Ni(111), respectively. Moreover, the 15 Å of artificial vacuum slab was introduced along z-axis to avoid the interaction between periodic images. The possible active sites of Ni-Au/Ni(111) surfaces are depicted in Figure 4.1c and 4.1f for Ni_3Au/Ni(111) and Ni_2Au/Ni(111), respectively.

There are atop sites of Ni and Au, bridge sites of Ni-Ni and Ni-Au, fcc site of Ni-Au-Ni, hcp site of Ni-Au-Ni as well as three fold site of Ni_3Au/Ni(111) surface; fcc site of Ni-Ni-Ni and hcp of Ni-Ni-Ni.

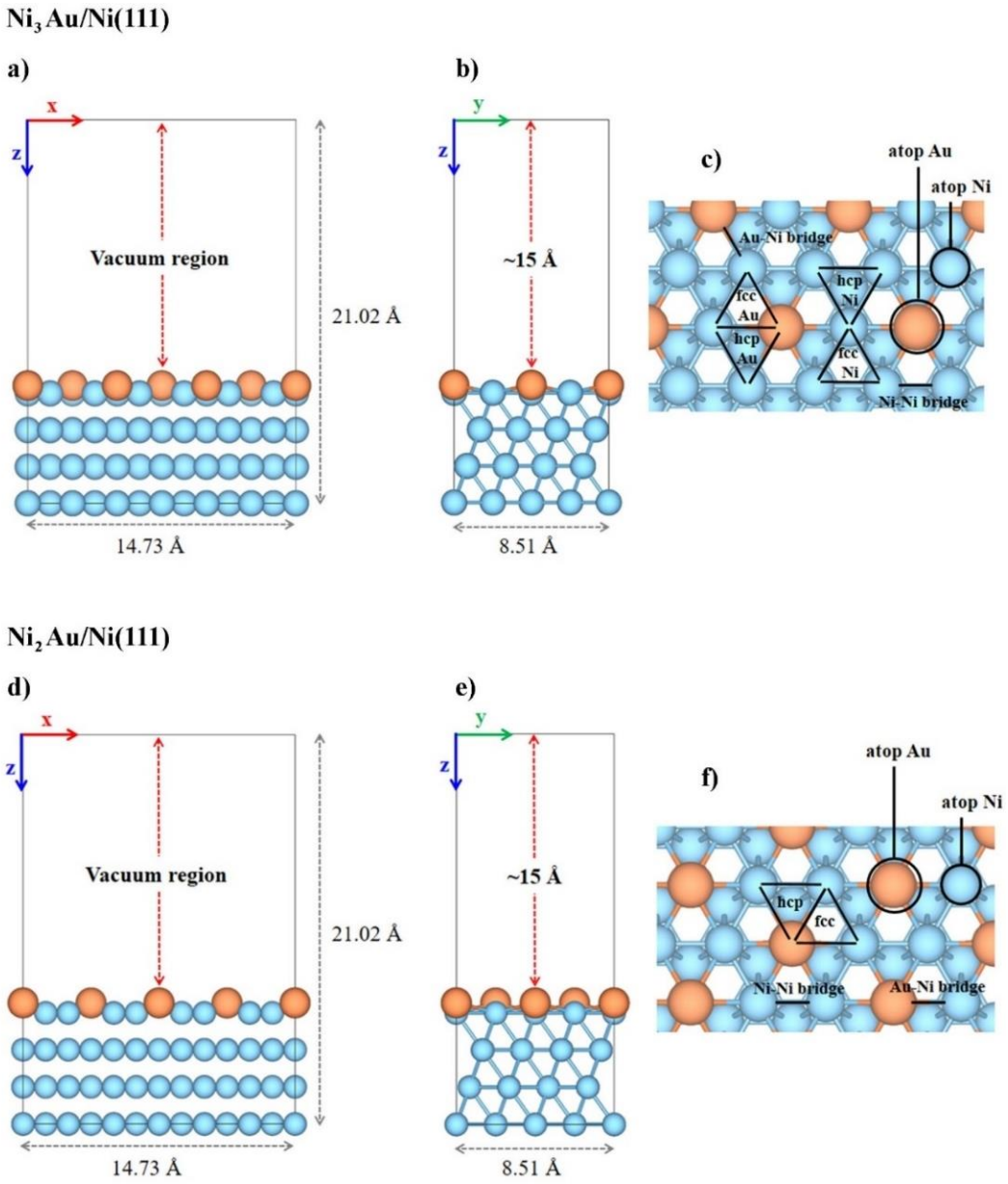

Figure 4.1 Unit cells of Ni_3Au/Ni(111) and Ni_2Au/Ni(111) projected along (a,d) the (010)-direction, (b,e) (100)-direction, and (c,f) the possible active sites on the Ni_3Au/Ni(111) and Ni_2Au/Ni(111) surfaces

During geometry optimization, two bottom layers of the slab were kept fixed to their bulk structure while two upper layers of Ni-Au/Ni(111) surfaces, together with the adsorbed species were allowed to fully relaxed.

4.2 Results and Discussion

4.2.1 Role of Au Doping for Propane and Propylene Adsorptions

The interactions between adsorbed propane and propylene on Ni-Au /Ni(111) surfaces, $Ni_3Au/Ni(111)$ and $Ni_2Au/Ni(111)$, are illustrated in Figure 4.2a and 4.2b and their corresponding E_{ads}, bond length and adsorbed position are summarized in Table 4.1. For propane adsorptions, a propane molecule prefers to be physiosorbed on both $Ni_3Au/Ni(111)$ and $Ni_2Au/Ni(111)$ surfaces with the E_{ads} of -0.59 and -0.58 eV, respectively. The most stable adsorption configuration of propane adsorption exhibits the parallel direction of adsorbed propane along with catalyst surfaces of $Ni_3Au/Ni(111)$ and $Ni_2Au/Ni(111)$. The adsorption height between the adsorbed propane and Ni-Au/Ni(111) surfaces is measured by the shortest distance between H atom of propane and Ni atom of Ni-Au/Ni(111) surfaces denoted as the H^2-Ni^2 interactions which are 2.41 and 2.50 Å for $Ni_3Au/Ni(111)$ and $Ni_2Au/Ni(111)$, respectively. For propylene adsorption, the most stable adsorption configuration shows that C^2 and C^3 atoms of propylene prefer to adsorb on atop of Ni^2 atom of $Ni_3Au/Ni(111)$ and $Ni_2Au/Ni(111)$ with the E_{ads} of -0.96 and -0.84 eV, respectively. The adsorption height of propylene on $Ni_3Au/Ni(111)$ and $Ni_2Au/Ni(111)$ surfaces are not significantly different (2.10 and 2.09 Å for $Ni_3Au/Ni(111)$ and $Ni_2Au/Ni(111)$, respectively). In this section, doping Au atoms in to Ni(111) surfaces has no effect for propane adsorption because the E_{ads} is not significantly different from that of Ni(111) surface (-0.60 eV) [133]. However, modification of Ni(111) surface by Au doping reduces the adsorption strength of propylene. Moreover, increasing Au composition also decreases the adsorption strength of propylene. The results of adsorption height indicate that addition of Au hinders adsorption of propylene on catalyst surface because all propane and propylene molecules avoid interacting with Au atom.

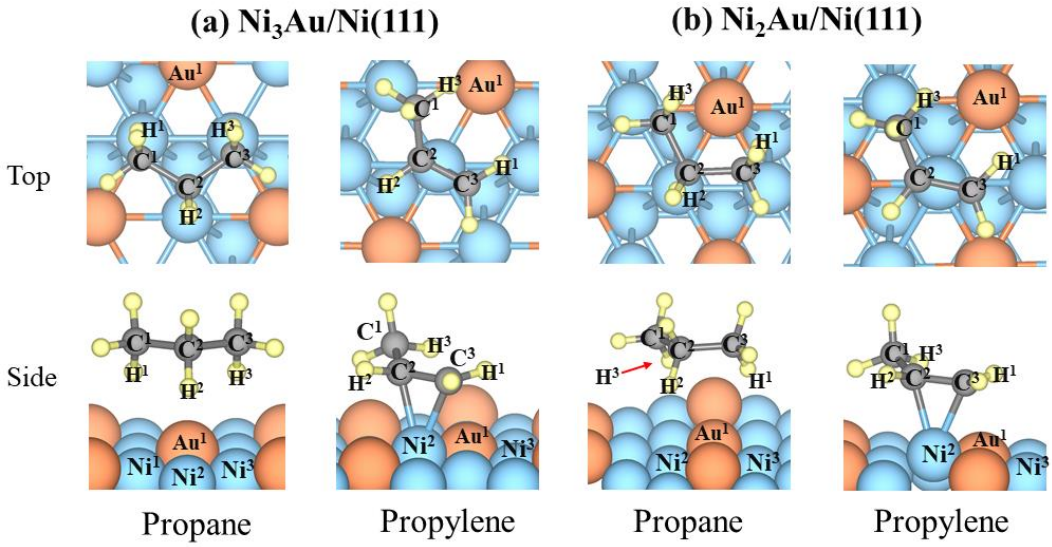

Figure 4.2 Adsorption configurations of propane and propylene on (a) $Ni_3Au/Ni(111)$ and (b) $Ni_2Au/Ni(111)$ surfaces

Table 4.1 Adsorption energies (E_{ads}) in eV and atomic distances (d) in Å of propane and propylene on $Ni_3Au/Ni(111)$ and $Ni_2Au/Ni(111)$ surfaces

Surface	Species	E_{ads} (eV)	Favored site	$d_{C\text{-}Ni}$ (Å)	$d_{H\text{-}Ni}$ (Å)	$d_{H\text{-}Au}$ (Å)	$d_{C\text{-}C}$ (Å)	$d_{C\text{-}H}$ (Å)
$Ni_3Au/Ni(111)$	**Propane**	-0.59	atop of Ni	C^1-Ni^1 = 3.48 C^2-Ni^2 = 3.45 C^3-Ni^3 = 3.46	H^1-Ni^1 = 2.64 H^2-Ni^2 = 2.41 H^3-Ni^3 = 2.64	H^1-Au^1 = 3.22 H^3-Au^1 = 2.64	C^1- C^2 = 1.52 C^2- C^3 = 1.52	C^1-H^1 = 1.11 C^2-H^2 = 1.11 C^3-H^3 = 1.11
	Propylene	-0.96	atop of Ni and hcp	C^2-Ni^2 = 2.12 C^3-Ni^2 = 2.10		H^1-Au^1 = 3.16 H^3-Au^1 = 2.83	C^1- C^2 = 1.50 C^2- C^3 = 1.40	
$Ni_2Au/Ni(111)$	**Propane**	-0.58	atop of Ni	C^1-Ni^1 = 3.67 C^2-Ni^2 = 3.50 C^3-Ni^3 = 3.50	H^1-Ni^1 = 3.02 H^2-Ni^2 = 2.50 H^3-Ni^3 = 2.98	H^1-Au^1 = 3.09 H^3-Au^1 = 3.02	C^1- C^2 = 1.53 C^2- C^3 = 1.53	C^1-H^1 = 1.10 C^2-H^2 = 1.11 C^3-H^3 = 1.11
	Propylene	-0.84	atop of Ni and Ni-Ni bridge	C^2-Ni^2 = 2.12 C^3-Ni^2 = 2.09		H^1-Au^1 = 2.96 H^3-Au^1 = 3.07	C^1- C^2 = 1.50 C^2- C^3 = 1.40	

4.2.2 Electronic Property of Propane and Propylene on Ni-Au/Ni(111) Surfaces

To understand the interaction of propane/propylene on Ni_3Au/Ni(111) and Ni_2Au/Ni(111) surfaces as well as the role of Ni and Au atoms during adsorption process, charge analyses such as charge density difference, and Bader charge are discussed in this section.

4.2.2.1 Charge Density Difference and Bader Charge Analysis

The interaction between H atom of propane and Ni atom of Ni-Au/Ni(111) surfaces (H^2-Ni^2 interactions) as well as C atoms of propylene and Ni atom of Ni-Au/Ni(111) surfaces (C^2-Ni^1 and C^3-Ni^1 interactions) during adsorption process are well described by charge density different as illustrated in Figure 4.3. The charge accumulation and charge depletion are depicted as the green and red contours, respectively. Moreover, a number of charge gaining and charge disappearing of adsorbed molecules and Ni-Au/Ni(111) surfaces are quantitively calculated by Bader charge analysis [125, 134] which are summarized in Table 4.2.

As clearly seen from Figure 4.3, charge density differences of propane and propylene adsorption on both Ni_3Au/Ni(111) and Ni_2Au/Ni(111) surfaces are not significantly different. For propane adsorption, charge depletion at H^2 indicates the interaction between H^2 position of propane and Ni-Au/Ni(111) surface. Moreover, the small contour of charge density difference reveals the weak adsorption interaction between propane and Ni-Au/Ni(111) surface (physisorption) as discussed in the adsorption section. For propylene adsorption, the green contour of charge accumulation noticeably appears at the Ni^2 of Ni-Au/Ni(111) surfaces and the red contour of charge depletion of C^2-C^3 bond of adsorbed propylene expresses that propylene adsorbs on Ni-Au/Ni(111) surfaces by creating Ni^2-C^2 and Ni^2-C^3 bond formations. The large area of charge different contour illustrates chemisorption of propylene on Ni-Au/Ni(111) surface.

The Bader charge results show the charge transfer from bare Ni-Au/Ni(111) surfaces to adsorbed molecules (~0.25 |e| to 0.27 |e| for propane adsorption and ~0.30|e| to 0.33|e| for propylene adsorption). These results indicate that Ni-Au/Ni(111) surfaces are electron donor while the adsorbed molecules are electron acceptor. Moreover, the

interaction between Ni-Au/Ni(111) surfaces and adsorbed propane mainly appears only at Ni^2-H^2 interaction while the major interaction between Ni-Au/Ni(111) surfaces and adsorbed propylene is observed at the double bond of C^2-C^3 of adsorbed propylene connecting to Ni^2 of Ni-Au/Ni(111) surface. Comparing with our previous study [133], the adsorbed propane shows three adsorption interactions with three nearest Ni atoms while the propylene also has four bonds connection with three Ni atoms on Ni(111) surface. Substitution of Au into Ni(111) surface decreases the electron donor site of Ni atom leading to weakening the adsorption interaction between molecules and surface particularly propylene-Ni-Au/Ni(111) and promoting the easy desorption of wanted propylene from Ni-Au/Ni(111) surface.

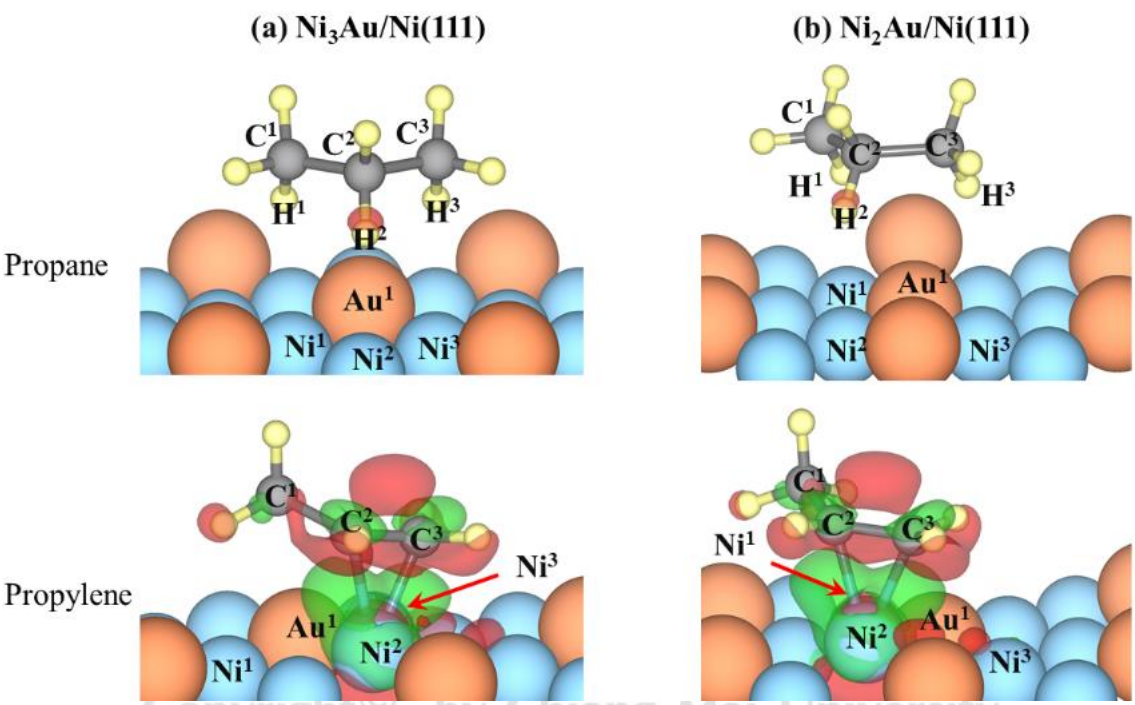

Figure 4.3 Charge density differences of propane and propylene adsorption differences (green for charge accumulation and red for charge depletion) on (a)-(b) $Ni_3Au/Ni(111)$ and (c)-(d) $Ni_2Au/Ni(111)$ with the isovalue of ±0.003 e $Å^{-3}$

Table 4.2 Bader charge analyses (charge gaining (+) and charge losing (-)) of propane and propylene adsorption on $Ni_3Au/Ni(111)$ and $Ni_2Au/Ni(111)$ surfaces

System	Bader charge change|e|					
		Surface		Adsorbed molecule		
		$Ni_3Au/Ni111$	$Ni_2Au/Ni111$		propane	propylene
	Total	(+0.00)	(+0.00)	Total	(+0.00)	(+0.00)
	Top layer	+0.90	+1.36	C^1	+0.18	-0.19
Isolated	Ni@Toplayer	-0.96	+0.26	C^2	-0.22	-0.10
phase	Au@Toplayer	+1.86	+1.10	C^3	+0.16	-0.11
	Ni^1	+0.01	-0.10	H^1	-0.05	
	Ni^2	-0.12	+0.15	H^2	-0.05	
	Ni^3	-0.28	+0.15	H^3	-0.04	
	Au^1	+0.31	+0.17			
		Surface		Adsorbed propane		
		$Ni_3Au/Ni111$	$Ni_2Au/Ni111$		$Ni_3Au/Ni111$	$Ni_2Au/Ni111$
	Total	-0.27	-0.25	Total	+0.27	+0.25
	Top layer	+0.64	+0.45	C^1	-0.39	-0.14
Propane	Ni@Toplayer	-0.64	-0.90	C^2	-0.17	-0.27
adsorption	Au@Toplayer	+1.28	+1.34	C^3	-0.38	-0.16
	Ni^1	+0.03	+0.03	H^1	+0.30	+0.08
	Ni^2	+0.23	-0.01	H^2	+0.08	+0.13
	Ni^3	-0.04	+0.04	H^3	+0.23	+0.09
	Au^1	+0.20	+0.10			
		Surface		Adsorbed propylene		
		$Ni_3Au/Ni111$	$Ni_2Au/Ni111$		$Ni_3Au/Ni111$	$Ni_2Au/Ni111$
	Total	-0.33	-0.30	Total	+0.33	+0.30
	Top layer	+1.06	+0.59	C^1	-0.52	-0.64
Propylene	Ni@Toplayer	-0.28	-1.04	C^2	+0.08	+0.11
adsorption	Au@Toplayer	+1.34	+1.62	C^3	-0.38	-0.78
	Ni^1	-0.06	-0.18			
	Ni^2	-0.09	-0.12			
	Ni^3	+0.23	-0.12			
	Au^1	+0.44	+0.16			

4.2.2.2 DOS Analysis

The interactions between propane/propylene on Ni-Au/Ni(111) surfaces as well as bond formation between atoms of adsorbed molecules and catalyst surfaces were investigated by PDOSs analysis. The PDOSs of isolated (propane, propylene and bare Ni-Au/Ni(111) surfaces) and adsorbed (adsorbed propane, propylene and Ni-Au/Ni(111) surfaces) systems are plotted in Figure 4.4a to 4.4d. The bonding (positive) and anti-bonding (negative) regions are separated by E_F at 0 eV. The density of states (DOSs) of H and C atoms of propane and propylene which are near to Ni atom of Ni-Au/Ni(111) surfaces are projected into the s-state and p-state, respectively. In addition, the DOSs of Ni is projected into d-state. The PDOSs of isolated propane and propylene are expressed in panel I while PDOSs of adsorbed propane and propylene are presented in panel II. Moreover, the d-DOS of Ni of Ni-Au/Ni(111) surfaces is plotted in panel III.

For isolated system of molecules (panel I) and bare surfaces (panel III), overlapping between s-DOS of H atoms and p-DOS of C atoms displays the C-H bond of propane and propylene molecules. For Ni-Au/Ni(111) surfaces, the reactivities of bare Ni-Au/Ni(111) are well described by shifting of ε_d. Herein, the ε_d values of Ni_3Au/Ni(111) and Ni_2Au/Ni(111) are 1.54 and 1.58 eV, respectively which are shifted further away from the E_F than that of Ni(111) surface (1.43 eV) [133]. This result indicates that doping Au and increasing amount of Au into Ni(111) surface significantly retard the reactivity of Ni-Au/Ni(111) catalysts.

For the adsorbed system of molecules (panel II) and Ni-Au/Ni(111) surfaces (panel III), shifting of s-DOSs of H^2 of adsorbed propane exhibits the interactions between propane and Ni-Au/Ni(111) surface. However, unchanged d-DOSs of associated Ni atoms on both Ni_3Au/Ni(111) and Ni_2Au/Ni(111) surfaces in propane adsorption system indicate that interaction between propane and Ni-Au/Ni(111) surface is weak interaction. For propylene adsorption, d-DOS peaks of Ni atom of Ni-Au/Ni(111) surface in propylene adsorption system appear in the range of -8.0 to -6.0 eV in panel III.

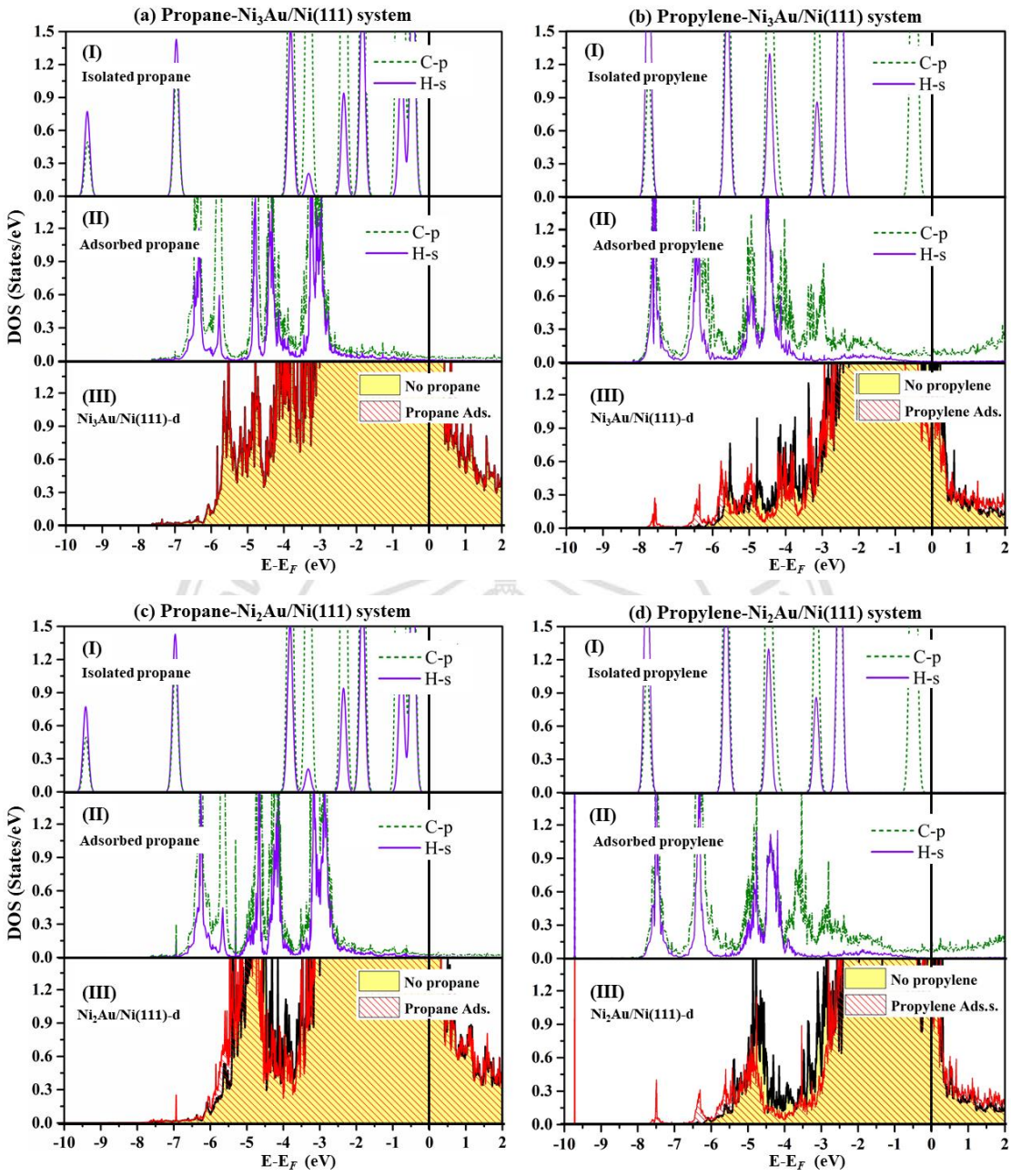

Figure 4.4 Projected density of state (PDOS) of propane and propylene adsorption on $Ni_3Au/Ni(111)$ (a),(b) and $Ni_2Au/Ni(111)$ (c),(d) systems, where I, II and III representing isolated molecule, adsorbed molecule, and surfaces (before and during adsorption), respectively

Furthermore, the interactions of propane/propylene on Au atom on Ni-Au/Ni(111) surfaces are also considered by DOS analysis as shown in Figure 4.5. The plots of s- and p-DOS of H atom and C atom of adsorbed propane are shown in panel I while the s- and p-DOS of adsorbed propylene are displayed in panel II. Moreover, the panel III illustrates

the d-DOS of the nearest Au atom on Ni-Au/Ni(111) surface in isolated and adsorbed systems. It is obviously seen that the d-DOS of Au after propane and propylene adsorption are not significantly different from that of isolated Au atom both in Ni_3Au/Ni(111) and Ni_2Au/Ni(111) surfaces indicating that adsorption of propane and propylene on Ni-Au/Ni(111) surface is generated by the adsorbed molecules-Ni without adsorbed molecules-Au interaction. Doping Au into Ni(111) surface plays the poisoning role to weaken the interaction between adsorbed molecule and the surface, particularly propylene-catalyst interaction. This result is in good agreement with diminishing E_{ads} of propylene on Ni-Au/Ni(111) compared with Ni(111) surface in the adsorption section (4.2.1).

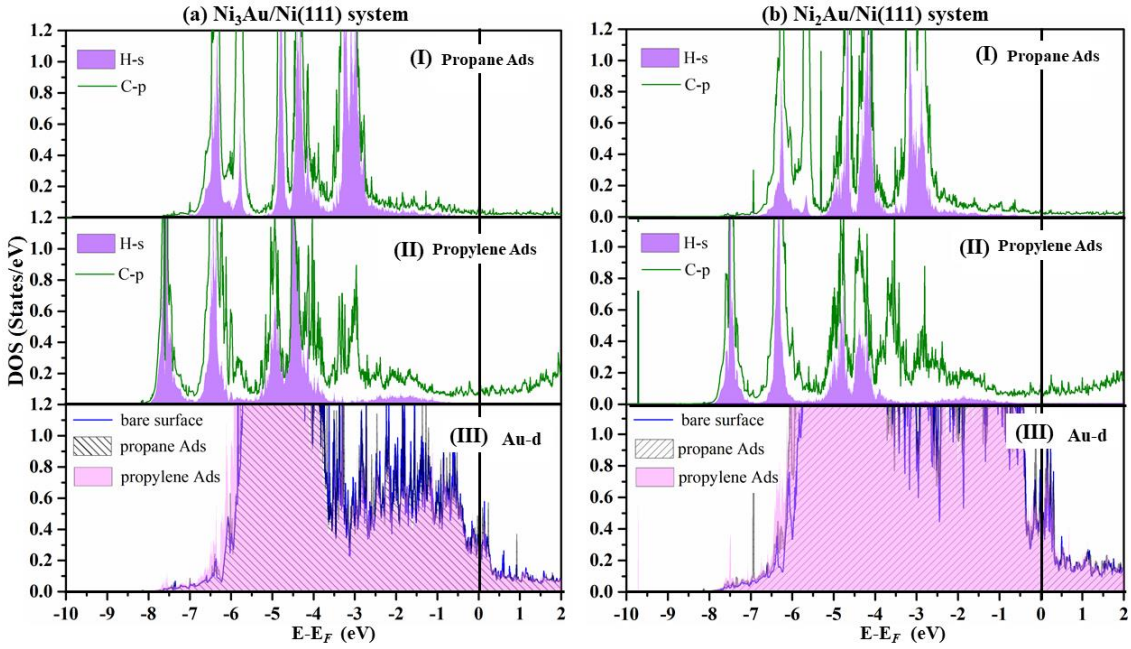

Figure 4.5 Projected density of state (PDOS) of propane and propylene adsorption on Au atom of Ni_3Au/Ni(111) (a) and Ni_2Au/Ni(111) (b) systems, where I, II and III representing isolated molecule, adsorbed molecule, and surfaces (before and during adsorption), respectively

4.2.3 Effect of Au Concentration on PDH Reaction on Ni-Au/Ni(111) Surfaces

The details of reaction mechanism of PDH on Ni-Au/Ni(111) surfaces are discussed in this section. The PDH reactions on Ni_3Au/Ni(111) and Ni_2Au/Ni(111) surfaces are noted as pathway A and pathway B, respectively. The geometries of IS, transition state structures (TSA1, TSA2, TSB1 and TSB2), intermediates (INTA and

INTB) and final state structures (FSA and FSB) are displayed in Figure 4.6a and 4.6b, respectively. Moreover, the activation energies of each elementary step on Ni(111), Ni_3Au/Ni(111) and Ni_2Au/Ni(111) surface are summarized in Table 4.3.

According to our previous investigation [133], the transformation of propane to be propylene can be taken place via two reaction steps: the first step is dehydrogenation of propane to be 1-propyl intermediate and the second step is dehydrogenation of 1-propyl intermediate to be propylene which is adsorbed on Ni-Au/Ni(111) surfaces. The reaction pathways of PDH on Ni_3Au/Ni(111) and Ni_2Au/Ni(111) are noted to be pathway A (blue line) and pathway B (black line), respectively which are plotted in Figure 4.7. The adsorbed propane configurations are defined as IS. For PDH reaction on Ni_3Au/Ni(111) surface, the first PDH reaction starts with detaching of H^1 atom of propane to the three-folds hollow site of three Ni atoms to transform adsorbed propane to be 1-propyl intermediate (FSA1) via transition state (TSA1) with the E_a of 1.48 eV. Then, the second PDH reaction is taken place to transform propyl intermediate to be propylene (FSA2) through TSA2 by detaching H^2 atom of propyl to the nearest fcc hollow site between three Ni atoms of Ni_3Au/Ni(111) surface with the E_a of 0.91 eV.

For PDH reaction on Ni_2Au/Ni(111) surface, transformation of adsorbed propane to 1-propyl intermediate (FSB1) can be accomplished via TSB1 with the E_a of 1.55 eV in the first PDH reaction. Subsequently, the 1-propyl intermediate continues with dehydrogenating to form propylene (FSB2) by detaching H^2 of adsorbed propyl with the E_a of 0.97 eV. For the overall PDH reactions on both Ni_3Au/Ni(111) and Ni_2Au/Ni(111) surfaces, the 1^{st} dehydrogenation of propane to form 1-propyl intermediate is the rate determining step. Comparison of PDH on Ni_3Au/Ni(111) and Ni_2Au/Ni(111) surfaces illustrates that increasing amount of Au into Ni(111) increases all energy barriers of PDH reaction as seen in pathway B of PDH reaction. These results indicate that increment of Au concentration suppresses the reactivity of Ni(111) surface for PDH reaction which is in accordance with the study by Yan and co-workers [96].

PDH mechanism on Ni_3Au/Ni(111)

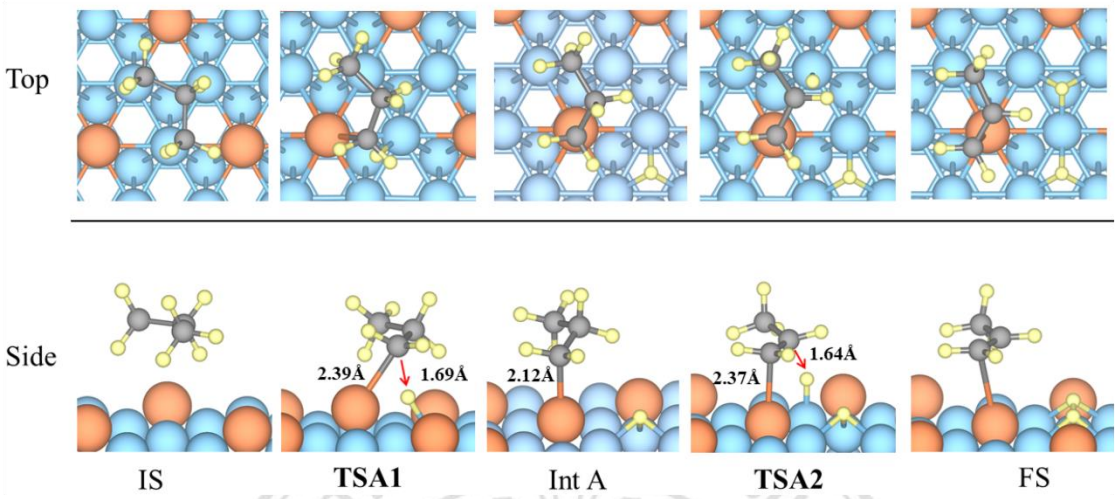

PDH mechanism on Ni_2Au/Ni(111)

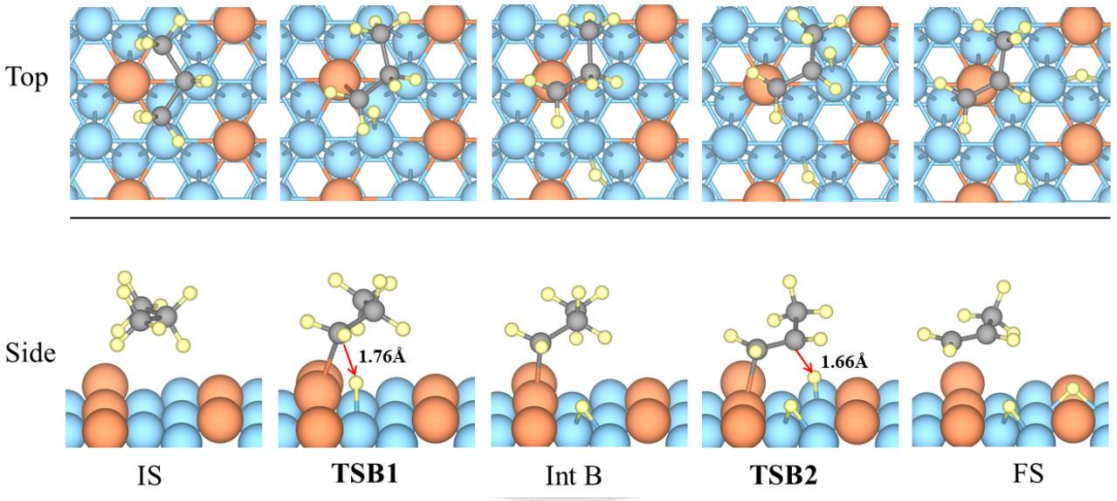

Figure 4.6 Optimized geometries of initial state (IS), transition state (TS) intermediate (Int) and final state (FS) structures of PDH reaction via Ni_3Au/Ni(111) and Ni_2Au/Ni(111) surfaces

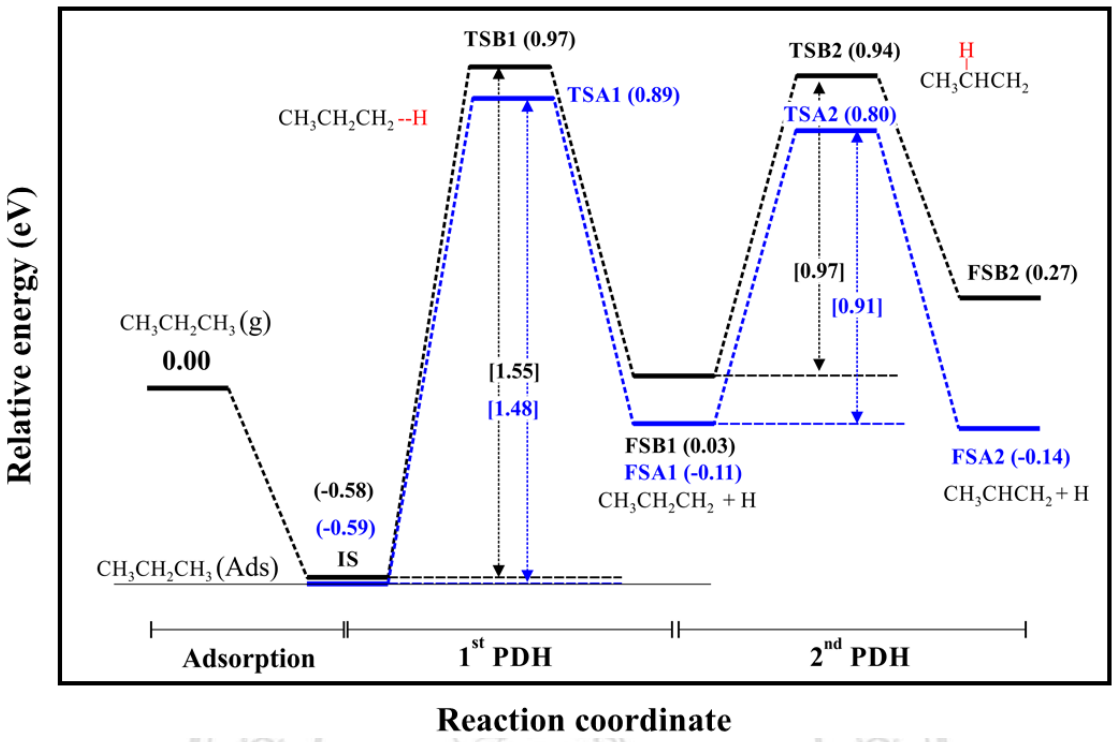

Figure 4.7 Potential energy profiles of PDH reaction on $Ni_3Au/Ni(111)$ (blue line) and $Ni_2Au/Ni(111)$ surfaces (black line)

Table 4.3 Activation energies (Ea) in eV of PDH, C-C cracking and deep dehydrogenation reactions on Ni(111), $Ni_3Au/Ni(111)$ and $Ni_2Au/Ni(111)$ surfaces

Reaction	Elementary step	Activation energy (E_a)		
		Ni(111)[133]	$Ni_3Au/Ni(111)$	$Ni_2Au/Ni(111)$
PDH	$CH_3CH_2CH_3 \longrightarrow CH_3CH_2CH_2^* + H^*$	0.69	1.48	1.55
	$CH_3CH_2CH_2^* \longrightarrow CH_3CH\,CH_2^* + H^*$	0.05	0.91	0.97
C-C cracking	$CH_3CH_2CH_3 \longrightarrow CH_3CH_2^* + CH_3^*$	2.39	2.25	2.23
	$CH_3CH_2CH_2^* \longrightarrow CH_3CH_2^* + CH_2^*$	1.45	1.81	2.04
	$CH_3CH\,CH_2^* \longrightarrow CH_3CH^* + CH_2^*$	1.14	2.69	2.35
Deep dehydrogenation	$CH_3CH\,CH_2^* \longrightarrow CH_3CH\,CH^* + H^*$	0.84	1.45	1.33
	$CH_3CH\,CH_2^* \longrightarrow CH_3CCH_2^* + H^*$	0.85	1.76	1.48
Desorption	$CH_3CH\,CH_2^* \longrightarrow CH_3CH\,CH_{2\,(g)}$	1.16	0.67	0.73

The energy profiles of overall PDH, cracking and deep dehydrogenation reactions on $Ni_3Au/Ni(111)$ surface are exhibited in Figure 4.8. The PDH reaction to form propylene is drawn in blue line plot while the side reactions C-C bond cracking during PDH process (red line plot) as well as two possible deep dehydrogenation reactions after

PDH process (green and purple plots) are included. During PDH process (1st to 2nd PDH), the C-C bond cracking [48, 133, 135] is reported as two C-C cracking steps: One is C-C cracking of adsorbed propane to be methyl and ethyl (IS to FSC1) with the E_a of 2.25 eV. Another is cracking of 1-propyl intermediate to be methylidene and ethyl (IntA to FSC2) with the E_a of 1.81 eV. Overall E_a C-C bond cracking is higher than that of PDH reaction (~0.91-1.48 eV) indicating that transformation of propane to be propylene on $Ni_3Au/Ni(111)$ is possible without C-C cracking which is similar to our previous study of PDH reaction on Ni(111) surface [133]. After PDH process, side reactions of C-C bond cracking and deep dehydrogenation are investigated as the competitive reaction with propylene desorption.

For C-C bond cracking, the adsorbed propylene possibly undergoes to methylidene and then ethylidene (FSA2 to FSC3) with the E_a of 2.69 eV. For deep dehydrogenation of propylene, there are two possible pathways of transformation of propylene to 1-propenyl (FSA2 to FSD3) and 2-propenyl (FSA2 to FSE3) with the activation energies of 1.45 and 1.76 eV, respectively. For consideration of propylene desorption, the propylene can desorb from $Ni_3Au/Ni(111)$ surface with the desorption energy of 0.67 eV which is lower than those of side reactions after PDH process including propylene cracking and deep dehydrogenation reactions while the E_a of propylene desorption from Ni(111) surface is higher than those of side reactions after PDH process [133]. These results suggest that introduction of Au into Ni(111) surface helps the desorption of propylene from catalyst surface, leading to increasing of the selectivity of propylene production on Ni-Au catalyst [58, 96].

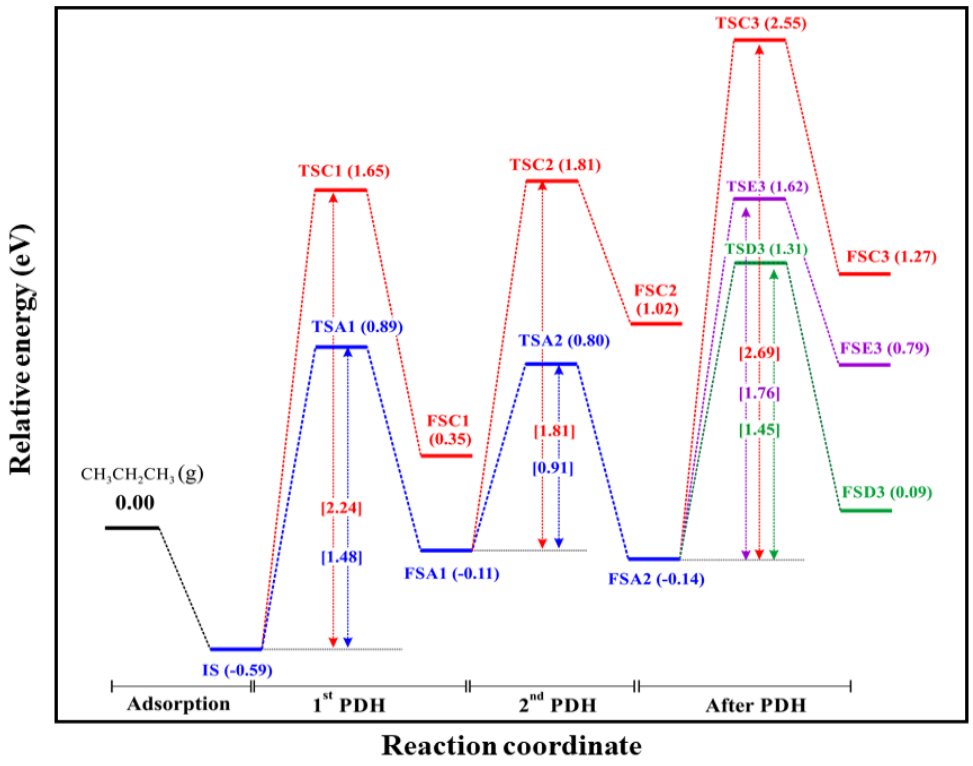

Figure 4.8 Energy profiles of PDH (blue line), C-C bond cracking (red line) and deep dehydrogenation (green line) and (purple line) reactions on $Ni_3Au/Ni(111)$ surfaces

4.2.4 Effect of Temperature on Propylene Selectivity on Ni-Au/Ni(111) Surfaces

To have more reliable information of mechanism study, the effect of temperature parameter in the PDH reaction rate is included in this path. For overall possible reaction steps of PDH reaction, there are two important processes that affect the production of propylene. One is the dehydrogenation of propane to form 1-propyl intermediate which is noted to be the rate determining step in previous section. Another is deep dehydrogenation of propylene after PDH process which generates undesired product reducing the selectivity of propylene production. The activation of the first PDH reaction and the deep dehydrogenation of propylene on Ni and Ni-Au/Ni(111) surfaces in the various temperature of 500 K to 1200 K are plotted in Figure 4.9a and 4.9b.

The activation energies of the 1st PDH reaction to form 1-propyl intermediate on Ni(111), $Ni_3Au/Ni(111)$ and $Ni_2Au/Ni(111)$ as a function of temperature are compared as shown in Figure 4.9a. In the temperature range of 500 to 1200K, the activation energies of the rate determining step of PDH reaction follow this order: $Ni_2Au/Ni(111)$ >

$Ni_3Au/Ni(111)$ > Ni(111) indicating that Ni(111) surface has the highest reactivity for PDH reaction followed by $Ni_3Au/Ni(111)$ and $Ni_2Au/Ni(111)$, respectively. For Ni(111) and $Ni_3Au/Ni(111)$ surfaces, the activation energies tend to decrease, 0.44 to 0.36 eV for Ni(111) and 0.78 to 0.61 eV for $Ni_3Au/Ni(111)$ surfaces, when the temperature is increased. On the other hand, the activation energies on $Ni_2Au/Ni(111)$ surface also tend to increase from 1.41 to 1.47 eV in the temperature range of 500 K to 1200K. These results indicate that larger amount of Au loading on Ni(111) diminishes the reactivity of Ni(111) surface for PDH reaction. Moreover, increment of the E_a on $Ni_2Au/Ni(111)$ surface is pronounced because introduction of Au into Ni(111) surface vanishes the 3Ni hollow site which is the active site for adsorbing the detached H atom, leading to higher E_a of PDH reaction. These results could well describe as losing the catalytic reactivity when increasing Au loading which is in line with experimental result reported by Yan and co-workers [96].

Another important process which greatly impacts the propylene desorption efficiency after PDH process is deep dehydrogenation of propylene. As previously discussed, two possible deep dehydrogenations are depicted in the Figure 4.8, however, the deep dehydrogenation via pathway D (FSA2 to FSD3) presents slightly lower barrier than that of another deep dehydrogenation (pathway E). Hence, deep dehydrogenation via pathway D is selected to further study and discuss in this section. The activation energies of forward and reverse reactions of deep dehydrogenation reactions are represented as filled and empty symbols, respectively as displayed in Figure 4.9b. For deep dehydrogenation on Ni(111) surface, insignificant deference between forward and reverse reactions indicates that the adsorbed propylene is possible to be dehydrogenated via deep dehydrogenation reaction which is competitive to propylene desorption after PDH process. For deep dehydrogenation on Ni-Au/Ni(111) surfaces, the activation energies of the forward reactions of deep dehydrogenation on both $Ni_3Au/Ni(111)$ and $Ni_2Au/Ni(111)$ surfaces are higher than that of the reverse reactions. The large difference between high E_a of forward reaction and low E_a of reverse reaction implies that deep dehydrogenations of propylene after PDH process on Ni-Au/Ni(111) are unfavorable to be continuously dehydrogenated. These results demonstrate that introduction of propylene is possible to impede occurrence of deep dehydrogenation of propylene after

PDH process, leading to enlargement of another pathway of propylene desorption after PDH process.

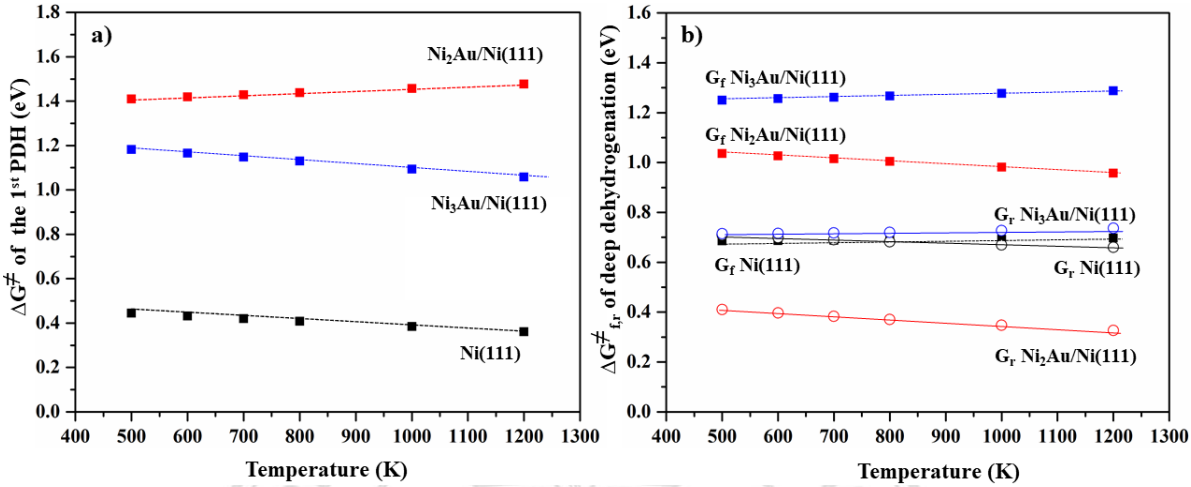

Figure 4.9 Activation energy of (a) the 1st PDH reaction and (b) deep dehydrogenation in the temperature range of 500 K to 1200K on Ni(111) (black line), $Ni_3Au/Ni(111)$ (blue line) and $Ni_2Au/Ni(111)$ surfaces (red line)

In addition, desorption of propylene from catalyst surface is also the key step for selectivity of propylene production. However, the side reactions after PDH process influence the desorption of propylene. Hence, kinetic simulation of PDH mechanism on Ni-Au/Ni(111) surfaces in this section will be focused on the 1st PDH reaction, propylene desorption and side reactions after PDH process.

4.2.5 Reaction Rate Constant of PDH Reaction on Ni(111) and Ni-Au/Ni(111) Surfaces

The information from energetic profile of PDH reaction describes which reactions from all proposed mechanism are possible to occur on Ni(111) as discussed in Chapter 3 for $Ni_3Au/Ni(111)$ and $Ni_2Au/Ni(111)$ surfaces. Among possible mechanisms (PDH and side reactions including C-C bond cracking and deep dehydrogenation) on Ni(111) and Ni-Au/Ni(111) surfaces, the side reaction of C-C bond cracking reaction is proven to be the most difficult to occur during PDH process. The K_{eq} of PDH and side reaction of deep dehydrogenation and C-C cracking in the temperature range of 500 K to 1200 K are summarized in Table 4.4 to 4.6. For Ni(111) system, the faster forward reaction of the 1st PDH reaction reveals that the adsorbed propane prefers to form 1-propyl intermediate. After the 1st PDH reaction, 1-propyl intermediate is possible to be continuously

dehydrogenated to form propylene. The 100 times faster of the 2nd PDH distinguishes the dehydrogenation of 1-propyl intermediate as kinetically favorable. After PDH process, there are three possible mechanisms of propylene desorption and the undesired side reactions of deep dehydrogenation and C-C cracking of propylene. By comparison of propylene desorption, deep dehydrogenation and C-C bond cracking reactions exhibit that the reaction rate follows this order: propylene desorption < C-C cracking < deep dehydrogenation. This order indicates that C-C cracking and deep dehydrogenation are more kinetically favorable than that of propylene desorption causing no propylene production on Ni(111) surface in the temperature range of 500 K to 1200K.

For Ni_3Au/Ni(111) system, the 10^5 to 10^3 times slower reaction of the 1st PDH indicates that existence of Au in the system reduces the reactivity of catalyst for PDH process. Increment of temperature increases the reaction rate of PDH reaction. However, the 1st PDH reaction is still thermodynamically unfavorable in the temperature range of 500 K to 1200K. Interestingly, the faster reaction rate of propylene desorption indicates that existence of Au improves the selectivity of propylene production.

For Ni_2Au/Ni(111) system, the 10^7 to 10^4 times slower reaction rate of the 1st PDH indicates that occurrence of PDH reaction on Ni_2Au/Ni(111) surface is kinetically unfavorable. Applying the temperature in higher temperature range slows down the reaction rate of PDH reaction as well as other reactions such as propylene desorption, deep dehydrogenation and C-C cracking. After PDH process, desorption of propylene is more possible to desorb from catalyst surface than to further undergo deep dehydrogenation and C-C bond cracking reaction because the K_{eq} of desorption is higher than those of deep dehydrogenation and C-C bond cracking reaction.

Comparison of the calculated reaction rate of PDH reaction on Ni(111) and Ni-Au/Ni(111) surfaces reveals that addition of Au significantly decreases the reactivity of Ni(111) surface for PDH reaction. However, by reducing of the reactivity Ni(111) surface with Au doping in turn improves the performance of propylene desorption and retards the side reactions of deep dehydrogenation and propylene cracking. These results are in good agreement with the experimental observation of selectivity improvement on Ni-Au surface which is reported by Yan and co-workers [58, 96]. Although Ni_2Au/Ni(111) exhibits highest desorption efficiency in terms of thermodynamic and

kinetic preferences, the energy barriers and reaction rate constants of the 1st PDH as the rate determining step illustrate that transformation of propane to form propylene on $Ni_2Au/Ni(111)$ surface is very difficult to occur. To compromise the catalytic activity for PDH reaction and selectivity of propylene production, the $Ni_3Au/Ni(111)$ surface alloy is suggested to be the best candidate for PDH.

Table 4.4 Equilibrium rate constants (K_{eq}) of PDH, propylene desorption and side reactions on Ni(111) from 500 K to 1200 K

Elementary step	Reaction	K_{eq}					
		500K	**600K**	**700K**	**800K**	**1000K**	**1200K**
$CH_3CH_2CH_3 \rightleftharpoons CH_3CH_2CH_2^* + H^*$	PDH	3.46×10^{0}	2.60×10^{0}	2.16×10^{0}	1.92×10^{0}	1.66×10^{0}	1.58×10^{0}
$CH_3CH_2CH_2^* \rightleftharpoons CH_3CHCH_2^* + H^*$		7.95×10^{3}	1.80×10^{3}	6.27×10^{2}	2.88×10^{2}	9.82×10^{1}	4.86×10^{1}
$CH_3CHCH_2^* \rightleftharpoons CH_3CHCH_{2\,(g)}$	Desorption	1.99×10^{-2}	7.22×10^{-1}	7.21×10^{0}	3.23×10^{1}	1.58×10^{2}	2.70×10^{2}
$CH_3CHCH_2^* \rightleftharpoons CH_3CHCH^* + H^*$	Deep dehydrogenation	1.75×10^{0}	1.29×10^{0}	1.05×10^{0}	9.12×10^{-1}	7.66×10^{-1}	6.96×10^{-1}
$CH_3CHCH_2^* \rightleftharpoons CH_3CCH_2^* + H^*$		2.98×10^{-3}	6.56×10^{-3}	1.17×10^{-2}	1.84×10^{-2}	3.52×10^{-2}	5.55×10^{-2}
$CH_3CHCH_2^* \rightleftharpoons CH_3CH^* + CH_2^*$	C-C cracking	3.64×10^{-2}	8.41×10^{-2}	1.57×10^{-1}	2.55×10^{-1}	5.21×10^{-1}	8.62×10^{-1}

Table 4.5 Equilibrium rate constants (K_{eq}) of PDH, propylene desorption and side reactions on $Ni_3Au/Ni(111)$ from 500 K to 1200 K

Elementary step	Reaction	K_{eq}					
		500K	**600K**	**700K**	**800K**	**1000K**	**1200K**
$CH_3CH_2CH_3 \rightleftharpoons CH_3CH_2CH_2^* + H^*$	PDH	5.22×10^{-5}	2.14×10^{-4}	5.96×10^{-4}	1.30×10^{-3}	3.97×10^{-3}	8.55×10^{-3}
$CH_3CH_2CH_2^* \rightleftharpoons CH_3CHCH_2^* + H^*$		1.19×10^{2}	7.08×10^{1}	4.99×10^{1}	3.89×10^{1}	2.82×10^{1}	2.32×10^{1}
$CH_3CHCH_2^* \rightleftharpoons CH_3CHCH_{2\,(g)}$	Desorption	8.98×10^{2}	4.13×10^{3}	1.07×10^{4}	1.95×10^{4}	3.66×10^{4}	4.54×10^{4}
$CH_3CHCH_2^* \rightleftharpoons CH_3CHCH^* + H^*$	Deep dehydrogenation	4.00×10^{-6}	2.91×10^{-5}	1.22×10^{-4}	3.61×10^{-4}	1.70×10^{-3}	4.88×10^{-3}
$CH_3CHCH_2^* \rightleftharpoons CH_3CCH_2^* + H^*$		2.98×10^{-5}	1.84×10^{-4}	6.84×10^{-4}	1.89×10^{-3}	8.03×10^{-3}	2.17×10^{-2}
$CH_3CHCH_2^* \rightleftharpoons CH_3CH^* + CH_2^*$	C-C cracking	1.84×10^{-14}	3.17×10^{-12}	1.28×10^{-10}	2.07×10^{-9}	1.04×10^{-7}	1.44×10^{-6}

Table 4.6 The equilibrium rate constants (K_{eq}) of PDH, propylene desorption and side reactions on $Ni_2Au/Ni(111)$ from 500 K to 1200 K

Elementary step	Reaction	K_{eq}					
		500K	**600K**	**700K**	**800K**	**1000K**	**1200K**
$CH_3CH_2CH_3 \rightleftharpoons CH_3CH_2CH_2^* + H^*$	PDH	4.39×10^{-7}	2.84×10^{-6}	1.11×10^{-5}	3.10×10^{-5}	1.36×10^{-4}	3.72×10^{-4}
$CH_3CH_2CH_2^* \rightleftharpoons CH_3CH\,CH_2^* + H^*$		3.01×10^{-1}	4.69×10^{-1}	6.52×10^{-1}	8.59×10^{-1}	1.29×10^{0}	1.73×10^{0}
$CH_3CH\,CH_2^* \rightleftharpoons CH_3CH\,CH_{2\,(g)}$	Desorption	1.10×10^{2}	6.76×10^{2}	1.89×10^{3}	3.26×10^{3}	4.19×10^{3}	2.93×10^{3}
$CH_3CH\,CH_2^* \rightleftharpoons CH_3CH\,CH^* + H^*$	Deep dehydrogenation	4.86×10^{-7}	5.10×10^{-6}	2.81×10^{-5}	1.02×10^{-4}	6.40×10^{-4}	2.24×10^{-3}
$CH_3CH\,CH_2^* \rightleftharpoons CH_3CCH_2^* + H^*$		7.82×10^{-9}	1.41×10^{-7}	1.11×10^{-6}	5.34×10^{-6}	4.90×10^{-5}	2.19×10^{-4}
$CH_3CH\,CH_2^* \rightleftharpoons CH_3CH^* + CH_2^*$	C-C cracking	3.99×10^{-14}	7.51×10^{-12}	3.26×10^{-10}	5.61×10^{-9}	3.10×10^{-7}	4.61×10^{-6}

4.3 Summary

In summary, the PDH and other deep dehydrogenation and side reactions of C-C bond cracking on Ni_3Au/Ni(111) and Ni_2Au/Ni(111) surfaces comparing to Ni(111) are depicted as follows:

i) Doping Au atom into Ni(111) has no significant effect on the adsorption strength of propane. Moreover, increment amount of Au loading insignificantly reduces the propane adsorption.

ii) Substitution of Au into Ni(111) surface disperses the active Ni atoms leading to reduction of propylene desorption energy, hence enhancing the probability of propylene desorption from Ni_3Au/Ni(111) and Ni_2Au/Ni(111) compared with Ni(111) [133].

iii) Existence of Au decreases the reactivity of Ni catalyst by increasing of barriers for all PDH and side reactions.

iv) After propylene formation, increment of deep dehydrogenation and propylene cracking barriers corresponding with reduction of desorption barrier enhances the selectivity of propylene production which is in good agreement with the previous experimental observation of Yan and co-workers [58, 96].

With the above results, therefore, this investigation uncovers that doping inactive Au can suppress propylene-Ni(111) interaction, which leads to the improvement of the selectivity of propylene production. On the other hand, this improvement significantly reduces the reactivity of catalyst for main PDH process. However, using precious Au as a dopant to Ni might lead to high cost consuming of catalytic materials but the increasing of selectivity toward propylene could be compromised. In literature, alloying Sn into Pt(111) surface was reported to increase the selectivity of propylene production [75, 135, 136]. Hence, important understanding the role of Au doping in Ni in term of improvement of the selectivity of propylene production derived our theoretical findings, could serve as a good guidance for developing the efficiency of Ni-based catalyst with cheaper metal such as Sn which might be also a good candidate for PDH reaction.

CHAPTER 5

Improvement of Ni with Sn Promoter and Coke Deposition on Ni-X/Ni(111)Surfaces (X=Au, Sn)

5.1 Effect of Sn Promoter on Ni

In the Chapter 3, the dehydrogenation of propane to produce propylene can be accomplished without the side reaction of C-C bond cracking during PDH process. However, the strong chemisorption of propylene induces the deep dehydrogenation of propylene, leading to low selectivity of propylene production on Ni surface. Hence, further modifying the Ni-based catalyst is needed for improvement the selectivity of propylene production. In the Chapter 4, doping of Au shows enhancement of propylene desorption by steric hindrance effect of the inactive Au dopant. However, the price of Au dopant could lead to the dramatic increment on the price of Ni-Au/Ni(111) material. Therefore, exploration of other cheaper dopants such Sn for improving Ni(111) catalyst is still needed. Recently, tin (Sn) as a good promoter for enhancing the propylene selectivity of PDH reaction on Pt/Al_2O_3 [137] was reported. Moreover, Sn also played an important role in terms of preventing Pt sintering on catalyst surface, lowering the acidity of the oxide support and removing the coke creation during the PDH process [138, 139]. According to those properties of Sn, the Sn dopant into Ni surface might improve its selectivity for propylene production for PDH. In this chapter, the role of Sn introduced into Ni(111) catalyst has been investigated.

The adsorption of propane and its E_{ads} values are given in Figure 5.1. Existence of Sn doping presents the higher effect on reactant (propane adsorption) than that of Au in which the E_{ads} values of $Ni_3Au/Ni(111)$ and $Ni_2Au/Ni(111)$ are -0.59 and -0.58 eV, respectively. This repulsion effect is also expected to react on the propylene on Ni-Sn/Ni(111) surface which might lead to enhancement of propylene desorption on Ni-Sn/Ni(111) surfaces.

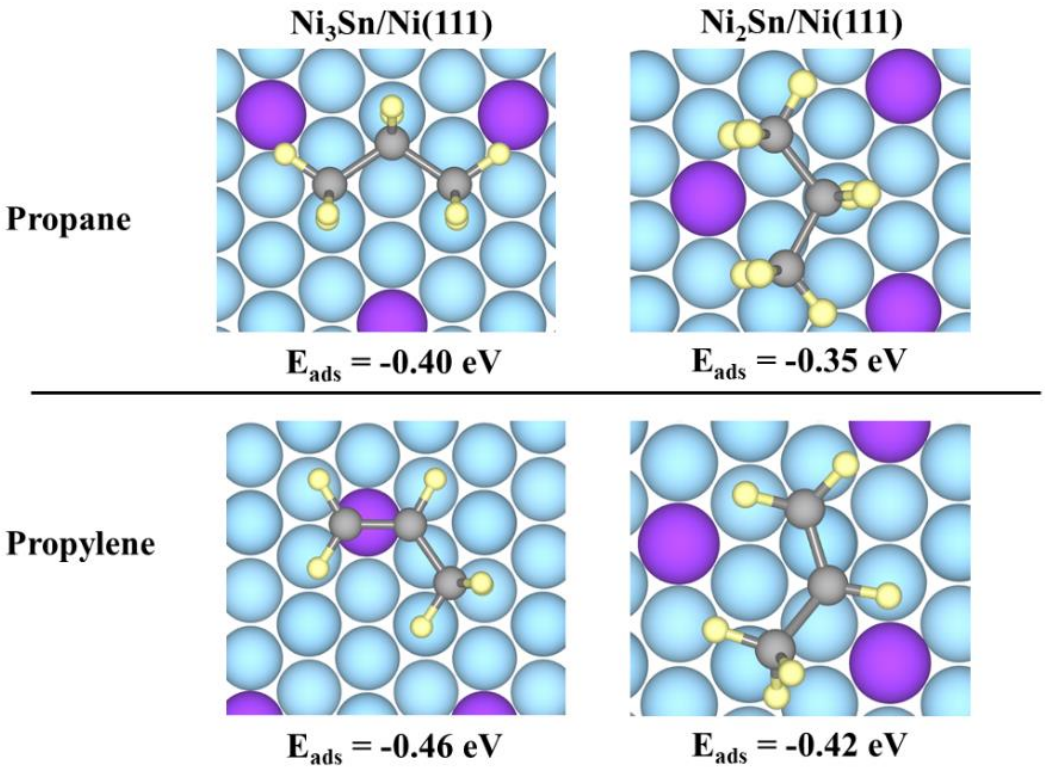

Figure 5.1 Stable configurations of propane and propylene on Ni_3Sn/Ni(111) and Ni_2Sn/Ni(111) surface

5.2 Coke Deposition on Ni-X/Ni(111) Surfaces (X=Au, Sn)

The coke formation reaction which has direct effect on deactivation of catalyst should be considered for development and improvement of a better Ni-based catalyst for PDH reaction. However, the mechanism of coke formation is very complicated and not completely understood yet. In this chapter, C adsorption on Ni-Au/Ni(111) and Ni-Sn/Ni(111) compared to Ni(111) surface is investigated. The slab models of different surfaces are shown in Figure 5.1.

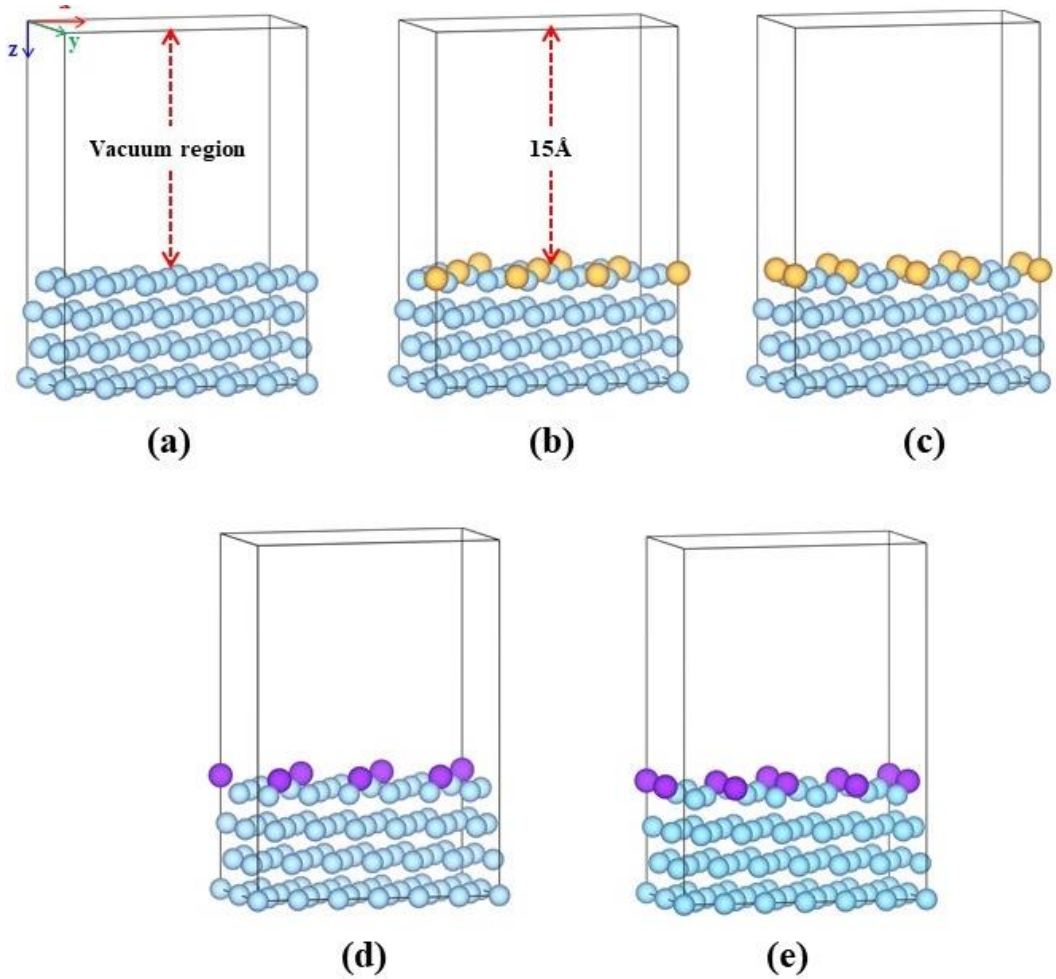

Figure 5.2 Slab models of (a) Ni(111), (b) Ni_3Au/Ni(111), (c) Ni_2Au/Ni(111), (d) Ni_3Sn/Ni(111) and (e) Ni_2Sn/Ni(111) surfaces

5.3 Adsorption of C Atom on Ni-X/Ni(111) Surfaces

According to the experimental investigations [58, 93, 96, 140-142], adding Au or Sn to Ni catalyst demonstrated an enhancement of coke resistance on catalyst surfaces. To understand that aspect, the adsorptions of a C atom, representing the initiation of coke formation, on Ni(111) Au- and Sn-doped on Ni(111) surfaces were investigated by DFT calculations. Herein, two compositions of Au and Sn dopants on Ni(111) surfaces are considered in this study, which are Ni_3Au/Ni(111), Ni_2Au/Ni(111), Ni_3Sn/Ni(111) and Ni_2Sn/Ni(111). All possible configurations of C atom adsorption were simulated as given in Table 5.1. The most stable configurations of C adsorption and selected bond distances between adsorbed C and catalyst surface of each Ni, Ni-Au/Ni(111) and Ni-Sn/Ni(111) systems are presented in Figure 5.3a to 5.3e.

Table 5.1 All possible adsorption configurations of C atom on Ni(111), Ni_3Au/Ni(111), Ni_2Au/Ni(111), Ni_3Sn/Ni(111) and Ni_2Sn/Ni(111) surfaces

Surface	Geometry	Favored site	E_{ads} (eV)
Ni(111)	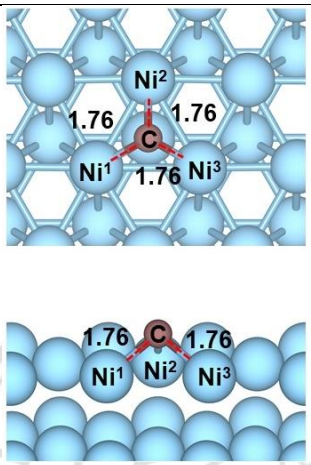	hcp	-6.99
	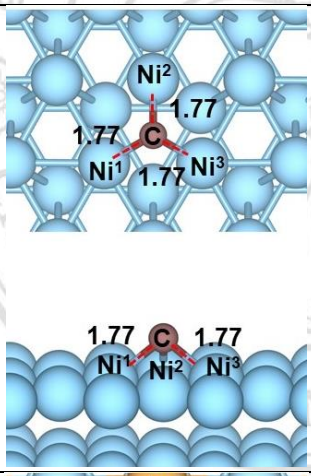	fcc	-6.95
Ni_3Au/Ni(111)	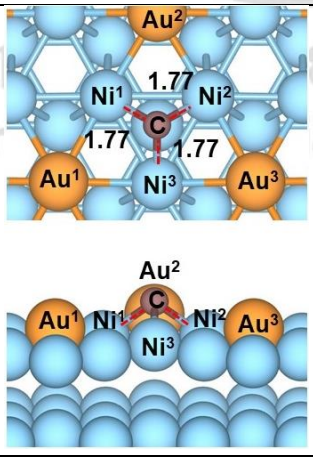	hcp	-6.66

Table 5.1 All possible adsorption configurations of C atom on Ni(111), Ni_3Au/Ni(111), Ni_2Au/Ni(111), Ni_3Sn/Ni(111) and Ni_2Sn/Ni(111) surfaces (continued)

Surface	Geometry	Favored site	E_{ads} (eV)
Ni_3Au/Ni(111)	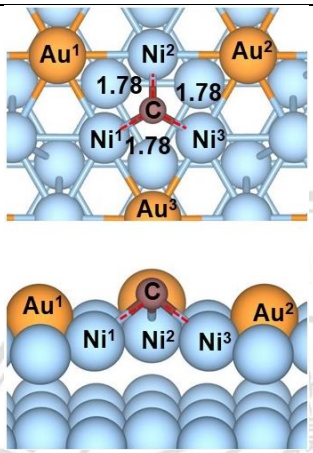	fcc	-6.64
	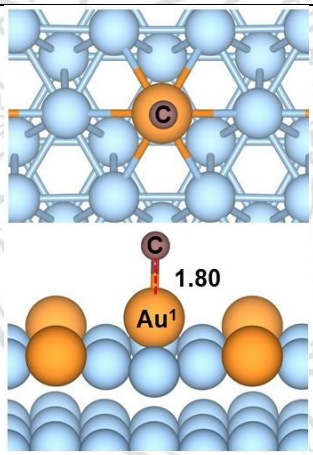	atop Au	-3.14
Ni_2Au/Ni(111)	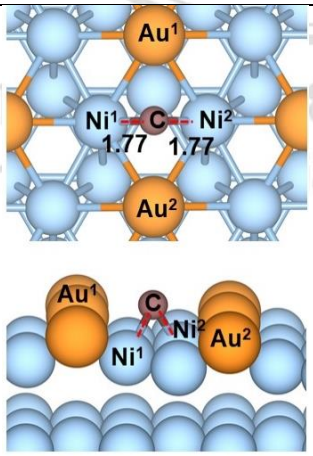	Ni-Ni bridge	-6.20

Table 5.1 All possible adsorption configurations of C atom on Ni(111), Ni_3Au/Ni(111), Ni_2Au/Ni(111), Ni_3Sn/Ni(111) and Ni_2Sn/Ni(111) surfaces (continued)

Surface	Geometry	Favored site	E_{ads} (eV)
Ni_2Au/Ni(111)	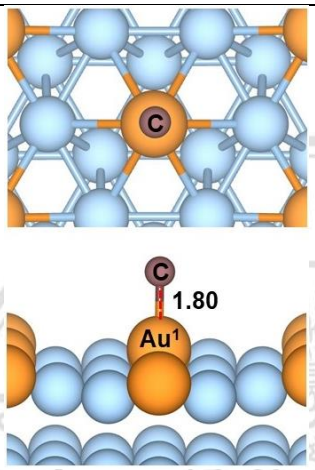	atop Au	-3.17
Ni_3Sn/Ni(111)	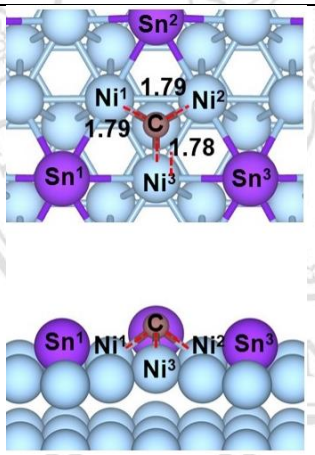	hcp	-6.23
	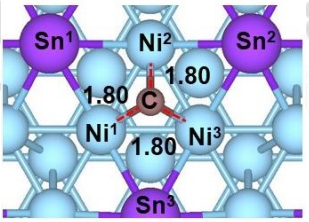	fcc	-6.22
	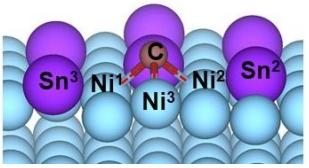		

Table 5.1 All possible adsorption configurations of C atom on Ni(111), Ni_3Au/Ni(111), Ni_2Au/Ni(111), Ni_3Sn/Ni(111) and Ni_2Sn/Ni(111) surfaces (continued)

Surface	Geometry	Favored site	E_{ads} (eV)
Ni_3Sn/Ni(111)	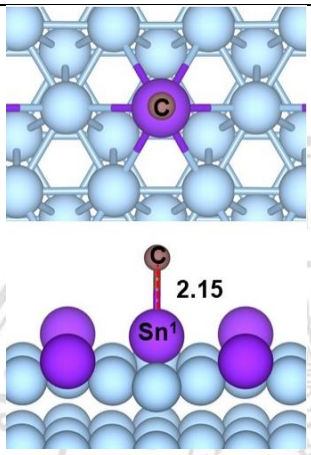	atop Sn	-1.96
Ni_2Sn/Ni(111)	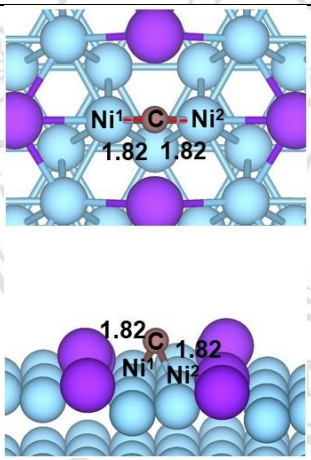 	Ni-Ni bridge	-5.10

For Ni(111) surface, the C atom prefers to adsorb on the hcp three-fold hollow site between Ni^1, Ni^2 and Ni^3 of Ni(111) surface with the E_{ads} value of -6.99 eV indicating the strong chemisorption between the C atom and Ni(111) surface. This calculated E_{ads} value is reasonably comparable with the literature [143]. The C atom initiates three bonds (1.76 Å) with Ni^1, Ni^2 and Ni^3 atoms as shown in Figure 5.2a.

For Ni-Au/Ni(111) systems, the two compositions of Ni_3Au/Ni(111) and Ni_2Au/Ni(111) surfaces are constructed to investigate effect of Au concentration for coke inhibition on Ni(111) surface. For Ni_3Au/Ni(111) system, the most stable adsorbed configuration of C adsorption on Ni3Au/Ni(111) surface is still the hcp three-fold hollow site between three Ni atoms of Ni^1, Ni^2 and Ni^3 with the E_{ads} of -6.66 eV as illustrated in

Figure 5.3b. The bond distances of three bond formations between adsorbed C and Ni^1, Ni^2 and Ni^3 are around 1.77 Å. For Ni_2Au/Ni(111) system, the C atom can be stably adsorbed on the bridge site between Ni^1 and Ni^2 atoms with the E_{ads} of -6.20 eV as depicted in Figure 5.3c. The bond lengths of C adsorption on Ni^1 and Ni^2 atoms are 1.77 Å.

For Ni-Sn/Ni(111) systems, two Sn doping concentrations on Ni(111) surface for C adsorption are also investigated in the similar reason to Au doping. Hence, the simulated structures of Ni_3Sn/Ni(111) and Ni_2Sn/Ni(111) were designed to study the effect of Sn concentration on hindering coke deposition on Ni(111) surface. For Ni_3Sn/Ni(111) surface, the C atom is chemisorbed on the hcp three-fold hollow site between Ni^1, Ni^2 and Ni^3 atoms with the E_{ads} of -6.23 eV. In Figure 5.3d, the bond lengths between the C atom and three neighboring Ni atoms of Ni^1, Ni^2 and Ni^3 are 1.79 Å. The adsorbed C atom is located far from Sn atoms approximately 2.98 Å. Comparing with other configurations in Table 5.2, the calculated results indicate that the adsorption of C atom near the Ni site is preferable than the Sn sites or the sites around Sn. For Ni_2Sn/Ni(111) surface, the C atom prefers to chemisorb on the bridge site between Ni^1 and Ni^2 atoms with the E_{ads} of -5.10 eV as exhibited in Figure 5.3e. The bond distances of C-Ni and C-Sn on this surface are 1.80 Å and 2.25 Å, respectively.

Comparison of the most favorite adsorption site of the C atom on Ni(111), Ni_3Au/Ni(111), Ni_2Au/Ni(111), Ni_3Sn/Ni(111) and Ni_2Sn/Ni(111) surfaces shown in Figure 5.3 reveals that the C atom prefers to interact with the Ni sites so it avoids to adsorb at the Au and Sn sites. The interaction between C and catalyst surface is weakened when doping Au and Sn in to Ni(111) surface. Moreover, increment of dopants loading from Ni_3M/Ni(111) to Ni_2M/Ni(111), where M is the dopants of Au and Sn, changes the adsorption site of C atom from the hcp three-fold hollow site of Ni_3M/Ni(111) surfaces to be the bridge site between two Ni atoms of Ni_2M/Ni(111) surfaces indicating that enhancement of dopants concentration on Ni(111) surface diminishes the most stable adsorption site of hcp hollow site between three Ni atoms. Hence, the C atom chooses to adsorb on the second most stable adsorption site of Ni^1 and Ni^2 atoms of Ni_2M/Ni(111) surfaces. Therefore, increment of Au and Sn doping also reduces the interaction between C atom and catalyst surfaces.

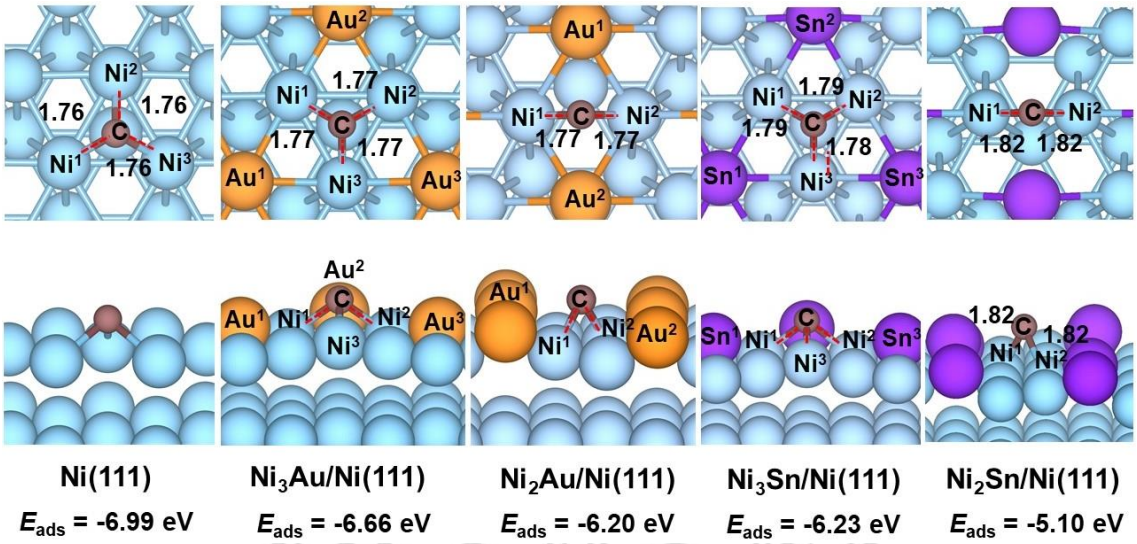

Figure 5.3 Top and side views of the most stable configurations of C atom on (a) Ni(111), (b) Ni_3Au/Ni(111), (c) Ni_2Au/Ni(111), (d) Ni_3Sn/Ni(111) and (e) Ni_2Sn/Ni(111) surfaces

5.4 Charge Analysis of Coking on Ni(111) and Ni-X/Ni(111) Surfaces

For deep understanding of interaction between adsorbed C atom and neighbor atoms of each catalyst surfaces, charge density difference analysis of those stable adsorbed configurations was performed and the results are depicted in Figure 5.4a to 5.4e. Charge accumulation and charge depletion are represented by the red and blue regions, respectively. As a result, charge accumulation appears around the adsorbed C atom in all five catalyst surfaces, while charge depletion can be observed around Ni atoms. This result implies that charge transfer happens from Ni atoms to the adsorbed C atom. At the same isovalue, the blue regions become smaller when amount of Au and Sn increases indicating the amount of charge transfer decreases as a function of dopants of Au and Sn compositions. The three interactions of adsorbed C atom and Ni^1, Ni^2 and Ni^3 of Ni(111) and Ni_3M/Ni(111) surfaces and two interactions of C and Ni^1 and Ni^2 of Ni_2M/Ni(111) surfaces are in good agreement with the number of bond formations in previous adsorption section 5.1. In addition, the interactions between nearest Au and Sn atoms and adsorbed C are not observed. So, the active species of Ni, Ni-Au/Ni(111) and Ni-Sn/Ni(111) surfaces for coke formation are Ni atoms.

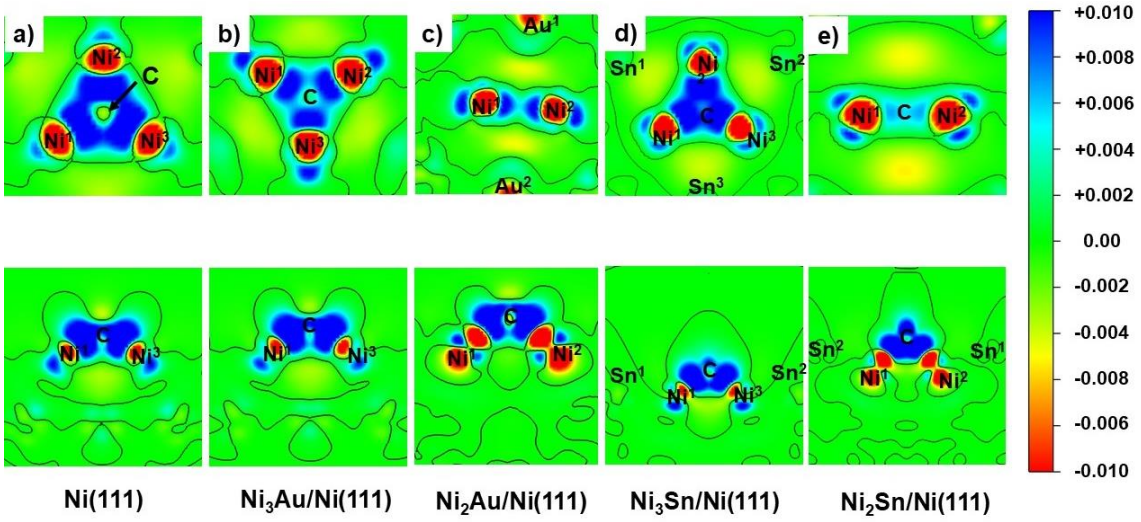

Figure 5.4 Contour plots of charge density differences (blue representing charge accumulation and red representing charge depletion) of C atom adsorption on (a) Ni(111), (b) Ni_3Au/Ni(111), (c) Ni_2Au/Ni(111), (d) Ni_3Sn/Ni(111) and (e) Ni_2Sn/Ni(111) at isovalue of ±0.010 e $Å^{-3}$

The DOS plots of five surfaces are given in Figure 5.5. The E_F is at 0.0 eV. As a result, the ε_d value of two upper layers of Ni(111) surface is -1.42 eV which is similar to the result reported by Hammer and Nørskov (-1.48 eV) [126]. Modification of Ni(111) surface by Au and Sn doping shifts ε_d to 1.39 and 1.38 eV for Ni_3Au/Ni(111) and Ni_2Au/Ni(111) surfaces and the same value of ε_d, -1.36 eV of both Ni_3Sn/Ni(111) and Ni_2Sn/Ni(111) surface. Shifting of the ε_d close to the Fermi level (at 0.0 eV) demonstrates that less valence states are filled when Au and Sn atoms are doped on Ni(111) surface. Moreover, the projected DOS information of selected atoms was further analyzed to compare the changes of before and during C adsorption states (Figure 5.5). Based on the configurations in Figure 5.3b and 5.3d, the PDOS peaks of the adsorbed C atom and three Ni sites (i.e. Ni^1, Ni^2 and Ni^3) in bare Ni(111) and Ni_3M/Ni(111) systems are plotted in panel I and II, respectively. The p-DOS peaks of three nearest Au and Sn dopant sites (i.e. Au^1, Au^2 and Au^3 of Ni_3Au/Ni(111) and Sn^1, Sn^2 and Sn^3 of Ni_3Sn/Ni(111) surfaces) are plotted in panel III of Figure 5.5b and d. According to the configuration in Figure 5.3c and 5.3e, the PDOS of two Ni and two Au atoms (i.e. Ni^1, Ni^2, Au^1 and Au^2) of Ni_2Au/Ai(111) surface and the PDOS of two Ni and two Sn atoms (i.e. Ni^1, Ni^2, Sn^1 and Sn^2) are projected for the C adsorption on Ni_2Sn/Ni(111) system (Figure 5.5c and 5.5e). As a result, the overlapping of the p-DOS of adsorbed C atom (panel I) and the d-DOS

of Ni atoms during C adsorption (panel II) indicates the d-p hybridization of between the states of the adsorbed C atom and its neighboring Ni atoms. This aspect results in the bond formation between Ni and C atoms. As shown in panel II of Figure 5.5, the valence d-peaks of Ni atoms are shifted to the lower energy level. This result indicates that more valence d-DOS states of Ni atoms in all systems are filled during the C adsorption compared to the pre-adsorption state. This result also corresponds well with the change of ε_d values in Table 5.2. From the panels III in Figure 5.5b to 5.5e, the d-DOS peaks of Au atom and p-DOS of Sn atoms are slightly changed during the C adsorption, since those Au and Sn atoms do not directly interact with the adsorbed C atom.

Table 5.2 The *d*-band center (ε_d) of the Ni atom on top layer surface

Surface	*d*-band center (ε_d) (eV)
Bare Ni(111)	1.42
Ni_3Au/Ni(111)	1.38
Ni_2Au/Ni(111)	1.39
Ni_3Sn/Ni(111)	1.36
Ni_2Sn/Ni(111)	1.36

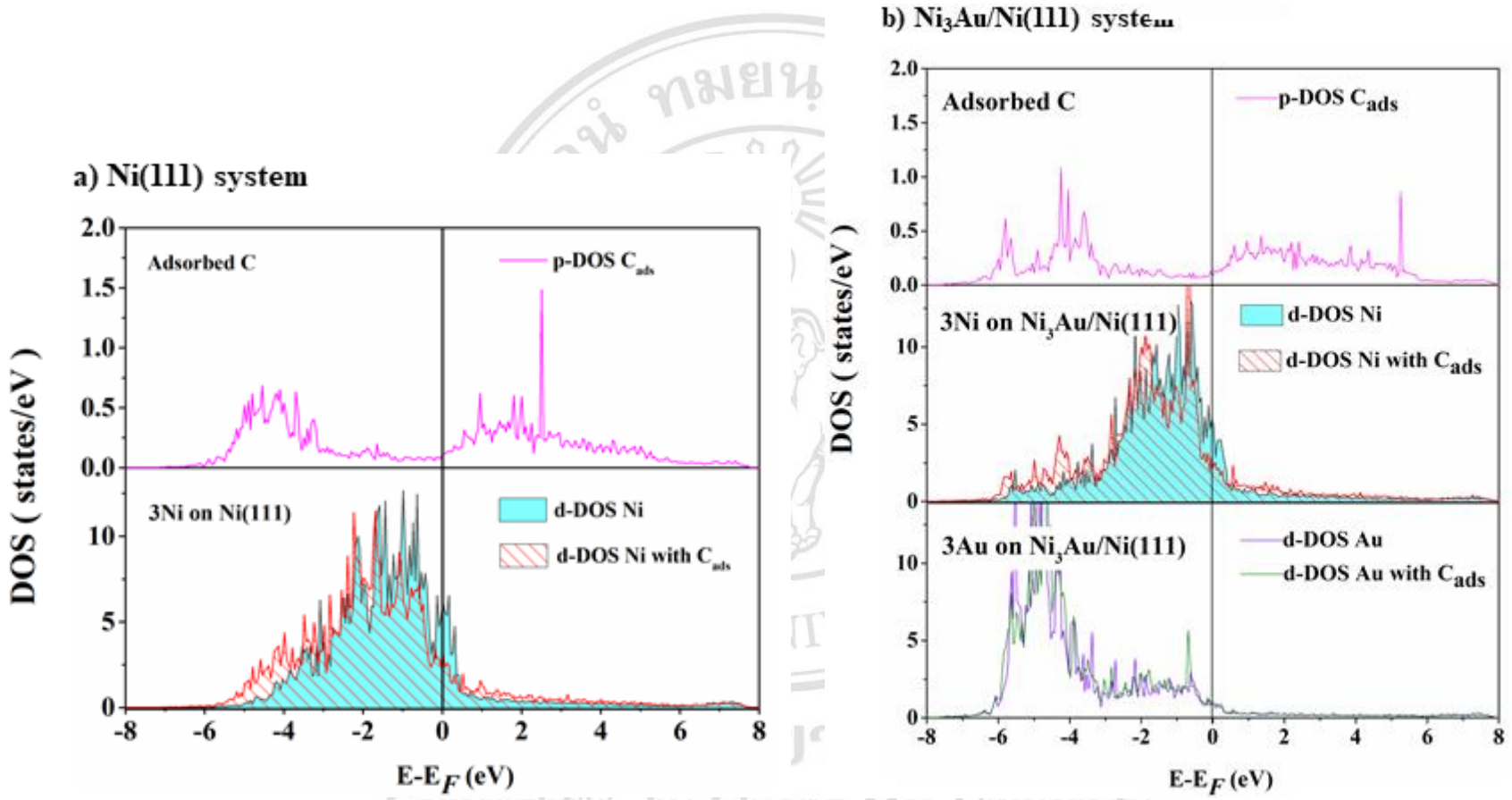

Figure 5.5 Projected density of state (PDOS) of all Ni atoms in the simulated models of bare Ni(111), (b) Ni_3Au/Ni(111), (c) Ni_2Au/Ni(111), (d) Ni_3Sn/Ni(111) and (e) Ni_2Sn/Ni(111) surfaces

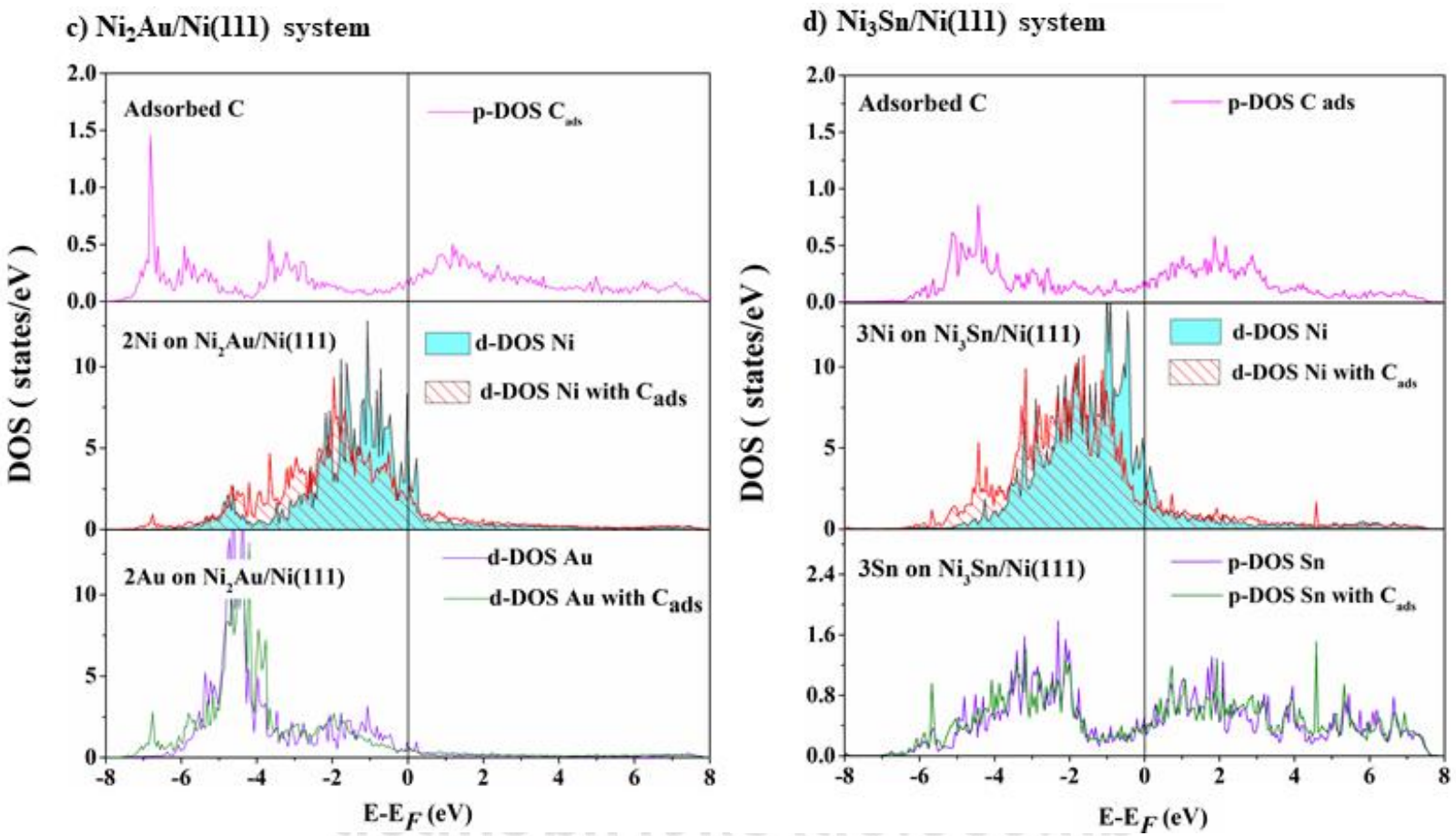

Figure 5.5 Projected density of state (PDOS) of all Ni atoms in the simulated models of bare Ni(111), (b) Ni_3Au/Ni(111), (c) Ni_2Au/Ni(111), (d) Ni_3Sn/Ni(111) and (e) Ni_2Sn/Ni(111) surfaces (continued)

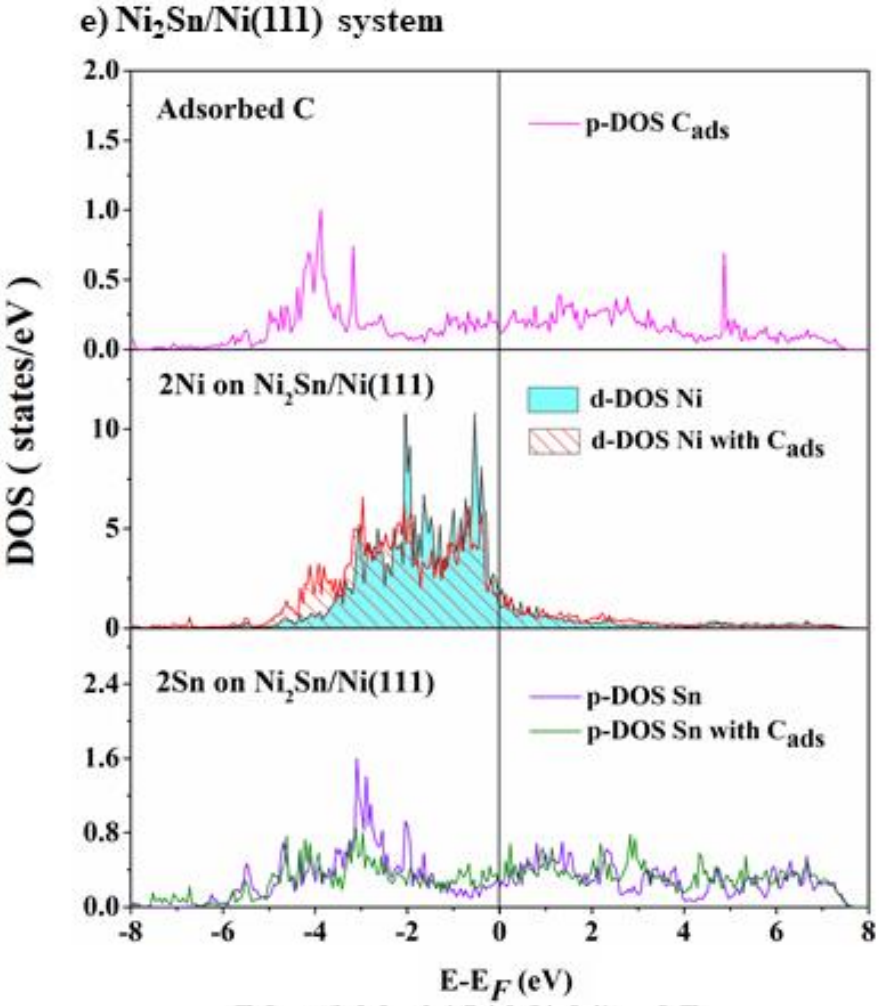

Figure 5.5 Projected density of state (PDOS) of all Ni atoms in the simulated models of bare Ni(111), (b) Ni_3Au/Ni(111), (c) Ni_2Au/Ni(111), (d) Ni_3Sn/Ni(111) and (e) Ni_2Sn/Ni(111) surfaces (continued)

Regarding to the electronegativity (EN), the EN values of Ni, Au, Sn and C are 1.91, 2.54, 1.96 and 2.55, respectively. For Ni-Au/Ni(111) system, the higher EN of Au affects the charge movement from electron rich Ni to the inactive Au dopant leading to decrement the efficiency of charge donation from Ni atom on Ni_3Au/Ni(111) and Ni_2Au/Ni(111) surfaces which leads to weakening the interaction between C atom and Ni atoms. For Ni-Sn/Ni(111) surface, the EN values of Ni and Sn are comparable, so they tend to form covalent-like interaction. This can be observed in the charge density difference contour proposed by Zhang and co-workers [144]. The d-p hybridization of Ni and Sn is slightly enhanced when amount of Sn is increased (see panels III in Figure

5.4d and 5.4e). According to d-DOS peaks of Ni atoms on pre-adsorbed surfaces, the d-DOS and ε_d values of Ni atoms are similar in pure Ni, Ni-Au/Ni(111) and Ni-Sn/Ni(111) systems (see panels II in Figure 5.4a to 5.4e). Addition of Au and Sn shows the small effect on the electronic properties of our simulated Ni models. On the other hand, Au and Sn are physically hindrance to the C adsorption as presented in their adsorption configurations. For Ni-Au/Ni(111) system, the large atomic radius of inactive Au affects distortion of Ni Au surfaces that the Au dopant moves up to the catalyst surface leading to the obstruction of geometry effect during C adsorption. For Ni-Sn/Ni(111) system, the doping Sn plays the indirect role on reducing the formation of coke by reducing the active Ni sites and might reduce the segregation of coke on the catalyst surface. Hence, modifications of Ni surface by Au and Sn doping are possible to enhance the lifetime of catalyst and to retard deactivation of catalytic surface by preventing the unwanted coke formation process. The extended catalyst lifetime by catalyst modification could slow down the deactivation and ultimately be beneficial and practical for industrial applications.

5.5 Summary

In summary, the coke formations on Ni(111), Ni_3Au/Ni(111), Ni_2Au/Ni(111), Ni_3Sn/Ni(111) and Ni_2Sn/Ni(111) surfaces are compared as follows:

i) The most preferable site of C adsorption on catalyst surface is the hcp three-fold hollow site between three nearest Ni atoms (Ni^1, Ni^2 and Ni^3).

ii) Doping Au and Sn into Ni(111) decreases the adsorption strength of C atom leading to coke reduction on catalyst surface.

iii) Increment of dopant concentration (Ni_2Au/Ni(111) and Ni_2Sn/Ni(111)) diminishes the most favorable active site of hcp site between three nearest Ni atoms resulting in lower adsorption strength of C atom to catalyst surface at higher dopant concentrations.

iv) At the same dopant concentration, Sn is more effective dopant than Au for inhibiting the coke formation on Ni(111) surface indicated by the lower E_{ads} of C atom on the surface of Ni-Sn/Ni(111) compared with that of Ni-Au/Ni(111).

Therefore, doping Sn into Ni(111) surface provides the better Ni-based catalyst than that of Au doping in term of coke inhibition during PDH process. However, the reaction mechanisms of PDH reaction as well as side reactions of deep dehydrogenation and C-C bond cracking on Ni-Sn/Ni(111) have not been proved in this investigation. To confirm the catalytic efficiency improvement for PDH reaction, the reaction mechanisms of PDH and other possible side reactions should be further investigated.

5.6 Suggestion and Future Work

Although doping of Sn plays the better role in term of coke inhibition than that of Au promoter, the reactivity loss of Ni-Sn/Ni(111) surface for PDH reaction as well as the efficiency of Ni-Sn/Ni(111) for inhibiting the side reaction of deep dehydrogenation and C-C bond cracking are still controversial. The important question is “Does the Sn dopant have a different or similar role to Au on selectivity improvement of propylene production?” To find the answer for this question, the reaction mechanism of PDH reaction on Ni-Sn/Ni(111) will have to be systematically investigated in the future.

CHAPTER 6

Conclusion

DFT calculations have been performed to investigate the reaction mechanism of PDH to form propylene as well as the side reactions of C-C bond cracking and deep dehydrogenation reaction on Ni (111) catalyst. Moreover, the charge density difference and partial density of state were performed to analyze the adsorption states of reactant, and product of the reaction. The investigated results reveal that adsorption of propane on Ni(111) is the physisorption while adsorption of propylene on Ni(111) surface is chemisorption. To improve catalytic performance in terms of selectivity enhancement of propylene production and inhibition of coking, two concentrations of Au and Sn dopants are introduced to Ni(111) surface, to form the surface alloys of Ni_3Au/Ni(111) and Ni_2Au/Ni(111), Ni_3Sn/Ni(111) and Ni_2Sn/Ni(111).

For Ni(111) surface, propane prefers to be physiosorbed on atop of three Ni atoms on catalyst surface but propylene prefers to be chemisorbed on catalyst surface with two adsorption sites (C^1 on hollow site and C^2 on atop site). The PDH mechanism on Ni(111) surface reveals that propane can be formed propyl species (1-propyl and 2-propyl) by the first dehydrogenation in two possible pathways; pathway A to form 1-propyl and pathway B to form 2-propyl intermediates. Then, both propyl intermediates can be dehydrogenated to yield the adsorbed propylene. From these two possible pathways, dehydrogenation of propane to form 1-propyl intermediate (pathway A) is more kinetically favorable than pathway B. Moreover, 1-propyl which is the intermediate of pathway A is more thermodynamically stable than that of pathway B. Hence, PDH reaction through pathway A is a major contribution to the formation of adsorbed propylene on Ni(111) surface without cracking reaction during PDH process. The activity of PDH reaction on Ni(111) surface is better than Pt(111) surface because the energy barriers of the first and second dehydrogenation on Ni(111) surface are lower than

that of Pt(111) surface. The selectivity of propylene production can be studied from desorption of propylene after PDH process. The strong chemisorption of propylene on Ni(111) surface causes high energy barrier of propylene desorption. Moreover, the high reactivity of Ni(111) surface is the cause of initiation of C-C bond cracking and deep dehydrogenation. The energy barrier of propylene desorption is higher than those of propylene cracking and deep dehydrogenation indicating that desorption of adsorbed propylene is more difficult, resulting in low selectivity of propylene production after PDH process.

For role of Au dopant, introduction of Au into Ni(111) surface shows insignificant effect on propane adsorption but reduces the adsorption strength of propylene adsorption. Moreover, increment of Au loading noticeably exhibits more decrement of E_{ads} of propylene on Ni_2Au/Ni(111) compared to Ni_3Au/Ni(111), leading to desorption improvement of the wanted propylene after PDH process. The result of DOS analysis supports that there are no charge association between Au dopant and adsorbed molecules during adsorption process. Furthermore, the Bader charge calculation reveals that charge movement from Ni donor to adsorbed propane and propylene accepters. Thus, the selectivity improvement of propylene production is caused by the steric hindrance effect of inactive Au blocking adsorption of propylene on Ni-Au/Ni(111) surface. For the mechanism investigation of PDH reaction, addition of Au dopant increases the energy barrier of PDH reaction, retarding the PDH reaction. After PDH process, reduction of propylene desorption barrier corresponding to faster desorption rate indicates that modification of Ni(111) surface by Au doping improves the propylene desorption. Although doping Au into Ni(111) surface illustrates the selectivity enhancement, the reactivity of catalytic surface for PDH reaction is reduced as a function of Au loading. Therefore, the compromise between catalytic selectivity and activity of catalyst as a function of Au concentration should be concerned. If the appropriate concentration of Au loading is optimized, the obtained information could be used for development of better Ni-based catalyst for PDH.

Although the mechanism exploration of PDH and other side reactions on undoped-Ni and doped-Ni(111), especially the coke formation is crucial for gaining the data on

improvement of better Ni catalyst on selectivity of propylene production, the complete mechanisms exploration takes a lot of computational cost in terms of computational time and memories. Thus, we have used computational screening that consumes less computational cost as given in Chapter 5. For the coke formation on catalyst surfaces, the results reveals that coking is easily formed on Ni(111) surface than other doped-Ni(111) because of the strong three bond formations between adsorbed C and three nearest Ni atoms. Moreover, doping Au and Sn into Ni(111) surface makes the positive effect for anti-coking by weakening the interaction between C and nearest Ni atoms. This anti-coking is further supported by charge density difference and DOS analysis in which the adsorbed C weakly interacts with nearest Ni atoms on Ni-Au/Ni(111) and Ni-Sn/Ni(111) surfaces and there is no bonding to Au and Sn atoms. In addition, increment of Au and Sn loading changes the most stable adsorption site from the hcp hollow site to the bridge site. Therefore, addition of Au and Sn promoters leads the decrement of coke formation, prolonging the lifetime of the catalyst.

REFERENCES

1. Weissermel K. and Arpe H. J., (2008), In: *Industrial Organic Chemistry*, Weissermel K. And Arpe H., Eds., WILEY-VCH Verlag GmbH & Co. KGaA, pp. 267-312.
2. Hocking M. B., (2005), In: *Handbook of Chemical Technology and Pollution Control (3rd Edition)*, Hocking M. B., Eds., Elsevier, pp. 637-668.
3. Dunn J. R. and Vara R. G., Oil resistant elastomers for hose applications, *Rubber Chemistry and Technology*, 56 (1983) 557-574.
4. Murata F., Suzuki S., Tsuyama S., Suganuma T., Imada M. and Furihata C., Application of rapid freezing followed by freeze-substitution acrolein fixation for cytochemical studies of the rat stomach, *The Histochemical Journal*, 17 (1985) 967-980.
5. Centi G., Grasselli R. K. and Trifiro F., Propane ammoxidation to acrylonitrile: An overview, *Catalysis Today*, 13 (1992) 661-666.
6. Dunn J. R., (2001), In: *Encyclopedia of Materials: Science and Technology*, K. H. J. Buschow, Cahn R. W., Flemings M. C., Ilschner B., Kramer E. J., Mahajan S. and Veyssière P., Eds., Elsevier, pp. 6163.
7. Niessner N. and Gausepohl H., (2003), In: *Modern Styrenic Polymers: Polystyrenes and Styrenic Copolymers*, John S. and Duane B. P., Eds., John Wiley & Sons, Ltd, pp. 25-42.
8. Dandekar A. B., Hryniszak M. and David Lawrence S., (2005). Process for producing cumene. (US 6,888,037). Retrieved from https://patents.google.com/ patent / WO2014003732A1.
9. Nijhuis T. A., Makkee M., Moulijn J. A. and Weckhuysen B. M., The production of propene oxide: catalytic processes and recent developments, *Industrial & Engineering Chemistry Research*, 45 (2006) 3447-3459.

10. Cools P., Mota C., Lorenzo M. I., Ghobeira R., De Geyter N., Moroni L. and Morent R., Acrylic acid plasma coated 3D scaffolds for cartilage tissue engineering applications, *Scientific Reports*, 8 (2018) 3830.

11. Tushar K. D., Prosenjit G. and Narayan C. D., Preparation, development, outcomes, and application versatility of carbon fiber-based polymer composites: A review, *Advanced Composites and Hybrid Materials*, 2 (2019) 214-233.

12. Olivera S, Muralidhara H. B., Venkatesh K., Gopalakrishna K. and Vivek C. S., Plating on acrylonitrile-butadiene-styrene (ABS) plastic: a review, *Journal of Materials Science*, 51 (2016) 3657-3674.

13. Yang T. H., Recent applications of polyacrylamide as biomaterials, *Recent Patents on Materials Science*, 1 (2008) 29-40.

14. Sojka R. E. and Entry J. A., Influence of polyacrylamide application to soil on movement of microorganisms in runoff water, *Environmental Pollution*, 108 (2000) 405-412.

15. Saito N., Aoki K., Usui Y., Shimizu M., Hara K., Narita N., Ogihara N., Nakamura K., Ishigaki N., Kato H., Haniu H., Taruta S., Ahm K. Y. and Endo M., Application of carbon fibers to biomaterials: A new era of nano-level control of carbon fibers after 30-years of development, *Chemical Society Reviews*, 40 (2011) 3824-3834.

16. Chand S., Review carbon fibers for composites, *Journal of Materials Science*, 35 (2000) 1303-1313.

17. Speight J. G., (2017), In: *Environmental Organic Chemistry for Engineers*, Speight J. G., Eds., Butterworth-Heinemann, pp. 87-151.

18. Roff W. J. and Scott J. R., (1971), In: *Fibres, films, plastics and rubbers*, Roff W. J. and Scott J. R., Eds., Butterworth-Heinemann, pp. 21-32.

19. Jansz J., (1999), In: *Polypropylene: An A-Z reference*, J. Karger-Kocsis, Eds., Springer Netherlands, pp. 643-651.

20. Martin J. and Pavol H., (1999), In: *Polypropylene: An A-Z reference*, J. Karger-Kocsis, Eds., Springer Netherlands, pp. 806-812.

21. Vaccaro F. J. and Klatte F. J., (1989), In: *Eleventh International Telecom munications Energy Conference*. "*Conference Proceedings*", Institute of Electrical and Electronics Engineers, pp. 1-5.

22. Han J. H., (2013), In: *Plastic Films in Food Packaging*, Ebnesajjad S., Eds., William Andrew Publishing, pp. 121-126.

23. Han J. H., Kissel W. J. and Meyer J. A., (2003), In: *Handbook of Polypropylene and Polypropylene Composites, Revised and Expanded (2nd Edition)*, Harutun K., Eds., CRC Press, pp. 10-27.

24. Qin Y., (2016), In: *Medical Textile Materials*, Qin Y., Eds., Woodhead Publishing, pp. 23-42.

25. Calafut T., (1998), In: *Plastic Films in Food Packaging*, Ebnesajjad S., Eds., William Andrew Publishing, pp. 17-20.

26. Marcilly C., Present status and future trends in catalysis for refining and petrochemicals, *Journal of Catalysis*, 216 (2003) 47-62.

27. Cavani F., Ballarini N. and Cericola A., Oxidative dehydrogenation of ethane and propane: How far from commercial implementation?, *Catalysis Today*, 127 (2007) 113-131.

28. Lavrenov A. V., Saifulina L. F., Buluchevskii E. A. and Bogdanets E. N., Propylene production technology: Today and tomorrow, *Catalysis in Industry*, 7 (2015) 175-187.

29. Shinya H., Azusa M., Shuhei W., Ryuichi K. and Fuyuki Y., Catalytic cracking of light-naphtha over MFI-zeolite/metal-oxide composites for efficient propylene production, *Research on Chemical Intermediates*, 41 (2015) 9615-9626.

30. Quazi Th. S., Akmm A. and Ma Q., Mechanical properties of polypropylene composites, *Journal of Thermoplastic Composite Materials*, 26 (2013) 362-391.

31. Van G. K. M, Reyniers M. F. and Marin G. B, Challenges of modeling steam cracking of heavy feedstocks, *Oil & Gas Science and Technology*, 63 (2008) 79-94.

32. Walther M., Refinery sources will fill the future "propylene gap", *Oil and Gas Journal*, 101 (2003) 52-54.

33. Yoshimura Y., Kijima N., Hayakawa T., Murata K., Suzuki K., Mizukami F., Matano K., Konishi T., Oikawa T., Saito M., Shiojima T., Shiozawa K., Wakui K., Sawada G., Sato K., Matsuo S. and Yamaoka N., Catalytic cracking of naphtha to light olefins, *Catalysis Surveys from Japan*, 4 (2001) 157-167.

34. Farshi A., Shaiyegh F., Burogerdi S. H. and Dehgan A., FCC process role in propylene demands, *Petroleum Science and Technology*, 29 (2011) 875-885.

35. Akah A., Al-Ghrami M., Saeed M. and Siddiqui M. A. B., Reactivity of naphtha fractions for light olefins production, *International Journal of Industrial Chemistry*, 8 (2017) 221-233.

36. Wang Y. and Wei F., (2017), In: *Multiphase Reactor Engineering for Clean and Low-Carbon Energy Applications,* Cheng Y., Wei F. and Jin Y., Eds., John Wiley & Sons, pp. 271-294.

37. Lwin S. and Wachs I. E., Catalyst activation and kinetics for propylene metathesis by supported WOx/SiO_2 catalysts, *ACS Catalysis*, 7 (2017) 573-580.

38. Anas K. J., Oki M., Masato Y., Adnan M. A.-A., Zain H. Y. and Toshiyuki Y., Selective production of propylene from methanol conversion over nanosized ZSM-22 zeolites, *Industrial & Engineering Chemistry Research*, 53 (2014) 19498-19505.

39. Jiang B., Feng X., Yan L., Jiang Y., Liao Z., Wang J. and Yang Y., Methanol to propylene process in a moving bed reactor with by products recycling: Kinetic study and reactor simulation, *Industrial & Engineering Chemistry Research*, 53 (2014) 4623-4632.

40. Khanmohammadi M., Amani S., Garmarudi A. B. and Niaei A., Methanol-to-propylene process: Perspective of the most important catalysts and their behavior, *Chinese Journal of Catalysis*, 37 (2016) 325-339.

41. Koempel H. and Liebner W., Lurgi's methanol to propylene MTP report on a successful commercialisation. In: *Symposium; 8th, Natural gas conversion*, Natal,

Brazil, Bellot Noronha F., Schmal M. and Falabella Sousa-Aguiar E., Eds; Elsevier: Amsterdam 2007: pp 261-267.

42. Amghizar I., Vandewalle L. A., Van Geem K. M. and Marin G. B., New trends in olefin production, *Engineering*, 3 (2017) 171-178.

43. Adam C., Minoux D., Nesterenko N., Van Donk S. and Dath J. P., (2016). Process to make propylene from isobutanol by dehydration and subsequent cracking. (US 9,334,202). Retrieved from https://patents.google.com/patent/US20150239801A1/en.

44. Sun J, Liu C., Wang Y., Martin K. and Venkitasubramanian P., (2017). Process and catalyst for conversion of acetic acid to isobutene and propylene. Retrieved from https://patents.google.com/patent/US9580365B2/en.

45. Aitani A., (2006), In: *Encyclopedia of Chemical Processing*, Lee S., Eds., Taylor & Francis, pp. 12-2461.

46. Sattler J. J. H. B., Ruiz-Martinez J., Santillan-Jimenez E. and Weckhuysen B. M., Catalytic dehydrogenation of light alkanes on metals and metal oxides, *Chemical Reviews*, 114 (2014) 10613-10653.

47. Rosenwasser M., James J. F. and Michael O'leary G., 2012, PetroLogistics LP-FORM S-1/A, veiwed 12 May 2019, <http://www.getfilings.com/sec-filings/120305/PetroLo gistics-LP_S-1.A/#bg42903a_main_toc>.

48. Yang M. L., Zhu Y. A., Fan C., Sui Z. J., Chen D. and Zhou X. G., DFT study of propane dehydrogenation on Pt catalyst: Effects of step sites, *Physical Chemistry Chemical Physics*, 13 (2011) 3257-3267.

49. Density functional study of the chemisorption of C1, C2 and C3 intermediates in propane dissociation on Pt(111), *Journal of Molecular Catalysis A*, 321 (2010) 42-49.

50. Burcat A., Cracking of propylene in a shock tube, *Fuel*, 54 (1975) 87-93.

51. Cremer P. S., Su X., Shen Y. R. and Somorjai G. A., Hydrogenation and dehydrogenation of propylene on Pt(111) studied by sum frequency generation

from UHV to atmospheric pressure, *The Journal of Physical Chemistry*, 100 (1996) 16302-16309.

52. Basaran D., Aleksandrov H. A., Chen Z. X., Zhao Z. J. and Rösch N., Decomposition of ethylene on transition metal surfaces M(111). A comparative DFT study of model reactions for M=Pd, Pt, Rh, Ni, *Journal of Molecular Catalysis A: Chemical*, 344 (2011) 37-46.

53. Yu C., Ge Q., Xu H. and Li W., Effects of Ce addition on the Pt-Sn/γ-Al_2O_3 catalyst for propane dehydrogenation to propylene, *Applied Catalysis A*, 315 (2006) 58-67.

54. Santhosh Kumar M., Chen D., Walmsley J. C. and Holmen A., Dehydrogenation of propane over Pt-SBA-15: Effect of Pt particle size, *Catalysis Communications*, 9 (2008) 747-750.

55. Andy P. and Davis M. E., Dehydrogenation of propane over platinum containing CIT-6, *Industrial & Engineering Chemistry Research*, 43 (2004) 2922-2928.

56. Kogan S. B., Schramm H. and Herskowitz M., Dehydrogenation of propane on modified Pt/θ-alumina performance in hydrogen and steam environment, *Applied Catalysis A*, 208 (2001) 185-191.

57. Martín N., Viniegra M., Lima E. and Espinosa G., Coke characterization on Pt/Al_2O_3-β-Zeolite reforming catalysts, *Industrial & Engineering Chemistry Research*, 43 (2004) 1206-1210.

58. Yan Z. and Goodman D. W., Silica-supported Au-Ni catalysts for the dehydrogenation of propane, *Catalysis Letters*, 142 (2012) 517-520.

59. Guanghui Z., Ce Y. and Jeffrey T. M., Tetrahedral nickel(II) phosphosilicate single-site selective propane dehydrogenation catalyst, *ChemCatChem*, 10 (2018) 961-964.

60. Liliana R. M., Osvaldo F. G. and Luis E. C., Chromium oxide supported on different Al_2O_3 supports: Catalytic propane dehydrogenation, *Industrial & Engineering Chemistry Research*, 38 (1999) 396-404.

61. Piotr M. and Jan O., Dehydrogenation of propane in the presence of carbon dioxide over oxide-based catalysts, *Reaction Kinetics and Catalysis Letters*, 78 (2003) 41-47.

62. Zhang X., Yue Y. and Gao Z., Chromium oxide supported on mesoporous SBA-15 as propane dehydrogenation and oxidative dehydrogenation catalysts, *Catalysis Letters*, 83 (2002) 19-25.

63. Jibril B. Y., Al-Zahrani S. M., Abasaeed A. E. and Hughes R., Oxidative dehydrogenation of propane over supported chromium-molybdenum oxides catalysts, *Catalysis Communications*, 4 (2003) 579-584.

64. Carrero C. A., Schloegl R., Wachs I. E. and Schomaecker R., Critical literature review of the kinetics for the oxidative dehydrogenation of propane over well-defined supported vanadium oxide catalysts, *ACS Catalysis*, 4 (2014) 3357-3380.

65. Liu G., Zhao Z. J., Wu T., Zeng L. and Gong J., Nature of the active sites of VOx/Al_2O_3 catalysts for propane dehydrogenation, *ACS Catalysis*, 6 (2016) 5207-5214.

66. Dai G. L., Li Z. H., Lu J., Wen N. W. and Kang N. F., Deep oxidations in the oxidative dehydrogenation reaction of propane over $V_2O_5(001)$: Periodic density functional theory study, *Journal of Physical Chemistry C*, 116 (2012) 807-817.

67. Chen K., Bell A. T. and Iglesia E., Kinetics and mechanism of oxidative dehydrogenation of propane on vanadium, molybdenum, and tungsten oxides, *Journal of Physical Chemistry B*, 104 (2000) 1292-1299.

68. Abello M. C., Gomez M. F. and Cadús L. E., Oxidative dehydrogenation of propane over molybdenum supported on $MgO{-}\gamma\text{-}Al_2O_3$, *Industrial & Engineering Chemistry Research*, 35 (1996) 2137-2143.

69. Liu Y., Li Z. H., Lu J. and Fan K. N., Periodic density functional theory study of propane dehydrogenation over perfect $Ga_2O_3(100)$ surface, *Journal of Physical Chemistry C*, 112 (2008) 20382-20392.

70. Zheng B., Hua W., Yue Y. and Gao Z., Dehydrogenation of propane to propene over different polymorphs of gallium oxide, *Journal of Catalysis*, 232 (2005) 143-151.

71. Sattler J. J. H. B., Gonzalez-Jimenez I. D., Luo L., Stears B. A., Malek A, Barton D. G., Kilos B. A., Kaminsky M. P., Verhoeven T. W. G. M., Koers E. J., Baldus M. and Weckhuysen B. M., Platinum-promoted Ga/Al_2O_3 as highly active, selective, and stable catalyst for the dehydrogenation of propane, *Angewandte Chemie International Edition*, 53 (2014) 9251-9256.

72. Chen C., Zhang J., Zhang B., Yu C., Peng F. and Su D., Revealing the enhanced catalytic activity of nitrogen-doped carbon nanotubes for oxidative dehydrogenation of propane, *Chemical Communications*, 49 (2013) 8151-8153.

73. Liu L., Deng Q. F., Agula B., Zhao X., Ren T. Z. and Yuan Z. Y., Ordered mesoporous carbon catalyst for dehydrogenation of propane to propylene, *Chemical Communications*, 47 (2011) 8334-8336.

74. Yang M. L., Zhu J., Zhu Y. A., Sui Z. J., Yu Y.-D., Zhou X. G. and Chen D., Tuning selectivity and stability in propane dehydrogenation by shaping Pt particles: A combined experimental and DFT study, *Journal of Molecular Catalysis A: Chemical*, 395 (2014) 329-336.

75. Yang M. L., Zhu Y. A., Zhou X. G., Sui Z. J. and Chen D., First-principles calculations of propane dehydrogenation over PtSn catalysts, *ACS Catalysis*, 2 (2012) 1247-1258.

76. Sandra C. D., Janaína C. E., Ricardo R. S. and Carla E. H., Effect of different promoters on $Ni/CeZrO_2$ catalyst for autothermal reforming and partial oxidation of methane, *Chemical Engineering Journal*, 156 (2010) 380-387.

77. Iglesias J. A., Beale A. M., Maaijen K., Weng T. C., Glatzel P. and Weckhuysen B. M., A combined in situ time-resolved UV-Vis, Raman and high-energy resolution X-ray absorption spectroscopy study on the deactivation behavior of Pt and PtSn propane dehydrogenation catalysts under industrial reaction conditions, *Journal of Catalysis*, 276 (2010) 268-279.

78. Zhang R. J., Xia G. F., Li M. F., Wu Y., Nie H. and Li D. D., Effect of support on the performance of Ni-based catalyst in methane dry reforming, *Journal of Fuel Chemistry and Technology*, 43 (2015) 1359-1365.

79. Kaihu H. and Ronald H., The kinetics of methane steam reforming over a Ni/α-Al_2O catalyst, *Chemical Engineering Journal*, 82 (2001) 311-328.

80. Mohsenzadeh A., Borjesson A., Wang J. H., Richards T. and Bolton K., The effect of carbon monoxide Co-adsorption on Ni-catalysed water dissociation, *International Journal of Molecular Sciences*, 14 (2013) 23301-23314.

81. Carrasco J., Barrio L., Liu P., Rodriguez J. A. and Ganduglia-Pirovano M. V., Theoretical studies of the adsorption of CO and C on Ni(111) and Ni/CeO_2(111): Evidence of a strong metal-support interaction, *The Journal of Physical Chemistry C*, 117 (2013) 8241-8250.

82. Chan F. L. and Tanksale A., Review of recent developments in Ni-based catalysts for biomass gasification, *Renewable and Sustainable Energy Reviews*, 38 (2014) 428-438.

83. Crampton A. S., Rötzer M. D., Schweinberger F. F., Yoon B., Landman U. and Heiz U., Ethylene hydrogenation on supported Ni, Pd and Pt nanoparticles: Catalyst activity, deactivation and the d-band model, *Journal of Catalysis*, 333 (2016) 51-58.

84. Biniwale R. B., Kariya N. and Ichikawa M., Dehydrogenation of cyclohexane over Ni based catalysts supported on activated carbon using spray-pulsed reactor and enhancement in activity by addition of a small amount of Pt, *Catalysis Letters*, 105 (2005) 83-87.

85. Heracleous E., Lee A. F., Wilson K. and Lemonidou A. A., Investigation of Ni-based alumina-supported catalysts for the oxidative dehydrogenation of ethane to ethylene: structural characterization and reactivity studies, *Journal of Catalysis*, 231 (2005) 159-171.

86. Boukhlouf H., Barama A., Benrabaa R., Caballero J. G., Löfberg A. and Bordes-Richard E., Catalytic activity in the oxidative dehydrogenation of ethane over Ni

and/or Co molybdate catalysts: Synthesis and characterization, *Comptes Rendus Chimie*, 20 (2017) 30-39.

87. Lin L. and Devon C. R., (2013). Non-oxidative patent dehydrogenative process. Retrieved from https://patents.google.com/patent/WO2012044415A1.

88. Shen W., Wang Y., Shi X., Shah N., Huggins F., Bollineni S., Seehra M. and Huffman G., Catalytic nonoxidative dehydrogenation of ethane over Fe–Ni and Ni catalysts supported on Mg(Al)O to produce hydrogen and easily purified carbon nanotubes, *Energy & Fuels*, 21 (2007) 3520-3529.

89. An W., Zeng X. C. and Turner C. H., First-principles study of methane dehydrogenation on a bimetallic Cu/Ni(111) surface, *The Journal of Chemical Physics*, 131 (2009) 174702.

90. Siahvashi A., Chesterfield D. and Adesina A. A., Nonoxidative and oxidative propane dehydrogenation over bimetallic Mo–Ni/Al_2O_3 catalyst, *Industrial & Engineering Chemistry Research*, 52 (2013) 4017-4026.

91. Mckee D. W., The kinetics of propane cracking on nickel, *Journal of the American Chemical Society*, 84 (1962) 4427-4431.

92. G. Wang S., Liao X. Y., Cao D. B., Li Y. W., Wang J. and Jiao H., Formation of carbon species on Ni(111): Structure and stability, *The Journal of Physical Chemistry C*, 111 (2007) 10894-10903.

93. Z. Wang, Cao X. M., Zhu J. and Hu P., Activity and coke formation of nickel and nickel carbide in dry reforming: A deactivation scheme from density functional theory, *Journal of Catalysis*, 311 (2014) 469-480.

94. Foppa L., Silaghi M. C., Larmier K. and Comas V. A., Intrinsic reactivity of Ni, Pd and Pt surfaces in dry reforming and competitive reactions: Insights from first principles calculations and microkinetic modeling simulations, *Journal of Catalysis*, 343 (2016) 196-207.

95. Ayabe S., Omoto H., Utaka T., Kikuchi R., Sasaki K., Teraoka Y. and Eguchi K., Catalytic autothermal reforming of methane and propane over supported metal catalysts, *Applied Catalysis A*, 241 (2003) 261-269.

96. Yan Z., Yao Y. and Goodman D. W., Dehydrogenation of propane to propylene over supported model Ni–Au catalysts, *Catalysis Letters*, 142 (2012) 714-717.

97. Anton K., Nicola B., Stefano De G., Carlo S., Guido F. and Stefano B., Methane dehydrogenation on Rh@Cu(111): A first-principles study of a model catalyst, *Journal of the American Chemical Society*, 128 (2006) 12448-12454.

98. Shephard F. E., Activity and properties of nickel catalysts in the hydrogenolysis of propane, *Journal of Catalysis*, 14 (1969) 148-167.

99. Zhang C. J. and Hu P., Methane transformation to carbon and hydrogen on Pd(100): Pathways and energetics from density functional theory calculations, *The Journal of Chemical Physics*, 116 (2002) 322-327.

100. Zhao Z. J., Chiu C. C. and Gong J., Molecular understandings on the activation of light hydrocarbons over heterogeneous catalysts, *Chemical Science*, 6 (2015) 4403-4425.

101. John A. K., Josef A., Payam K. and Timo J., (2011), In: *Modeling and Simulation of Heterogeneous Catalytic Reactions*, Olaf D., Eds., Wiley-VCH Verlag GmbH & Co. KGaA, pp. 1-38.

102. Zha S., Sun G., Wu T., Zhao J., Zhao Z. J. and Gong J., Identification of Pt-based catalysts for propane dehydrogenation via a probability analysis, *Chemical Science*, 9 (2018) 3925-3931.

103. Barghi B., Fattahi M. and Khorasheh F., Kinetic modeling of propane dehydrogenation over an industrial catalyst in the presence of oxygenated compounds, *Reaction Kinetics, Mechanisms and Catalysis*, 107 (2012) 141-155.

104. Hook A. and Celik F. E., Predicting selectivity for ethane dehydrogenation and coke formation pathways over model Pt–M surface alloys with ab initio and scaling methods, *The Journal of Physical Chemistry C*, 121 (2017) 17882-17892.

105. Houk K. N. and Cheong P. H. Y., Computational prediction of small-molecule catalysts, *Nature*, 455 (2008) 309-313.

106. Gregg J., What in the (quantum) world is macroscopic?, *American Journal of Physics*, 82 (2014) 896-905.

107. Werner Heisenberg, (1984), In: *Scientific Review Papers, Talks, and Books Wissenschaftliche Übersichtsartikel, Vorträge und Bücher*, Walter Blum, Hans-Peter Dürr and Helmut Rechenberg, Eds., Springer Berlin Heidelberg, pp. 226-237.

108. Pauli W., Über den zusammenhang des abschlusses der elektronengruppen im atom mit der komplexstruktur der spektren, *Zeitschrift für Physik*, 31 (1925) 765-783.

109. Slater J. C., The theory of complex spectra, *Physical Review*, 34 (1929) 1293-1322.

110. Kohn W. and Sham L. J., Self-consistent equations including exchange and correlation effects, *Physical Review*, 140 (1965) A1133-A1138.

111. Perdew J. P., Chevary J. A., Vosko S. H., Jackson K. A., Pederson M. R., Singh D. J. and Fiolhais C., Atoms, molecules, solids, and surfaces: Applications of the generalized gradient approximation for exchange and correlation, *Physical Review B*, 46 (1992) 6671-6687.

112. Germain Salvato-Vallverdu, 2009, Periodic boundaries conditions, veiwed 12 May 2019 <http://www.texample.net/tikz/examples/periodic-boundaries-conditions/>.

113. Kresse G. and Furthmüller J., Efficiency of ab-initio total energy calculations for metals and semiconductors using a plane-wave basis set, *Computational Materials Science*, 6 (1996) 15-50.

114. Kresse G. and Hafner J., Ab initio, *Physical Review B*, 48 (1993) 13115-13118.

115. Blöchl P. E., Projector augmented-wave method, *Physical Review B*, 50 (1994) 17953-17979.

116. Kresse G. and Joubert D., From ultrasoft pseudopotentials to the projector augmented-wave method, *Physical Review B*, 59 (1999) 1758-1775.

117. Perdew J. P., Burke K. and Ernzerhof M., Generalized gradient approximation made simple, *Physical Review Letters*, 77 (1996) 3865-3868.

118. Monkhorst H. J. and Pack J. D., Special points for Brillouin-zone integrations, *Physical Review B*, 13 (1976) 5188-5192.

119. Methfessel M. and Paxton A. T., High-precision sampling for Brillouin-zone integration in metals, *Physical Review B*, 40 (1989) 3616-3621.

120. Stefan G., Jens A., Stephan E. and Helge K., A consistent and accurate ab initio parametrization of density functional dispersion correction (DFT-D) for the 94 elements H-Pu, *The Journal of Chemical Physics*, 132 (2010) 154104.

121. Henkelman G., Uberuaga P. B. and Jónsson H., A climbing image nudged elastic band method for finding saddle points and minimum energy paths, *The Journal of Chemical Physics*, 113 (2000) 9901-9904.

122. Henkelman G. and Jónsson H., A dimer method for finding saddle points on high dimensional potential surfaces using only first derivatives, *The Journal of Chemical Physics*, 111 (1999) 7010-7022.

123. Olsen R. A., Kroes G. J., Henkelman G., Arnaldsson A. and Jónsson H., Comparison of methods for finding saddle points without knowledge of the final states, *The Journal of Chemical Physics*, 121 (2004) 9776-9792.

124. Henkelman G. and Jónsson H., Long time scale kinetic Monte Carlo simulations without lattice approximation and predefined event table, *The Journal of Chemical Physics*, 115 (2001) 9657-9666.

125. Fampiou L. and Ramasubramaniam A., Binding of Pt nanoclusters to point defects in graphene: Adsorption, morphology, and electronic structure, *Journal of Physical Chemistry C*, 116 (2012) 6543-6555.

126. Hammer B. and Nørskov J. K., Electronic factors determining the reactivity of metal surfaces, *Surface Science*, 343 (1995) 211-220.

127. Lilja K. and Egill S., A systematic DFT study of hydrogen diffusion on transition metal surfaces, *Surface Science*, 606 (2012) 1400-1404.

128. Koestner R. J., Frost J. C., Stair P. C., Van H. M. A. and Somorjai G. A., Evidence for the formation of stable alkylidyne structures from C3 and C4 unsaturated hydrocarbons adsorbed on the Pt(111) single crystal surface, *Surface Science*, 116 (1982) 85-103.

129. Song L. and Rees L. V. C., Diffusion of propane in theta-1 and silicalite-1 zeolites, *Microporous and Mesoporous Materials*, 41 (2000) 193-200.

130. Busca G., (2014), In: *Heterogeneous Catalytic Materials*, Busca G., Eds., Elsevier, pp. 297-343.

131. Saerens S., Sabbe M. K., Galvita V. V., Redekop E. A., Reyniers M. F. and Marin G. B., The positive role of hydrogen on the dehydrogenation of propane on Pt(111), *ACS Catalysis*, 7 (2017) 7495-7508.

132. Celik F. E. and Mavrikakis M., Stability of surface and subsurface hydrogen on and in Au/Ni near-surface alloys, *Surface Science*, 640 (2015) 190-197.

133. Saelee T., Namuangruk S., Kungwan N. and Junkaew A., Theoretical insight into catalytic propane dehydrogenation on Ni(111), *The Journal of Physical Chemistry C*, 122 (2018) 14678-14690.

134. Henkelman G., Arnaldsson A. and Jónsson H., A fast and robust algorithm for bader decomposition of charge density, *Computational Materials Science*, 36 (2006) 354-360.

135. Feng J., Zhang M. and Yang Y., Dehydrogenation of propane on Pt or PtSn catalysts with Al2O3 or SBA-15 Support, *Chinese Journal of Chemical Engineering*, 22 (2014) 1232-1236.

136. Nykänen L. and Honkala K., Density functional theory study on propane and propene adsorption on Pt(111) and PtSn alloy surfaces, *The Journal of Physical Chemistry C*, 115 (2011) 9578-9586.

137. Vu B. K., Song M. B., Ahn I. Y., Suh Y. W., Suh D. J., Kim W. I. L., Koh H. L., Choi Y. G. and Shin E. W., Propane dehydrogenation over Pt–Sn/Rare-earth-doped Al_2O_3: Influence of La, Ce, or Y on the formation and stability of Pt–Sn alloys, *Catalysis Today*, 164 (2011) 214-220.

138. Praserthdam P., Grisdanurak N. and Yuangsawatdikul W., Coke formation over Pt–Sn–K/Al_2O_3 in C3, C5–C8 alkane dehydrogenation, *Chemical Engineering Journal*, 77 (2000) 215-219.

139. Seo H., Lee J. K., Hong U. G., Park G., Yoo Y., Lee J., Chang H. and Song I. K., Direct dehydrogenation of n-butane over Pt/Sn/M/γ-Al_2O_3 catalysts: Effect of third metal (M) addition, *Catalysis Communications*, 47 (2014) 22-27.

140. Reangchim P., Saelee T., Itthibenchapong V., Junkaew A., Chanlek N., Eiad-Ua A., Kungwan N. and Faungnawakij K., Role of Sn promoter in Ni/Al_2O_3 catalyst for the deoxygenation of stearic acid and coke formation: Experimental and theoretical studies, *Catalysis Science & Technology*, (2019). 3361-3372.

141. Liu J., Peng H., Liu W., Xu X., Wang X., Li C., Zhou W., Yuan P., Chen X., Zhang W. and Zhan H., Tin modification on Ni/Al_2O_3: Designing potent coke-resistant catalysts for the dry reforming of methane, *ChemCatChem*, 6 (2014) 2095-2104.

142. Wang F., Zhang J.-C., Li W.-Z. and Chen B.-H., Coke-resistant Au–Ni/$MgAl_2O_4$ catalyst for direct methanation of syngas, *Journal of Energy Chemistry*, 39 (2019) 198-207.

143. Dong C., An L., Yang Y. and Zhang J., A density functional investigation on C atom adsorbed on Ni (111) surface in the steam seforming of acetic acid, *Asia-Pacific Power and Energy Engineering Conference*, (2010). 1-4.

144. Zhang Y., Fu Z., Dong S. and Yan Z., The mechanisms for the high resistance to sulfur poisoning of the Ni/yttria-stabilized zirconia system treated with Sn vapor, *Physical Chemistry Chemical Physics*, 16 (2014) 1033-1040.

LIST OF PUBLICATIONS

1. Rathawat Daengngern, Rusrina Salaeh, **Tinnakorn Saelee,** Khanittha Kerdpol, Nawee Kungwan, Excited-state intramolecular proton transfer reactions of 2,5-bis(2′-benzoxazolyl)hydroquinone and its water cluster exhibiting single and double proton transfer: A TD-DFT dynamics simulation. *J. Mol. Liq.* 2019, 286, 110889-110898 [*IF4.48, Q2*]

2. Promporn Reangchim, **Tinnakorn Saelee**, Vorranutch Itthibenchapong, Anchalee Junkaew, Narong Chanlek, Apiluck Eiad-ua, Nawee Kungwan, Kajornsak Faungnawaki, Role of Sn promoter in Ni/Al_2O_3 catalyst for the deoxygenation of stearic acid and coke formation: experimental and theoretical studies. *Catal. Sci. Technol.* 2019, 9, 3361-3372 [*IF5.73, Q1*]

3. **Tinnakorn Saelee**, Supawadee Namuangruk, Nawee Kungwan, Anchalee Junkaew, Theoretical insight into catalytic propane dehydrogenation on Ni(111). *J. Phys. Chem. C.* 2018, 122, 14678-14690 [*IF4.48, Q1*]

4. Sutinee Girdthep, Wenuka Sankong, Asamaporn Pongmalee, **Tinnakorn Saelee**, Winita Punyodom, Puttinan Meepowpan, Patnarin Worajittiphon, Enhanced crystallization, thermal properties, and hydrolysis resistance of poly(L-lactic acid) and its stereocomplex by incorporation of graphene nanoplatelets. *Polym. Test*. 2017, 61, 229-239. [*IF2.45, Q1*]

5. Sunan Tacha, **Tinnakorn Saelee,** Woothichai Khotasen, Winita Punyodom, Robert Molloy, Patnarin Worajittiphon, Puttinan Meepowpan, Kiattikhun Manokruang, Stereocomplexation of PLL/PDL–PEG–PDL blends: Effects of blend morphology on film toughness. *Eur. Polym. J.* 2015, 69, 308-318. [*IF3.67, Q1*]

APPENDIX A

Scholarships and Experiences

Scholarship

2015 - 2019 Thailand Graduate Institute of Science and Technology Scholarship (TGIST), Thailand

2017 Graduate Research Scholarship from Chiang Mai University Research

Short-Term Visit

1. 2019 (Feb 20th - June 15st) four months short visiting researcher at School of Chemical and Biomolecular, University of Sydney, Australia.
2. 2018 (May 29th - Aug 1st) three months visiting researcher at Ibaraki University, Japan.
3. 2017 (June 13th - Sep 9th) three months visiting researcher at Ibaraki University, Japan.

Working skill/Certificate

1. Staff: The 22nd International Annual Symposium on Computational Science and Engineering (ANSCSE22), Chulalongkorn University, Bangkok, Thailand.
2. Staff: The 2nd Thai-Japan Symposium in Chemistry and The 13th Thai Summer School of Computational Chemistry (13rd TS_2C_2) Workshop organized by Material Research Center, Chiang Mai University.
3. Staff: Molecular Designs for Advanced Materials: Workshop and Conference organized by Material Research Center, Chiang Mai University.
4. Staff: The 2014 IUPAC World Polymer Congress (MACRO 2014) organized by Chemical Society of Thailand (CST), Chiang Mai University.

APPENDIX B

Conferences and Workshops

Conference

1. 2018 (November 8th - 9th) participated in the 15th Thai Summer School of Computational Chemistry (TS2C2), Department of Chemistry, Faculty of Science, Ubon Ratchathani University
2. 2018 (May 30th - June 2nd) Asian Workshop of Experiment and Theory in Quantum Beam Molecular Science at Ibaraki University, Ibaraki, Japan "Mechanistic investigations of propane dehydrogenation on Ni-based catalyst: A DFT study"
3. 2016 (September 19th - October 9th) successfully achieved the course of Japan-Asia Youth Exchange Program in Science, Yokohama City University, Yokohama, Japan
4. 2015 (March 6th -10th) selected participant for attending the Asian Academic Seminar (AAS 2014) Kolkata, India

Workshop

1. 2018 (November 8th - 9th) The Excited State Theory and Application Workshop, Department of Chemistry, Faculty of Science, Ubon Ratchathani University
2. 2017 (July 14th - 15th) Japan-Thai Workshop on Theoretical and Computational Chemistry 2017, Yokohama City University, Yokohama, Japan.
3. 2016 (November 15th - 17th) The Thai-Japan Symposium in Chemistry and The 13th Thai Summer School of Computational Chemistry Workshop (13th TS_2C_2), Chiang Mai University, Chiang Mai, Thailand.
4. 2016 (July 27th - 29th) The Workshop on Computational Biomolecular Modelling in ANSCSE 20, Kasetsart University, Thailand.

APPENDIX C

Publications and Posters

European Polymer Journal 69 (2015) 308–318

Contents lists available at ScienceDirect

European Polymer Journal

journal homepage: www.elsevier.com/locate/europolj

Stereocomplexation of PLL/PDL–PEG–PDL blends: Effects of blend morphology on film toughness

Sunan Tacha [a], Tinnakorn Saelee [a], Wootichai Khotasen [a], Winita Punyodom [a,b], Robert Molloy [a,b], Patnarin Worajittiphon [a,b], Puttinan Meepowpan [a], Kiattikhun Manokruang [a,b,*]

[a] Department of Chemistry, Faculty of Science, Chiang Mai University, Chiang Mai 50200, Thailand
[b] Materials Science Research Center, Faculty of Science, Chiang Mai University, Chiang Mai 50200, Thailand

ARTICLE INFO

Article history:
Received 25 April 2015
Received in revised form 8 June 2015
Accepted 9 June 2015
Available online 10 June 2015

Keywords:
Stereocomplex
Poly(lactide)
Toughness
Atomic force microscopy (AFM)

ABSTRACT

Polylactide (PL) finds its use in a wide variety of applications ranging from medical devices to engineering plastics. However, the use of PL is limited to certain applications due to its brittle characteristic and low heat distortion temperature, which indicate its poor mechanical and thermal properties, respectively. This present work demonstrated the toughening of PL by stereocomplexation adopting poly(D-lactide)–poly(ethylene glycol)–poly(D-lactide) (PDL–PEG–PDL) copolymers with various PDL segment length. The DSC results showed that the complete stereocomplexation was reached when 40 wt% copolymer was blended with poly(L-lactide) (PLL). In addition, the crystallization of PEG was interrupted and, thus, prohibited by either adding PDL or PLL in the system. AFM images showed that, for the first time, the stereocomplex crystallites (Sc-crystallites) formed by the enantiomer pairs were dispersed in a continuous amorphous phase of PL and the non-crystallizing PEG. The increase of PDL segment length in the copolymer leaded to the increase of the Sc-crystallite size, which, consequently, resulted in the increase of the tensile strength of the blended-films. Elongation at break of the films was found to rely on the determined amorphous area. To maximize the toughness of the films, the specific ratio of PDL and PEG segment length in the copolymer must be achieved to provide the optimum balance between Sc-crystallite size and % amorphous area.

1. Introduction

Polylactide (PL), one of the well-known aliphatic polyesters, has received much interest due to its enzymatic-/hydrolytic-degradability as well as biocompatibility [1–3]. PL finds its use in a wide variety of applications ranging from medical devices to engineering plastics [4–7]. Since its monomer can be derived from renewable agricultural sources, this polymer is considered as a "green" alternative thermoplastic which can potentially replace a number of petrochemical based polymers in the next era. However, the use of PL is limited to certain applications due to its brittle characteristic and low heat distortion temperature, which indicate its poor mechanical and thermal properties, respectively. Many approaches adopted to improve heat distortion temperature of PL such as plasticization and nucleation [8,9], and blending PLL with its

* Corresponding author at: Department of Chemistry, Faculty of Science, Chiang Mai University, Chiang Mai 50200, Thailand.
E-mail address: kiattikhun.m@cmu.ac.th (K. Manokruang).

Contents lists available at ScienceDirect

Polymer Testing

journal homepage: www.elsevier.com/locate/polytest

Enhanced crystallization, thermal properties, and hydrolysis resistance of poly(L-lactic acid) and its stereocomplex by incorporation of graphene nanoplatelets

Sutinee Girdthep [a], Wenuka Sankong [b], Asamaporn Pongmalee [b], Tinnakorn Saelee [b], Winita Punyodom [b, c], Puttinan Meepowpan [b], Patnarin Worajittiphon [b, c, d, *]

[a] Department of Chemistry, Faculty of Science, Silpakorn University, Nakhon Pathom 73000, Thailand
[b] Department of Chemistry, Faculty of Science, Chiang Mai University, Chiang Mai 50200, Thailand
[c] Center of Excellence in Materials Science and Technology, Chiang Mai University, Chiang Mai 50200, Thailand
[d] Center of Excellence for Innovation in Chemistry, Faculty of Science, Chiang Mai University, Chiang Mai 50200, Thailand

ARTICLE INFO

Article history:
Received 10 January 2017
Received in revised form
20 April 2017
Accepted 9 May 2017
Available online 19 May 2017

Keywords:
Polylactide
Graphene
Stereocomplex
Nanocomposite
Hydrolytic degradation
Thermal property

ABSTRACT

Poly(D-lactic acid) (PDLA) and graphene nanoplatelets were used as nucleating agents for poly(L-lactic acid) (PLLA). The graphene (1 wt%) shows a more pronounced effect than PDLA in facilitating PLLA crystallization. Graphene effect on crystallization of stereocomplex (SC) polylactide is also demonstrated. Although medium molecular weight PLLA was blended with a limited content (1 wt%) of low molecular weight PDLA in the presence of graphene (0.5 phr), SC melting temperature is slightly increased without the use of high molecular weight polylactide pair. Also, optimal graphene content (0.5 phr–1.5 phr) promotes crystallization of PLLA homocrystals in the three-component system (PLLA/PDLA/graphene). Graphene additionally enhances Young's modulus and barrier property to thermal degradation of both PLLA and SC systems. Furthermore, PLLA/graphene is more resistant to hydrolysis than PLLA. Likewise, PLLA/PDLA/graphene is more stable than PLLA/PDLA during hydrolysis.

1. Introduction

Poly(L-lactic acid) (PLLA) is a commercial polymer that has drawn much attention because it is biodegradable and derived from renewable resources [1]. However, the major bottlenecks to practical uses of PLLA are its properties of low crystallinity and low crystallization rate which significantly suppress associated mechanical and thermal properties and stability of PLLA-based products [2,3]. Blending of polylactide enantiomeric forms between PLLA and poly(D-lactic acid) (PDLA) results in stereocomplex (SC) crystals which are used as nucleating agents to increase the PLLA crystallization rate [4,5]. A series of PDLA contents, ranging up to 10 wt%, was previously added to PLLA [4,6,7]. Based on these reports, adding low contents of PDLA (<5 wt%) to PLLA for nucleation purpose was shown to be efficient in promoting PLLA crystal formation. In addition to using PDLA, use of other nucleating agents for PLLA was also reported, for instance, talc [8], fullerene [8], montmorillonite [8], multi-walled carbon nanotubes [9,10], graphene [10,11], and graphene oxide (GO) [12].

Graphene (or graphene nanoplatelets, GNPs) and GO have been studied and used in a wide range of applications due to their excellent properties such as high thermal conductivity [13], high mechanical strength [14], and high carrier transport ability [15]. Due to their layered morphology with high aspect ratio and high surface area, graphene nanosheets embedded in such PLLA/graphene systems can act as effective nucleating sites for PLLA crystal formation. Thus, graphene and GO were incorporated into PLLA to aid lamellar packing of polymer chains for crystallization studies [10,11,16,17]. Using graphene and GO in the content range of 0.05–2 wt% resulted in a positive effect on PLLA crystallization because the nucleation site number was increased and the nucleation was more readily introduced to the PLLA/graphene composite compared to the neat PLLA [10,16,17].

* Corresponding author. Department of Chemistry, Faculty of Science, Chiang Mai University, Chiang Mai 50200, Thailand.
E-mail address: pworajittiphon@gmail.com (P. Worajittiphon).

THE JOURNAL OF PHYSICAL CHEMISTRY C

Article

Cite This: J. Phys. Chem. C 2018, 122, 14678−14690

pubs.acs.org/JPCC

Theoretical Insight into Catalytic Propane Dehydrogenation on Ni(111)

Tinnakorn Saelee,[†] Supawadee Namuangruk,[§] Nawee Kungwan,*[,†,‡] and Anchalee Junkaew*[,§]

[†]Department of Chemistry, Faculty of Science, Chiang Mai University, Chiang Mai 50200, Thailand

[‡]Center of Excellence in Materials Science and Technology, Chiang Mai University, Chiang Mai 50200, Thailand

[§]National Nanotechnology Center (NANOTEC), National Science and Technology Development Agency (NSTDA), Pathum Thani 12120, Thailand

Supporting Information

ABSTRACT: Here, propane dehydrogenation (PDH) to propylene and side reactions, namely, cracking and deep dehydrogenation on Ni(111) surface, have been theoretically investigated by density functional theory calculation. On the basis of adsorption energies, propane is physisorbed on Ni(111) surface, whereas propylene exhibits chemisorption supported by electronic charge results. In the PDH reaction, possible pathways can occur via two possible intermediates, i.e., 1-propyl and 2-propyl. Our results suggest that PDH reaction through 1-propyl intermediate is both kinetically and thermodynamically more favorable than another pathway. The C−C bond cracking during PDH process is more difficult to occur than the C−H activation reaction because of higher energy barrier of the C−C bond cracking. However, deep dehydrogenation is the preferable process after PDH, owing to the strong adsorption of propylene on Ni(111) surface, resulting in low selectivity of propylene production. This work suggests that Ni(111) has superior activity toward PDH; however, the enhancement of propylene desorption is required to improve its selectivity. The understanding in molecular level from this work is useful for designing and developing better Ni-based catalysts in terms of activity and selectivity for propane conversion to propylene.

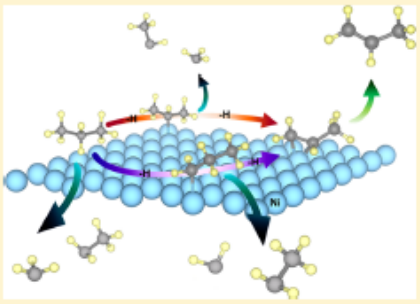

1. INTRODUCTION

Propylene is an important monomer to produce polypropylene, which is a useful polymer for automotive part, textile, furniture, clothing, tube, and packaging applications.[1,2] Moreover, it is a crucial chemical feedstock to synthesize other important chemicals, such as propylene oxide, acrylic acid, acrylonitrile, cumene, and alcohols. Those chemicals are precursors in many products for painting, coating, and automotive parts.[3,4] Typically, propylene can be produced from steam cracking of liquid feedstocks,[5] catalytic cracking refinery units,[5,6] and propane dehydrogenation (PDH) reaction.[7] Among those processes, PDH is a simple approach to generate propylene by direct elimination of two H atoms from propane using effective heterogeneous catalysts.[8−10] The PDH mechanisms and side reactions, including C−C bond cleavage and deep dehydrogenation on catalyst surface, have been proposed as illustrated in Scheme 1.[11] The PDH mechanisms can be classified into two possible pathways based on the order of eliminated H position. One is through 1-propyl ($*CH_2CH_2CH_3$) intermediate (Int) in pathway A, where one H of the primary carbon is eliminated first. Another is via 2-propyl (CH_3*CHCH_3) intermediate in pathway B, where one H of the secondary carbon is eliminated first. However, the side reactions of the C−C bond cracking of propane, propyl intermediates, and propylene, which are described in steps 1C, 2C, 2C′ during PDH, and 3C after PDH, can take place.[12−14] Moreover, another side reaction, namely, the deep dehydrogenation of propylene to 1-propenyl (CH_3CHCH*) and 2-propenyl ($CH_2^*CCH_3$) via steps 3D and 3E leading to coke formation, is also possible resulting in deactivation on the active site of the catalyst surface. Thus, high effective catalysts with high selectivity of propylene are very essential for PDH reaction. On the other hand, good selectivity of propylene can be achieved by inhibiting the side reactions of C−C bond cracking and deep dehydrogenation on the surface of catalyst.

Many catalysts have been proposed in the literature for PDH reaction, including (1) metals as nonoxidative dehydrogenation catalysts, such as platinum (Pt)[15−19] and nickel (Ni);[20,21] (2) metal oxides as oxidative catalysts, such as chromium oxide (CrO_x),[22−25] vanadium oxide (VO_x),[26−29] molybdenum oxide (MoO_x),[29,30] and gallium oxide (GaO_x);[23,31−33] (3) carbon-based materials, such as carbon nanofibers[34] and mesoporous carbon;[35] (4) zeolites;[36−38] and so on. Among metal-based catalysts, Pt has been widely employed in industries due to its high reactivity on PDH and minimum cracking, leading to high conversion of propane.[7,8,12] However, the poisoning of the

Received: April 26, 2018
Revised: May 27, 2018
Published: June 15, 2018

DOI: 10.1021/acs.jpcc.8b03939
J. Phys. Chem. C 2018, 122, 14678−14690

Catalysis Science & Technology

PAPER

View Article Online
View Journal | View Issue

Cite this: Catal. Sci. Technol., 2019, 9, 3361

Role of Sn promoter in Ni/Al_2O_3 catalyst for the deoxygenation of stearic acid and coke formation: experimental and theoretical studies†

Promporn Reangchim,[ab] Tinnakorn Saelee,[ac] Vorranutch Itthibenchapong,[*a] Anchalee Junkaew,[a] Narong Chanlek,[d] Apiluck Eiad-ua,[b] Nawee Kungwan[ce] and Kajornsak Faungnawakij[a]

Received 6th February 2019,
Accepted 22nd April 2019

DOI: 10.1039/c9cy00268e

rsc.li/catalysis

The effect of Sn promoter on a $Ni/\gamma\text{-}Al_2O_3$ catalyst towards the catalytic activity and catalyst stability *via* the deoxygenation of stearic acid for the production of diesel-range hydrocarbons has been investigated herein. The decarboxylation (DCO_2) and decarbonylation (DCO) of stearic acid using NiSn catalysts are proposed as the main pathways to produce *n*-heptadecane ($n\text{-}C_{17}H_{36}$), whereas hydrodeoxygenation (HDO) is a minor pathway, as confirmed by the high ratio of C17 to C18 alkanes. Moreover, the Sn promoter in $Ni/\gamma\text{-}Al_2O_3$ significantly improves the catalyst reusability by enhancing the tolerance to the carbon-induced deactivation. This improvement was investigated by a density functional theory (DFT) calculation. The calculation results clearly explained that the Sn promoter can weaken the interaction between carbon and the catalyst surface, tending to prevent carbon segregation on the NiSn surface. This retardation of coke formation expands the life time of the catalyst, leading to a cost-effective approach for industrial processes.

1. Introduction

Along with the rapidly accelerating energy consumption, the depletion of conventional petroleum resources has attracted worldwide attention. This concern has driven research and development in renewable energy technologies. Among the available alternative energy resources, biofuels derived from biomass, plant and animal oils, and industrial wastes *via* catalytic reactions have gained high attention due to their environmental benefits.[1–3] Bio-hydrogenated diesel (BHD) or green diesel product and biochemicals from sugar and lignin derived from biomass can be mainly produced *via* a deoxygenation reaction.[3,4] Typically, there are three well-known deoxygenation pathways. First, hydrodeoxygenation (HDO) in which the oxygenated components are removed from the reactants under H_2 gas to obtain a hydrocarbon with retained chain length and a water molecule as the by-product. The other two reactions are decarboxylation (DCO_2) and decarbonylation (DCO) in which a carboxyl group or a carbonyl group is removed to obtain a hydrocarbon with a shorter chain length and CO_2 or CO as the by-product, respectively.[5]

In the literature, various monometallic and bimetallic catalysts deposited on a variety of supports such as SiO_2, Al_2O_3, zeolites and carbon have been explored for the green diesel production applications.[5–10] Not only the reaction conditions, but the different types of catalysts and supports also play decisive roles in the selectivity of each deoxygenation pathway. For instance, MoS_2-based catalysts including a Co (or Ni) promoter have been known to be highly selective and efficient catalysts for HDO[4,11–13] as well as hydrodesulfurization (HDS). Metal oxides (*e.g.* MoO_3, $NiMoO_3$)[14–17] and metal carbides (*e.g.* Mo_2C, W_2C)[18–20] have also been reported as promising catalysts for HDO. Transition metal catalysts (*i.e.* Pt, Pd, Ni, Cu, Co, Mo, W) including monometallic and their bimetallic forms,[7,21–26] metal phosphides (*e.g.* Ni_2P, Co_2P, Cu_2P, MoP),[8,27,28] and metal organic frameworks (MOFs)[29,30] have been reported to be selective for DCO_2 and DCO.

Among these choices of catalysts, Ni metal has become an attractive catalyst for the deoxygenation reaction due to its high reactivity, being sulfur-free, relatively low cost compared with noble metals, and lower H_2 consumption *via* DCO and DCO_2 pathways.[21,31] An enhancement in the deoxygenation

[a] National Nanotechnology Center (NANOTEC), National Science and Technology Development Agency (NSTDA), 111 Thailand Science Park, Pathum Thani 12120, Thailand. E-mail: vorranutch@nanotec.or.th; Fax: +66 2 564 6981; Tel: +66 2 564 7100 ext. 6615
[b] College of Nanotechnology, King Mongkut's Institute of Technology Ladkrabang, Bangkok, 10520 Thailand
[c] Department of Chemistry, Faculty of Science, Chiang Mai University, Chiang Mai, 50200, Thailand
[d] Synchrotron Light Research Institute (Public Organization), 111 University Avenue, Muang District, Nakhon Ratchasima, 30000 Thailand
[e] Center of Excellence in Materials Science and Technology, Chiang Mai University, Chiang Mai 50200, Thailand

† Electronic supplementary information (ESI) available. See DOI: 10.1039/c9cy00268e

Contents lists available at ScienceDirect

Journal of Molecular Liquids

journal homepage: www.elsevier.com/locate/molliq

Excited-state intramolecular proton transfer reactions of 2,5-bis(2′-benzoxazolyl)hydroquinone and its water cluster exhibiting single and double proton transfer: A TD-DFT dynamics simulation

Rathawat Daengngern [a,b,*], Rusrina Salaeh [c], Tinnakorn Saelee [c], Khanittha Kerdpol [c], Nawee Kungwan [c,d]

[a] Department of Chemistry, Faculty of Science, King Mongkut's Institute of Technology Ladkrabang, Bangkok 10520, Thailand
[b] Integrated Applied Chemistry Research Unit, Faculty of Science, King Mongkut's Institute of Technology Ladkrabang, Bangkok 10520, Thailand
[c] Department of Chemistry, Faculty of Science, Chiang Mai University, Chiang Mai 50200, Thailand
[d] Center of Excellence in Materials Science and Technology, Chiang Mai University, Chiang Mai 50200, Thailand

ARTICLE INFO

Article history:
Received 4 January 2019
Received in revised form 13 April 2019
Accepted 1 May 2019
Available online 2 May 2019

Keywords:
2,5-Bis(2′-benzoxazolyl)hydroquinone
TD-DFT
Excited-state proton intramolecular transfer
Dynamics simulations

ABSTRACT

Detailed pictures of the excited-state intramolecular proton transfer (ESIPT) of 2,5-bis(2′-benzoxazolyl)hydroquinone (BHQ) and its water cluster have been investigated by dynamics simulations on the first lowest-excited energy using time-dependent density functional theory (TD-DFT). We focused on the structural, photophysical and dynamic properties of BHQ in the absence and presence of water molecules through intermolecular hydrogen bonds (interHBs). Our dynamics simulations reveal three possible mechanisms of the ESIPT processes: i) no proton transfer (No PT); ii) single PT (SPT); and iii) double PT (DPT), that could take place within the PT time of 160 fs via intrinsic intramolecular hydrogen bonds (intraHBs). The ESIPT mechanism of isolated BHQ elucidates that back PT is likely to be found at 64% rather than the SPT (32%) and DPT (4%), which is in good agreement with the experiments of dual fluorescence from di-enol and mono-keto emissions. Notably, the results from BHQ with water (BHQ-$(H_2O)_2$) reveal that the participation of water might produce a remarkable effect on promoting the SPT process up to 60% and DPT up to 7 times when compared to conditions of no water. The simulated probability of PT is well related to possible PT mechanisms regarding different tautomers in the fluorescence spectra found in previous experiments. The existence of di-keto tautomer arose from the DPT of BHQ and its water cluster and was not observed in the UV/Vis spectrum.

1. Introduction

One of the most significant and simplest processes that have recently been gaining increased levels of attention is proton transfer (PT), especially with regard to the excited-state intramolecular proton transfer (ESIPT) that takes place in biochemistry and chemistry [1–3]. Owing to the remarkable photophysical properties of ESIPT molecules [4–7], a large Stokes shift arising from the ESIPT process may lead to many applicational uses, such as in light-emitting devices [8–10], photoswitches [11–14], and fluorescent probes [15,16], etc. Most of the ESIPT processes occur in the molecules having moieties of proton donors (O—H, N—H) and proton acceptors (C═N, C═O) through intrinsic intramolecular hydrogen bonds (intraHBs) [10,15,17]. The ESIPT processes occur via the four-level photocycle (Enol → Enol* → Keto* → Keto) of phototautomerization between the proton donor and acceptor sites in the bifunctional molecules [15,18]. ESIPT molecules favor the enol form in the ground state (S_0), which is stabilized by intramolecular hydrogen bonding. However, upon photoexcitation, a fast PT reaction from the excited enol triggers to yield the excited keto tautomer on a subpicosecond timescale. Due to the close position between the proton donor and acceptor, the back PT in the excited state is then possibly found if the PT barrier is not too high and barrier energy is close to zero, as illustrated in Scheme 1. In this process, the enol form could not proceed to the keto tautomer because the phenolic proton is not acidic enough to be deprotonated in the ground state. In the excited state, however, the enhancement in the acidity or photoacid is more pronounced for the proton donating group, as well as the basicity of the proton acceptor group, to facilitate the ESIPT process via the enol form [19], which is known as the mono-enol form for only one enol moiety. A lot of relevant reports upon the ESIPT of the mono-enol form, such as 2-(2′-hydroxyphenyl)benzoxazole (HBO) [6,7,20,21] and its derivatives [22–25], have been intensively investigated in ESIPT via single PT (SPT).

Since only the SPT reaction is not adequate to represent the complicated PT behavior in the chemical and biological systems involving multiple PT processes [4–7,26]. To this point, the compounds containing

* Corresponding author at: Department of Chemistry, Faculty of Science, King Mongkut's Institute of Technology Ladkrabang, Bangkok 10520, Thailand.
E-mail address: rathawat.da@kmitl.ac.th (R. Daengngern).

PROPANE DEHYDROGENATION ON Ni-BASED CATALYST

Tinnakorn Sae-Lee[a], Supawadee Namuangrak[b], Nawee Kungwan[a,*], Anchalee Junkaew[b,*]

[a]Department of Chemistry, Faculty of Science, Chiang Mai University, Chiang Mai 50200, Thailand

[b]National Nanotechnology Center (NANOTEC), National Science and Technology Development Agency, Pathumthani, 12120, Thailand.

naweekung@gmail.com

Introduction

Propylene, a product from refining petroleum gas, is a monomer of polypropylene (PP) which is used in a variety of applications. Production of propylene can be done via propane dehydrogenation (PDH) reaction by eliminating hydrogen atoms from propane as shown in figure1. PDH is an interesting approach, because this method can add a value and expand applications of propane. Nowadays, platinum- (Pt-) and chromium- (Cr-) based catalysts are widely used for PDH process due to their high reactivity and good stability at high temperatures. However, the catalyst's price and environment concerned are the limitations of Pt and Cr-based catalysts, respectively. Therefore, nickel-(Ni-) based catalysts are the good candidate for PDH reaction [2] because Ni metal is cheaper than Pt and it is more ecological friendly than Cr. However, the high reactivity of Ni results in hydrogenolysis process by breaking of C-C bond as depicted in figure 2. This side reaction directly decreases the selectivity of the Ni catalyst. This research focuses on the propane adsorption on Ni surface, PDH and hydrogenolysis of propane after adsorption on Ni (111) surface.

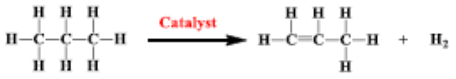

Figure.1 Propane dehydrogenation (PDH) reaction [1]

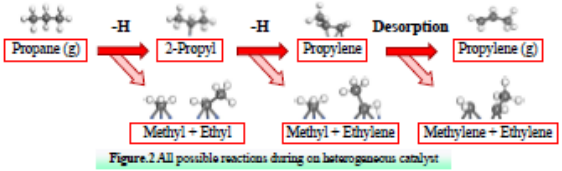

Figure.2 All possible reactions during on heterogeneous catalyst

Computational details

Information of surface slabs

- 6 x 4 x 4 of bare-Ni (111)

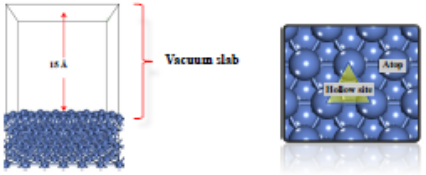

Periodic Density Functional Theory

- Vienna Ab-initio Simulation Package (VASP)
  - Potentials: PAW-PBE
  - Energy cutoff : 400 eV
  - k-points: Monkhorst-Pack 3x3x1
  - Energy convergence criteria: $1x10^{-6}$ eV
  - Force convergence criteria: 0.01 eV/Å
  - Spin polarizable with dispersion correction (DFT+D3)

Nudge elastic band (NEB)

Energetic calculation:

Adsorption energy is calculated by : $E_{ads} = E_{System} - E_{Surface} - E_{Adsorbate}$

Objectives

- To study propane adsorption on bare Ni (111) surface
- To study the mechanisms of PDH and hydrogenolysis of propane on bare Ni (111) surface

Acknowledgements

We gratefully acknowledge the financial support from Thailand Graduate Institute of Science and Technology (TGIST) and the Graduated School, Chiang Mai University. Computational resources are provided by National Nanotechnology Center (NANOTEC) and the National e-Science Infrastructure Consortium. We thank the Computational Chemistry Laboratory, Chiang Mai University (CCL-CMU) for all instrumental supports.

Results and Discussion

Adsorption of propane on bare-Ni surface

Atop site

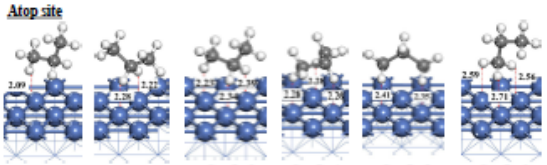

Config.1	Config.2	Config.3	Config.4	Config.5	Config.6
-0.47 eV	-0.51 eV	-0.50 eV	-0.61 eV	-0.53 eV	-0.38 eV

Hollow site

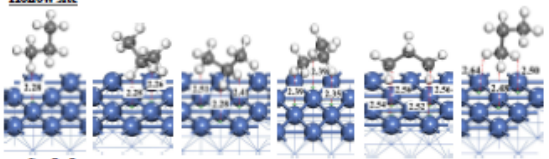

Config.7	Config.8	Config.9	Config.10	Config.11	Config.12
-0.38 eV	-0.47 eV	-0.48 eV	-0.57 eV	-0.51 eV	-0.36 eV

The most favorable configuration of adsorbed propane on bare-Ni(111) surface is the config.4. This configuration provides the highest contact points between the propane molecule and Ni atoms on the Ni surface.

Energy profile of PDH and C-C scission reactions on bare-Ni surface

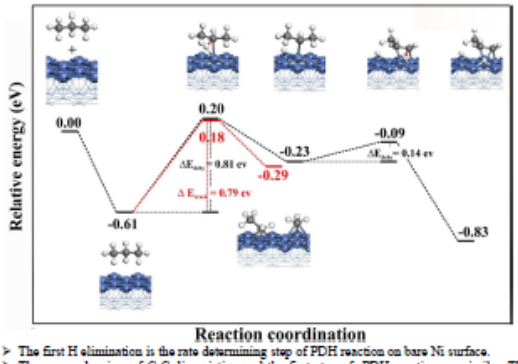

- The first H elimination is the rate determining step of PDH reaction on bare Ni surface.
- The energy barriers of C-C dissociation and the first step of PDH reaction are similar. This result indicates that the hydogenolysis and PDH reactions are competitive on the Ni(111) surface. They can occur after propane molecule is adsorbed on bare-Ni surface.

Conclusions

- The most stable structure of propane adsorption on Ni (111) is the parallel configuration of propane over Ni surface plane.
- Rate determining step of PDH reaction is the first H elimination.
- The PDH and hydogenolysis reactions are competitive on the Ni(111) surface.

References

[1]. X. Cao, Insight into mechanism and selectivity of propane dehydrogenation over the Pd-doped Cu(111) surface, RSC Advances, 6 (2016) 65524-65532.

[2]. Morris D. Argyle and Calvin H. Bartholomew * Catalysts 2015, 5, 145-269

[3]. Z. Yan, Y. Yao, D.W. Goodman, Dehydrogenation of Propane to Propylene over Supported Model Ni–Au Catalysts, Catalysis Letters, 142 (2012) 714-717.

Theoretical study of propane dehydrogenation on Ni-based catalyst

Tinnakorn Sae-Lee[a], Supawadee Namuangrak[b], Anchalee Junkaew[b,*], Nawee Kungwan[a,**]

[a]Department of Chemistry, Faculty of Science, Chiang Mai University, Chiang Mai 50200, Thailand
[b]National Nanotechnology Center (NANOTEC), National Science and Technology Development Agency, Pathumthani, 12120, Thailand
anchalee@nanotec.or.th* and naweekung@gmail.com**

Introduction

Propane dehydrogenation (PDH) is an important process to produce propylene from propane using catalysts. Among metal-based catalysts, nickel (Ni) has been reported as an active catalyst for hydrogenation and dehydrogenation reactions of small alkanes [1]. However, cracking and deep dehydrogenation in PDH decrease selectivity of propylene production, resulting in fast deactivation of catalysts. In literature, experimental observation suggested that doping Au to Ni can enhance the selectivity of propylene production. Mechanistic insights of PDH and C-C bond cracking in Ni and Ni-Au catalysts have not been well understood yet. In this work, PDH and C-C bond cracking reactions on Ni and 0.33 monolayer equivalent (MLE) of Au on Ni(111) (Ni-Au) catalysts have been systematically investigated by using plane-wave based density functional theory (DFT) calculations. Our results show that the active site of catalysts for propane adsorption is atop Ni site. Electronic charge properties have been elucidated to explain nature of these catalysts. Modifying Ni catalyst by Au increases energy barriers of C-C bond and decreases propylene adsorption. Therefore, Ni-Au catalyst is more selective toward propylene production than Ni catalyst.

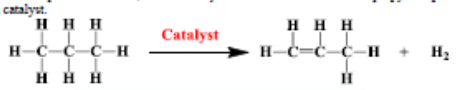

Figure 1. Propane dehydrogenation (PDH) reaction [2].

Computational Details

Slab models

Ni(111) surface

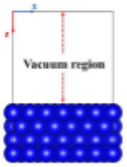

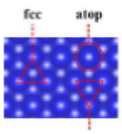

0.33 MLE Au-Ni surface

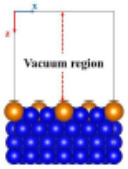

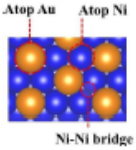

Periodic Density Functional Theory

- Vienna Ab-initio Simulation Package (VASP)
- Potential: PAW-PBE
- Energy cutoff : 400 eV
- K-points: Monkhorst-Pack 3x3x1
- Energy convergence criterion: $1x10^{-5}$ eV
- Force convergence criterion: 0.01 eV/Å
- Spin polarizable
- Dispersion correction (DFT+D3)
- Nudge elastic band (NEB) and Dimer

Adsorption energy (E_{ads}) is calculated by :

$$E_{ads} = E_{System} - E_{Surface} - E_{Adsorbate}$$

Objectives

- To investigate the effect of Au in Ni-based catalysts for PDH reaction
- To study the PDH mechanisms on Ni (111) and Ni-Au surfaces
- To compare reactivity of Ni (111) and Ni-Au surfaces

Acknowledgements

We gratefully acknowledge the financial support from Thailand Graduate Institute of Science and Technology (TGIST) and the Graduated School, Chiang Mai University. Computational resources are provided by National Nanotechnology Center (NANOTEC) and the National e-Science Infrastructure Consortium. We thank the Computational Chemistry Laboratory, Chiang Mai University (CCL-CMU) for all supports.

References

[1] L. Luo, D.C. Rosenfield, Non-Oxidative Patent Dehydrogenative Process in, DOW Global Technologies LLC,Midland, MI (US), 2013
[2] Z. Yan, Y. Yao, D.W. Goodman, Dehydrogenation of Propane to Propylene over Supported/Model Ni–Au Catalysts, Catalysis Letters, 142 (2012) 714-717
[3] X. Cao, Insight into mechanism and selectivity of propane dehydrogenation over the Pd-doped Cu(111) surface, RSC Advances, 6 (2016) 65524-65532.
[4] M.-L. Yang, Y.-A. Zhu, C. Fan, Z.-J. Sui, D. Chen, X.-G. Zhou, DFT study of propane dehydrogenation on Pt catalyst: effects of step sites, Physical Chemistry Chemical Physics, 13 (2011) 3257-3267.

Results and Discussion

Adsorption of propane on bare-Ni surface

Adsorbent	Adsorption energy (eV)		
	Pt(111) [3]	Ni(111)	Ni-Au
Propane	-0.42	-0.61	-0.58
Propylene	-0.97	-0.91	-0.84

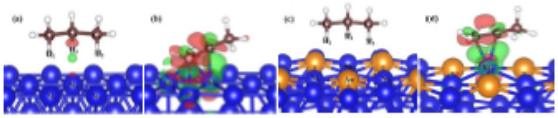

- Atop Ni sites are the active sites of Ni and Ni-Au catalysts for propane and propylene adsorption.
- Doping of Au into Ni(111) catalyst can increase the efficiency of propylene desorption because Au as inactive site can reduce the active site of Ni surface.
- The d-band center of Ni-Au (-1.58 eV) is lower than that of Ni(111) (-1.43 eV), indicating that Ni-Au catalyst is less reactive than Ni(111).

Energy profile of PDH and C-C cracking reactions on Ni(111) and Ni-Au surfaces

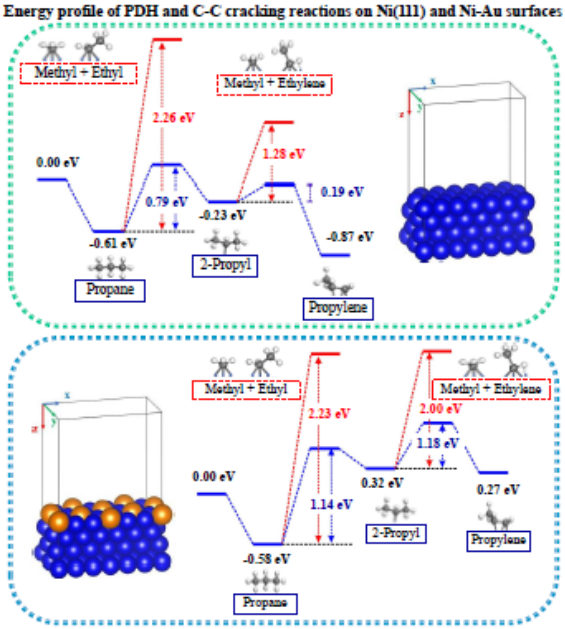

- By comparing energy barriers, PDH reactions proceed easier than C-C bond cracking in both systems.
- The first H elimination is the rate determining step of PDH reaction on Ni and Ni-Au surfaces.
- Doping of Au to Ni(111) increases energy barriers of C-C bond cracking and PDH reaction because the active sites of Ni catalyst are suppressed by inactive Au.

Conclusions

- Doping Au into Ni(111) surface has no effect on propane adsorption but decreases adsorption energy of propylene.
- Doping Au into Ni(111) surface increases energy barriers of PDH and C-C cracking reactions.
- Desorption of propylene from Ni-Au surface is easier than that of Ni(111), indicating better selectivity of propylene production.

Theoretical Investigation of Propane Dehydrogenation on Ni(111) Surface

Tinnakorn Sae-Lee[a], Supawadee Namuangrak[b], Nawee Kungwan[a,*], Anchalee Junkaew[b,*]

[a]Department of Chemistry, Faculty of Science, Chiang Mai University, Chiang Mai 50200, Thailand
[b]National Nanotechnology Center (NANOTEC), National Science and Technology Development Agency, Pathumthani 12120, Thailand
naweekung@gmail.com and anchalee@nanotec.or.th

Introduction

Propylene, a product from refining petroleum gas, is a monomer of polypropylene (PP) which is used in a variety of applications. It can be produced via propane dehydrogenation (PDH) reaction by eliminating two hydrogen atoms from propane using the high effective catalyst. Nowadays, platinum (Pt) is the conventional catalyst for PDH process due to its high reactivity and good stability at high temperatures. However, the low selectivity of propylene production on Pt catalyst leads to exploration the new effective catalyst for PDH process. Recently, nickel (Ni) metal has been reported as the good candidate for PDH reaction [2] due to its high reactivity for alkane reaction and cheaper than Pt. Nevertheless, the reaction mechanism of PDH as well as the side reactions of C-C bond cracking on Ni are still unclear. Therefore, possible PDH reaction and side reactions (Figure1.) are theoretically investigated by DFT study.

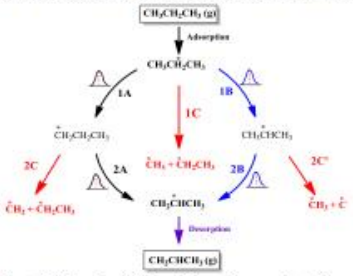

Figure 1. Mechanisms of PDH and side reactions on catalyst surface

Objectives

- To study adsorption process of propane and propylene on Ni(111) surface
- To investigate insight mechanism of PDH reaction on Ni(111) surface
- To understand the cause of low selectivity of propylene production on Ni(111) for designing the better Ni-based catalyst in the future

Computational details

Periodic Density Functional Theory

- Vienna Ab-initio Simulation Package (VASP)
  - Potentials: PAW-PBE
  - k-points: Monkhorst-Pack 3x3x1
  - Energy convergence criteria: $1x10^{-5}$ eV
  - Force convergence criteria: 0.01 eV/Å
  - Spin polarizable with dispersion correction (DFT+D3)

Nudge elastic band (NEB) and Dimer

Energetic calculations

Adsorption energy is calculated by : $E_{ads} = E_{System} - E_{Surface} - E_{Adsorbate}$

Ni(111) surface

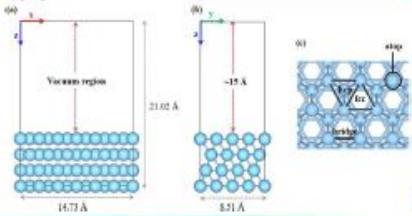

Acknowledgements

We gratefully acknowledge the financial support from Thailand Graduate Institute of Science and Technology (TGIST) and the Graduated School, Chiang Mai University. Computational resources are provided by National Nanotechnology Center (NANOTEC) and the National e-Science Infrastructure Consortium. We thank the Computational Chemistry Laboratory, Chiang Mai University (CCL-CMU) for all instrumental supports.

Results and Discussion

Adsorption of propane and propylene on Ni(111) surface

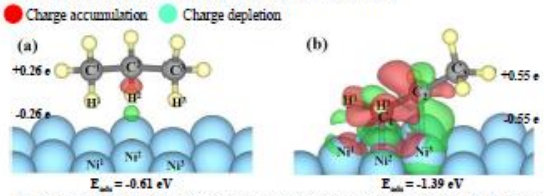

Figure 2. Charge density differences of (a) propane and (b) propylene adsorption on the Ni(111) surface

Mechanisms of PDH reaction on Ni(111)

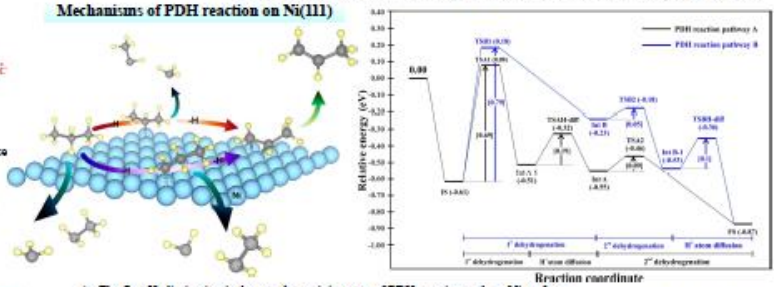

- The first H elimination is the rate determining step of PDH reaction on bare Ni surface.
- Dehydrogenation of propane to form 1-propyl intermediate via pathway A is more kinetically favorable than that of 2-propyl intermediate (pathway B).

Energy profile of PDH and C-C scission reactions on Ni(111) surface

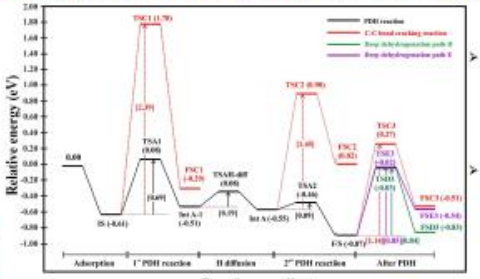

- The C-C cracking barriers are much higher than PDH barriers indicating that the hydrogenolysis reaction cannot occur during PDH process on Ni(111) surface.
- Deep hydrogenation of propylene after PDH process is a predominant reaction leading to low selectivity of propylene production on Ni(111) surface.

Conclusions

- Propane and propylene interact with Ni(111) via physisorption and chemisorption processes, respectively.
- Pathway A via 1-propyl intermediate is the most kinetically favorable pathway for the PDH reaction.
- The C-C bond cracking reaction is impossible to take place during PDH process.
- The low desorption ability of propylene from Ni(111) surface causes the low selectivity of propylene production.
- Modification of Ni(111) surface for facilitating desorption ability of propylene is essential for improving the selectivity of propylene production on Ni(111) surface.

References

(1) Nerlekar, J. K.; Schreffler, M.; Toffoletto, M. MRS Bulletin 2011, 31, 669.
(2) Yan, Z.; Goodman, D. W. Catal. Lett. 2012, 142, 517.
(3) Yan, Z.; Yao, Y.; Goodman, D. W. Catal. Lett. 2012, 142, 714.
(4) Yang, M.-L.; Zhu, J.; Zhu, Y.-A.; Sui, Z.-J.; Yu, Y.-D.; Zhou, X.-G.; Chen, D. J. Mol. Catal. A: Chem. 2014, 395, 329.
(5) Yang, M.-L.; Zhu, Y.-A.; Fan, C.; Sui, Z.-J.; Chen, D.; Zhou, X.-G. J. Mol. Catal. A: Chem. 2010, 321, 42.
(6) Saelee, T.; Namuangrak, S.; Kungwan, N.; Junkaew, A. J Phys Chem C 2018, 122, 14678.

Influence of Au Promoter on Catalytic Properties of Ni-Au for Propane Dehydrogenation Reaction: A DFT Study

Tinnakorn Sae-Lee[a,b], Supawadee Namuangrak[b], Suwit Suthirakun[c,d], Nawee Kungwan[a,*], Anchalee Junkaew[b,*]

[a]Department of Chemistry, Faculty of Science, Chiang Mai University, Chiang Mai 50200, Thailand
[b]National Nanotechnology Center (NANOTEC), National Science and Technology Development Agency, Pathumthani, 12120, Thailand
[c]School of Chemistry, Institute of Science, Suranaree University of Technology, Nakhon Ratchasima 30000, Thailand
[d]Center of Excellence in Advanced Functional Materials, Suranaree University of Technology, Nakhon Ratchasima 30000, Thailand
anchalee@nanotec.or.th* and naweekung@gmail.com**

Introduction

Propane dehydrogenation (PDH) is an important process to produce propylene from propane using catalysts. Among metal-based catalysts, nickel (Ni) has been reported as an active catalyst for dehydrogenation reactions of small alkanes [1]. However, the coke formation declines selectivity of propylene production. In literature, experimental observation suggested that doping Au to Ni can enhance the selectivity of propylene production. However, mechanistic insights of PDH and side reaction of coke formation on Ni and Ni-Au catalysts have not been well understood yet. In this work, PDH reaction and C adsorption on Ni and 0.33 monolayer equivalent (MLE) of Au on Ni(111) (Ni-Au) catalysts have been systematically investigated by using plane-wave based density functional theory (DFT) calculations. Our results show that the active site of catalysts for propane adsorption is atop Ni site. Electronic charge properties have been elucidated to explain nature of these catalysts. Modifying Ni catalyst by Au enhance the efficient of propylene desorption and inhibit C formation. Therefore, Ni-Au catalyst is more selective toward propylene production than Ni catalyst.

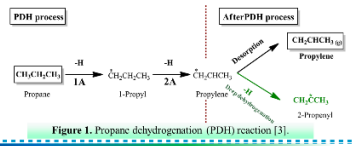

Figure 1. Propane dehydrogenation (PDH) reaction [3].

Computational Details

Slab information

Ni(111) surface

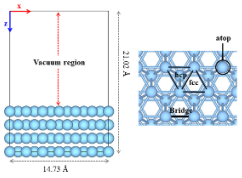

0.33 MLE Ni-Au surface

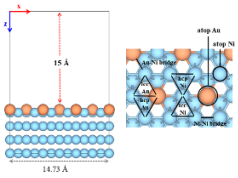

Periodic Density Functional Theory

- Vienna Ab-initio Simulation Package (VASP)
- Potential: PAW-PBE
- Energy cutoff : 400 eV
- K-points: Monkhorst-Pack 3x5x1
- Energy convergence criterion: $1x10^{-5}$ eV
- Force convergence criterion: 0.01 eV/Å
- Spin polarizable
- Dispersion correction (DFT+D3)
- Nudge elastic band (NEB) and Dimer

Adsorption energy (E_{ads}) is calculated by :

$$E_{ads} = E_{System} - E_{Surface} - E_{Adsorbate}$$

Objectives

- To elucidate the effect of Au in Ni-based catalysts for PDH reaction
- To compare selectivity of propylene production on Ni(111) and Ni-Au surfaces
- To investigate coke adsorption on Ni(111) and Ni-Au surface

Acknowledgements

The authors gratefully acknowledge the financial support from Thailand Graduate Institute of Science and Technology (TGIST) contract No. SCA-CO-2559-2292-TH, the Graduated School, Chiang Mai University for the financial support. N.K. would like to thank the Thailand Research Fund (RSA6180044). This research work was partially supported by Chiang Mai University. The computational resources are provided by National Nanotechnology Center (NANOTEC). All supports from Computational Chemistry Laboratory, Department of Chemistry, Faculty of Science, Chiang Mai University are also acknowledged.

References

[1] L. Tao, D.C. Rosenfeld, Non-Oxidative Butane Dehydrogenation Process in, DOW Global Technologies LLC,Midland, MI (US), 2013
[2] Z. Yan, Y. Yao, D.W. Goodman, Dehydrogenation of Propane to Propylene over Supported Model Ni-Au Catalysts, Catalysis Letters, 142 (2012) 714-717
[3] M.-L. Yang, Y.-A. Zhu, C. Fan, Z.-J. Sui, D. Chen, X.-G. Zhou, DFT study of propane dehydrogenation on Pt catalyst: effects of step sites, Physical Chemistry Chemical Physics, 13 (2011) 3257-3267.

Results and Discussion

Adsorption of propane on bare-Ni surface

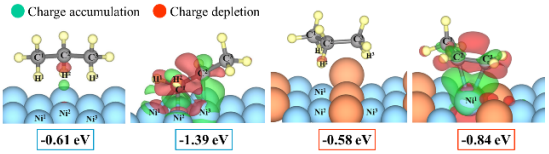

- The active sites of Ni and Ni-Au catalysts for propane and propylene adsorption are similar. (Ni site)
- During adsorption process, electron density moves from Ni site of surface (Donor) to adsorbed molecules (Acceptor)
- Doping of Au into Ni(111) catalyst has no effect for propane adsorption but it decrease the binding energy of propylene adsorption.

Energy profile of PDH reactions on Ni(111) and Ni-Au surfaces

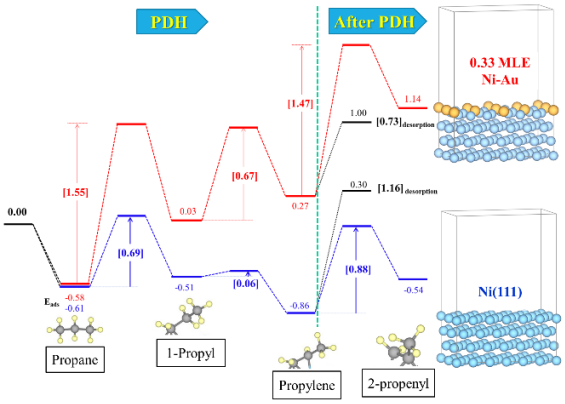

Coke formation on Ni(111) and Ni-Au surfaces

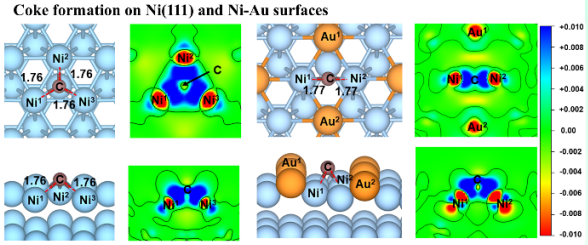

- By comparing energy barriers, PDH reactions on Ni(111) surface proceed easier than that of 0.33 MLE Ni-Au.
- Doping of Au to Ni(111) decreases the energy barrier of propylene desorption.
- Existence of Au on Ni(111) surface reduce charge exchanging between Ni-Au surface and C atom

Conclusions

- Doping Au into Ni(111) surface has no effect on propane adsorption but decreases adsorption energy of propylene.
- Doping Au into Ni(111) surface enhance the efficiency of propylene desorption increasing the selectivity of propylene production from Ni-Au surface.
- Weakening of C adsorption on Ni-Au indicates that doping Au is possible to reduce coke formation on Ni surface.

CURRICULUM VITAE

Author's Name	Mr. Tinnakorn Sae-Lee
Date/Year of Birth	5 March 1989
Education	2007 Bachelor of Engineering (Petrochemical and Polymeric Materials), Silpakorn University 2012 Master of Science (Chemistry), Chiang Mai University 2014 Doctor of Philosophy (Chemistry), Chiang Mai University
Scholarship	2016 – 2019 Thailand Graduate Institute of Science and Technology Scholarship (TGIST)
Specialized Programs	Gaussian 09, VASP, Surface science, *etc*.